SUPERCONDUCTOR
TECHNOLOGIES

THE PROCESSING OF HIGH TEMPERATURE CERAMIC SUPERCONDUCTING DEVICES

Contract No.: N00014-88-C-0713

Principal Investigator: Dr. James H. Long, Jr.

ARPA Order No.: 06268

Contract Dates: 9-1-88 to 12-31-91

DTIC
ELECTE
APR 01 1992
D

FINAL REPORT
Volume 1
January 31, 1992

AD-A248 176

Submitted by Program Manager

James H. Long, Jr.

SUPERCONDUCTOR TECHNOLOGIES INC.
460 WARD DRIVE, SUITE F
SANTA BARBARA, CA 93111-2310
Phone (805) 683-7646
Fax (805) 683-8527

92-07620

92 3 25 066

460 WARD DRIVE, SUITE F, SANTA BARBARA, CALIFORNIA 93111-2310
TELEPHONE (805) 683-7646 FAX (805) 683-8527

THE PROCESSING OF HIGH TEMPERATURE CERAMIC SUPERCONDUCTING DEVICES

Volume 1

TABLE OF CONTENTS

Accesion For		
NTIS CRA&I		☑
DTIC TAB		☐
Unannounced		☐
Justification		
By		
Dist ibution /		
Availability Codes		
Dist	Avail and / or Special	
A-1		

LIST OF TABLES AND FIGURES

LIST OF TABLES AND FIGURES

EXECUTIVE SUMMARY

This report describes the objectives and the results achieved in a three-year research effort. The goals of the program included:

(a)   development of a process to grow high critical current, low surface resistance high temperature superconducting thin films on 2" substrates,

(b)   development of fabrication processes to support the development of passive microwave and IR focal plane interconnect devices,

(c)   design and implementation of passive microwave and IR focal plane interconnect devices, and

(d)   theoretical analysis of microwave losses in HTS thin films.

High performance, microwave TlCaBaCuO thin films have been developed and put into pilot production in a 2" wafer process. Films are made in both single and double side configurations. The films have the lowest surface resistance at 77K of any material in existence, nearly 100 times better than OFHC Cu at 10 GHz and 77K.

Fabrication processes to produce passive microwave and IR focal plane interconnect devices have been developed: patterning, contacts, bonding, passivation, crossover metallization, and die attach.

Passive microwave devices have been demonstrated that show orders of magnitude improvement over conventional technologies including resonators, bandpass filters, bandreject filters, delay lines, couplers, and resonator-stabilized oscillators.

IR focal plane interconnects have been demonstrated that show dramatic improvement over existing technologies.

The primary loss mechanism in HTS films has been identified as weak links occurring at high angle grain boundaries.

This report begins with an introduction and background that describes the original program objectives and summarizes the major research results. Then there are six sections that address the specific research results: Thin Film Processes, Device Fabrication Processes, Microwave Devices, Measurement Development, Cryocooling and Packaging, and the FM CW Radar Prototype. Following this are five sections that summarize the research results of the subcontractors: BEI Electronics, Avantek, Lockheed Missiles and Space Company, Hughes, and Lockheed/Sanders. Finally there is a section of Summary and Conclusions, a section of Recommendatinos for Future Work, and an appendix that includes the five subcontractor final reports (in Volume 2).

INTRODUCTION AND BACKGROUND

The original objectives of this three-year program were to develop a manufacturable process for the fabrication of superconducting thallium thin films with surface resistances 10× less than cryogenic copper at 10 GHz and 50K and 100× less at 77K. The precursor films would be deposited by sol-gel or laser ablation and then thermally processed at high temperatures to form the desired superconducting compound. The resulting HTS thallium films would be used for the fabrication of passive microwave, IR focal plane interconnect, and linear actuator coil devices.

Characterization of the films was a significant element of the program. Identifying the relationship of deposition and processing conditions to microstructure was crucial in developing the manufacturing process. Understanding the relationship between transport properties and microstructure allowed the structure, chemistry and morphology of the HTS thin film to be tailored to meet the needs of a particular device application.

The following summarizes the original program objectives:

- Thallium Thin films: 1 cm to 3" wafers, $J_c=10^5$ A/cm^2, $R_s=0.01$ Cu at 10 GHz 77K, Substrates: MgO, zirconia, LaAlO$_3$, sapphire

- Develop Manufacturing process

- Microwave Devices: local oscillator, phase shifter

- Theory: theoretical model for Rs limits

- Sol-gel for IR interconnect: 10^3 A/cm^2, 0.03 system thermal conduct.

- Interconnect device on rigid substrate (laser ablation taken to manufacturing)

- Fibers: redirected to thin films

- Linear actuator: redirected to PMD package development.

During the course of the program the goals and objectives were modified somewhat by mutual agreement between DARPA, ONR, STI, and the subcontractors. The changes were made due to the rapid progress in the field and the priority to speed development of applications.

In the first year, sol-gel work was discontinued because it was determined that laser ablation produced better films. The fiber work was discontinued also during the first year and efforts were focused on rigid substrate approaches to fabricate IR focal plane interconnects. The linear actuator work was discontinued and the effort was redirected toward packaging of HTS

1

microwave devices. Originally, MgO was identified as the most attractive microwave substrate, but was changed to $LaAlO_3$ during the second year of the program due to better performance of this newly available substrate material.

A major accomplishment in the first two years was the production of superconducting thallium thin films with microwave surface resistance more than one hundred times lower than cryogenic copper at 10 GHz and 77K. These films were manufactured in a two step batch process of deposition followed by post deposition thermal annealing. The films were produced on 1 cm^2 $LaAlO_3$. The process was successfully taken into pilot production during the second year.

Device design and development was started in the second year. The performance of prototype passive microwave and IR focal plane interconnect devices was excellent. Resonators with Q values of 30,000 at low temperature (20K) and in excess of 20,000 at 80K were routinely produced. In conjunction with Avantek, Inc., we demonstrated oscillator performance using a superconducting resonator. The performance of the oscillator was much better than one which used a gold thin-film resonator and approached that achievable with DRO oscillators. Microwave bandpass and band reject filter structures were patterned and tested. Performance of these devices was significantly better than gold structures.

In the first year of the program we were successful in developing a weak link model of microwave losses in thin film HTS. This model predicted strongly power dependent losses due to weak links in the films. The weak links arose from in-plane grain boundaries in the film. We determined that no large angle in plane grain boundaries could be tolerated in the manufacture of high performance microwave films. As a result we developed the ELF process to produce fully oriented epitaxial films.

A major accomplishment in the final year of the program was the production of 2-inch thallium superconducting thin films with microwave surface resistance 50 times lower than cryogenic copper at 10 GHz and 77K. It is significant that this low surface resistance was measured in an actual thin film microwave device. Films of equal microwave quality were produced on one or both sides of the double-side polished substrates. An early goal for the program was to produce films on 3-inch wafers. We successfully produced precursor deposits on 5-inch areas and designed a ELF reactor for 3 inch films, but did not complete the implementation of this process before the end of the program, due to only recent availability of 3" wafers.

The final year emphasized device fabrication development and showed significant progress. A low resistance, less than 1 $\mu\Omega$ cm^2, MIL SPEC bondable contact metallization process was developed and put into routine production. In addition, a patternable passivation layer was

2

developed for thallium films. The passivation did not degrade microwave performance of the films. The patternability and excellent microwave performance of the passivation dielectric also allowed the development of a gold crossover metallization process. This enabled a dramatic improvement in HTS delay lines and lumped element filters. Also, we developed a thermal expansion-matched chip carrier for mounting finished devices.

Performance in prototype passive microwave devices was excellent in the final year of the program. Microstrip resonator Qs up to 33,000 were demonstrated at 77K, 5 GHz. A 29 nsec superconducting delay line was realized on a 1.2 inch square substrate with less than 0.1 dB per nsec loss at 2 GHz. A Lange coupler with less than 0.1 dB loss from 9.5 GHz to 10.5 GHz was demonstrated. A ninth order 4% bandpass 10 GHz microstrip filter with less than 0.4 dB insertion loss was demonstrated. A low noise, compact, 10 GHz reflection oscillator with phase noise -100 dBc at 10 kHz was developed. Finally, a novel Q-switch that permits rapid switching of resonator Q from extremely high to extremely low values, e.g., 10,000 to 10 was fabricated.

Significant progress was made in cryogenic packaging. Numerous devices were packaged in custom liquid nitrogen dewars. These included filters, resonators and delay lines. Also, our deliverable demonstration device represents the most significant advance in the field in this area: a superconducting delay line packaged in a closed cycle Stirling cooler. An FMCW radar unit was constructed and delivered to DARPA for demonstration purposes.

RESULTS AND DATA

Film Process Development

Overview

The objectives for the overall program were to manufacture microwave devices, IR focal plane interconnects and a linear actuator. A prerequisite to these end products was to develop a thin film manufacturing capability. The 2" round Tl-Ba-Ca-Cu oxide (TBCCO) thin films on one or both sides of a substrate, which are currently being produced at STI, demonstrate the tremendous progress made in HTS thin film technology over the past three years. The significant contributions made by STI in developing this capability are listed below.

- First TBCCO film using sol-gel
- First epitaxial TBCCO film
- First double-sided superconducting $1cm^2$ film
- First 2" round HTS film

3

- First double-sided 2" round HTS film
- First production process for the manufacture of HTS films.

As the program developed emphasis on microwave devices increased. Microwave devices represented a goal where the advantages of superconductivity would be significant over the current technology. The improvements in performance are best seen by comparing the surface resistance of films made at the end of year 1 of this program with those currently available as 2" films from wafer production.
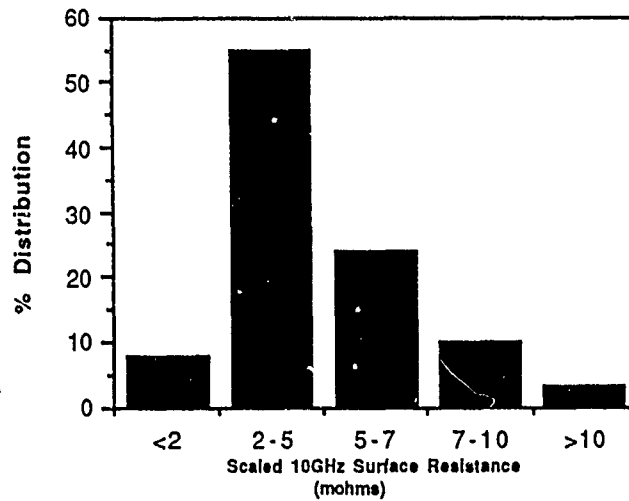
Figure 1. Distribution of scaled 10 GHz surface resistance at 77K (May, 1989).
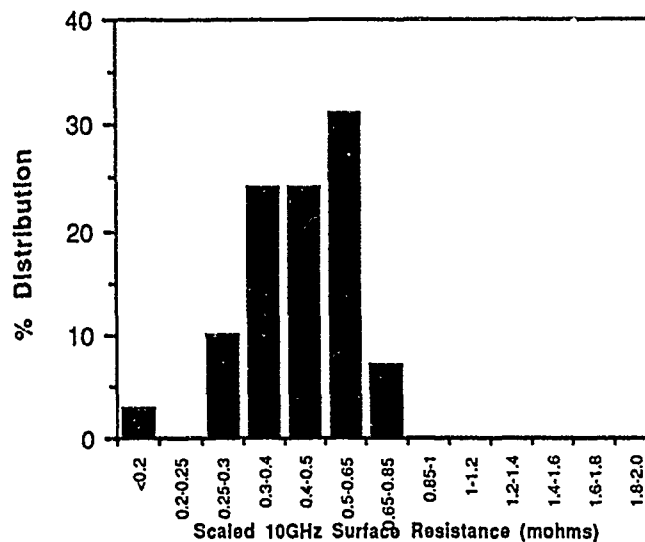
Figure 2. Distribution of scaled 10 GHz surface resistance at 77K (November, 1991).

The two figures above clearly show the improvement in film quality. The scales for surface resistance do not overlap; an order of magnitude improvement in the surface resistance has been achieved. However, the improvement is even more dramatic when considering how these measurements were taken. The R_s data shown in Figure 1 were measured using a 10 GHz cavity in which the whole film is measured and the data represents an average value over the 1cm^2 wafer. Figure 2, on the other hand, is data extracted from actual device performance, in this case a 0.006" wide, straight line resonator, where any defects will degrade the performance. Thus, the resonator data represents an upper bound on the average R_s value. In addition, all of the data shown in the latter figure is from 2" round wafers.

Over the three years of this contract, the thin film process has developed from an uncontrolled, research experiment into a reproducible, pilot scale process, with process documentation and specifications. The evolution of the thin film process is shown in Figure 3.
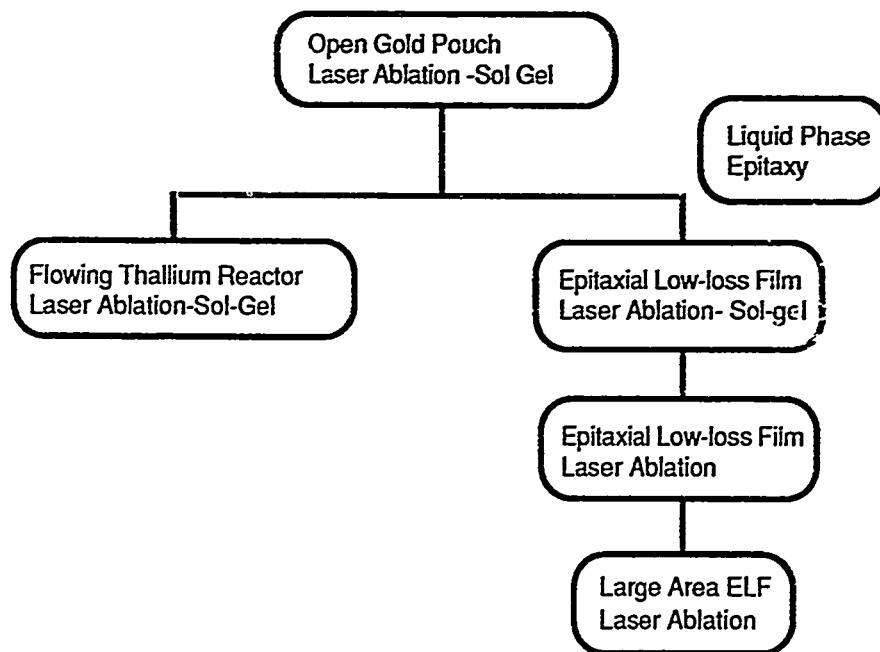
Figure 3. Evolution of the TBCCO thin film process. The process name and deposition technique are given.

At the start of the contract STI had focused on TBCCO superconducting thin films because of its higher intrinsic T_c and the early results of high J_c in thin films from Sandia. In the first process employed, two methods were used to deposit the amorphous precursor--sol-gel and laser ablation. The high temperature processing was carried out in a gold container, with TBCCO pellets acting as thallium sources to prevent depletion of thallium from the film (the OGP process). This still remains the standard method of making TBCCO films in the scientific community.

However, at STI it was realized this process was difficult to control and reproduce, and that a quite different approach was necessary. Consequently three techniques were investigated: the Flowing Thallium Reactor (FTR), Epitaxial Low-loss Film process (ELF) and Liquid Phase Epitaxy (LPE). These processes represented what STI saw as a significant improvement in control and reproducibility. Work on LPE was halted when it was found, as other groups later discovered, that producing a stable, equilibrated melt was very difficult, if not impossible. The two remaining processes both produced high quality, epitaxial TBCCO films; however, the ELF process was chosen to develop into production because of its simplicity and scaleability.

Laser ablation was chosen over sol-gel as the deposition method of choice, since laser ablation produced more uniform and smoother surfaces. Also pyrolysis of the organic in the sol-gel precursor was difficult because of the volatility of the thallium itself. The ELF process, using precursors deposited by laser ablation, is currently used at STI to produce the 2" round, epitaxial TBCCO thin films.

The improvement in the microwave properties after the transition from OGP to ELF is shown in Figure 4, where the surface resistance as a function of microwave field is illustrated. "Old process" is the gold pouch method originally used at STI and "New Process" is the ELF process, and as can be seen, the quality of the films and the ability to handle high fields without degradation in performance has improved dramatically even after focusing on the ELF process.
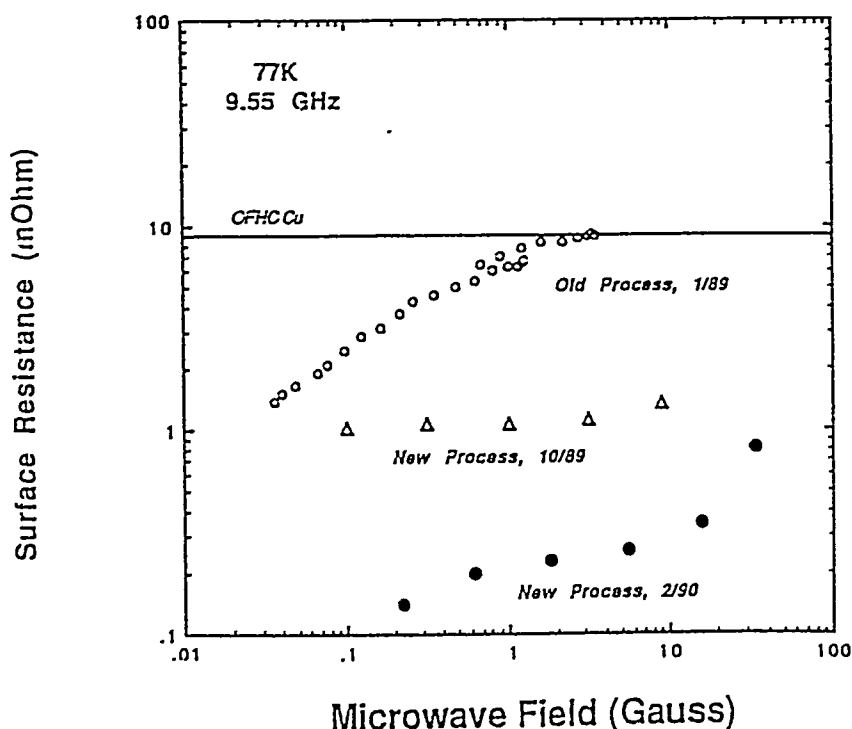
Figure 4. Surface resistance as a function of input power for different process methods.

Choosing laser ablation as the deposition technique required considerable advances to improve uniformity and reproducibility, and these efforts are continuing. The increasing sophistication and control in laser deposition is shown in the layout schematic, Figure 5, which shows the current setup of the laser ablation deposition system at STL
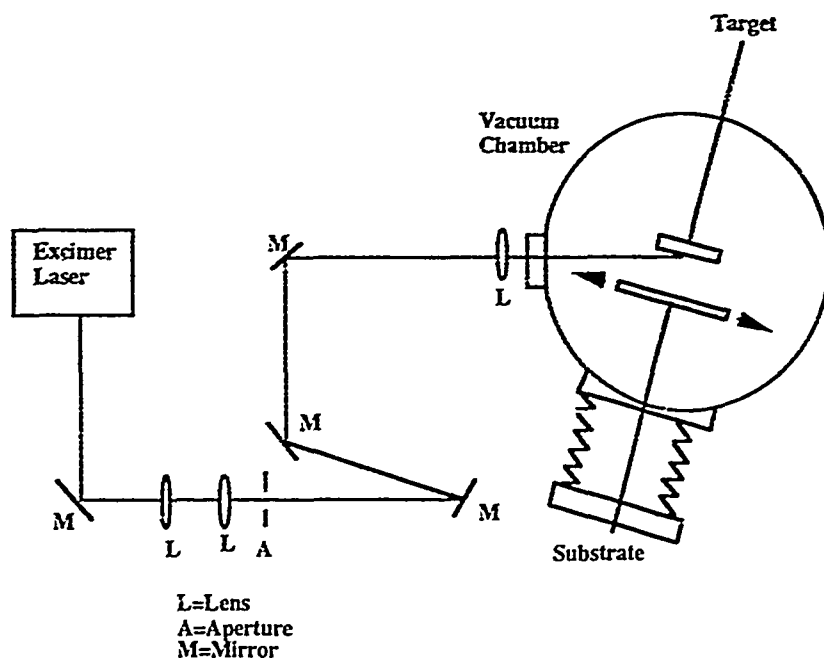
Figure 5. Layout of the laser ablation deposition equipment at STI.

A Lambda Physik 315i-F is used to provide the 248nm radiation. This is operated at a repetition rate of 50 Hz. Complex substrate motion using both rotation and translation produces deposits uniform in both thickness and composition. A typical deposit on 2" round wafers takes ~20 minutes.

The culmination this process development work has been the demonstration of a manufacturing process for the production of 2" round TBCCO films. The process is operated according to manufacturing procedures, with quality control monitored according to specifications. It is this production process, shown in Figure 6, which provides films for sales and internal use.
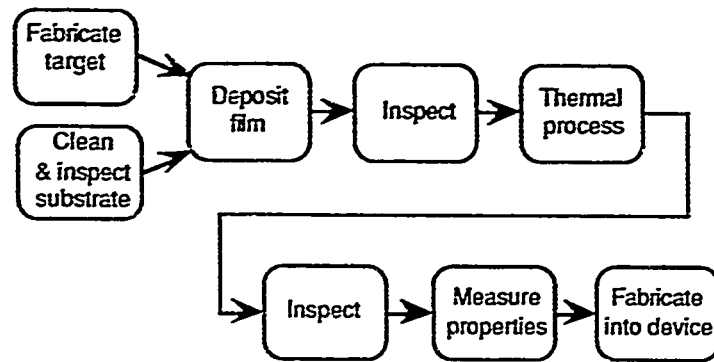
Figure 6. Block diagram of the ELF process at STI.

The following sections give a more detailed review of the progress made and the various stages of the process evolution.

Deposition Technique Development (Sol-gel--Laser Ablation)

Sol-gel

The first task towards developing a sol-gel thin film deposition technology was to evaluate various precursor chemistries for preparing amorphous deposits of Tl-Ca-Ba-Cu oxides for thermal processing. A precursor composed of Tl, Ca, Ba and Cu carboxylate compounds (*viz.*, neodecanoates, 2-ethyl hexanoates) was selected for coating. These precursors were selected on the basis of their comparable solubility properties, low pyrolysis temperatures, high net ceramic yields and excellent rheological (i.e., coating) properties.

Thallium precursor films were deposited and thermally processed to obtain superconducting thin films on a variety of substrate materials including MgO, sapphire and polycrystalline zirconia. The thermal process development effort soon confirmed the existence of an transient liquid phase during pyrolysis that controlled the structural and morphological development of the film at high temperature. This unique development was exploited to obtain polycrystalline c-axis oriented thin films on a wide variety of substrates and epitaxial thin films on MgO and LaAlO$_3$.

The crystallographic orientation of the film was verified by performing selected area electron channeling experiments. Large area electron channeling patterns have been obtained for thermally processed thallium thin films on LaAlO$_3$. The excellent quality of the channeling pattern and orientation with respect to the substrate was consistent with the formation of an epitaxial 2122 structure with its c-axis normal to, and the (100) and (010) axes coincident with, the (100) and (010) substrate axes .

8

Laser Ablation

In parallel with the sol-gel chemical processing effort, a laser ablation system for depositing thallium precursor films was constructed. The system included an excimer laser and vacuum deposition chamber, with a heated substrate holder and activated oxygen source capability for *in-situ* growth experiments. This equipment was used to prepare amorphous Tl-Ca-Ba-Cu oxide deposits of 2223 stoichiometry which were subsequently processed at high temperature.

At this point in the program we began addressing the development of laser ablation to produce larger area, uniform deposits. In the original configuration we could only achieve a ±20% thickness variation on a single 1 cm^2 substrate. By positioning the substrate slightly off axis in relation to the target axis and continuously rotating the sample during the deposition, we increased the area of uniform deposit (within ±20%) to approximately a 40 mm diameter, as shown in Figure 7. This new configuration has allowed us to simultaneously deposit on four 1 cm^2 substrates while maintaining a thickness variation of less than ±20% across the substrate as well as substrate to substrate.
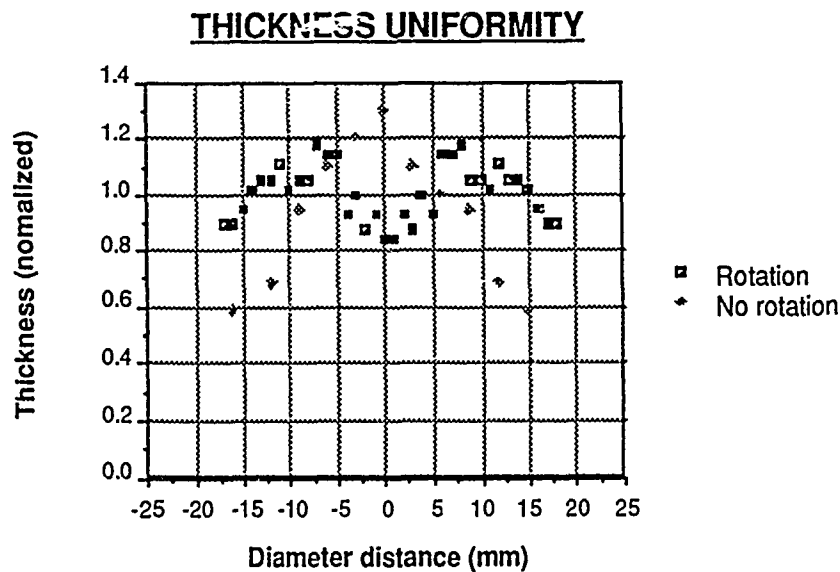
Figure 7. Lateral thickness uniformity of deposits from laser ablation.

As larger substrates have become available and the demand for large area devices has increased, the production of large wafers became a necessity. Consequently, STI is now developing sophisticated substrate motion of the substrate to deposit over areas as large as 5". This will allow the simultaneous deposition of three 2" wafers. The preliminary data for such a system is shown in Figure 8. This shows the the thickness uniformity over one of the 2" wafers coated. The thickness uniformity is +/-10%.
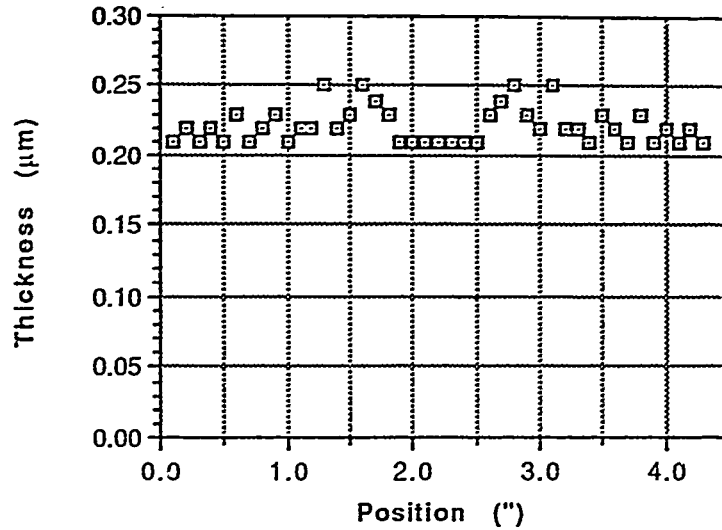
Figure 8. Thickness uniformity over one of the 2" round wafers from a large area deposition.

Thermal Processing Development

The amorphous precursors must be annealed at a high temperature (750-900°C) to form the superconducting phase(s). The high volatility of thallium oxides above 350°C increases the difficulty of preparing superconducting thallium thin films with attractive transport properties. Control of the volatility is a key step to crystallizing the films at high temperatures. Early experiments with sol-gel precursor deposits indicated that complete thallium volatilization from the deposit occurred at 300°C if the film was heated in a thallium-free environment at atmospheric pressure. Laser ablation deposits are much more stable, not losing thallium below 700°C.

In the sections following the OGP and ELF process developments will be described. These are the two processes which have been focused upon over the program.

Open Gold Pouch (OGP)

Early attempts to obtain superconducting thallium thin films were plagued by thallium loss at high temperature. After considerable effort, we developed a thermal process capable of producing isolated platelets of the 2122 material on MgO. These early films were prepared by placing an amorphous sol-gel or laser ablation deposited film and a thallium source material in a sealed gold pouch and firing the pouch/powder/film assemblage at 860°C for several minutes. A large excess of Tl_2O_3-CaO-BaO-CuO powder was necessary in the pouch to limit volatilization of thallium from the film at high temperature.

We discovered during optimizing the thermal process that under the process conditions that produced superconducting material, a substantial fraction of the film had formed a liquid phase during heating. In fact, the final morphology of the films bore a striking similarity to films grown by LPE. This observation culminated in our discovery that under the proper thermal process conditions that c-axis oriented, epitaxial 2122 or 2223 thin films could be fabricated from *either* sol-gel or laser ablation deposited films.

The thermal process that was used to prepare our first low surface resistance thallium film was based on a hermetically sealed gold pouch that contained a pellet to provide a source of thallium vapor during processing. Experimentation with a variety of pouch designs indicated that improved results could be obtained using an open pouch process geometry (the OGP process).

After spending considerable effort in defining and controlling all process variables relating to deposition and thermal processing of the films, we achieved a significant improvement in the reproducibility of the thermal process. Specific examples of the process improvements we implemented include: (i) utilization of high purity chemicals from preferred vendors; (ii) use of controlled-atmosphere glove boxes for all powder weighing and handling; (iii) definition and observation of detailed process specifications relating to substrate preparation, film deposition and firing.

The variations in surface resistance for films made by the OGP process are shown in Figure 9. All data was collected in a 10 GHz cavity and, as shown, the R_S at 77K varies from ~0.3 to 600mΩ, over three orders of magnitude. The 2" ELF production process, currently produces films which, measured at 100 GHz and extrapolated to 10 GHz for comparison, have R_S values ranging from 0.15 to 0.6mΩ, representing a significant improvement.

11
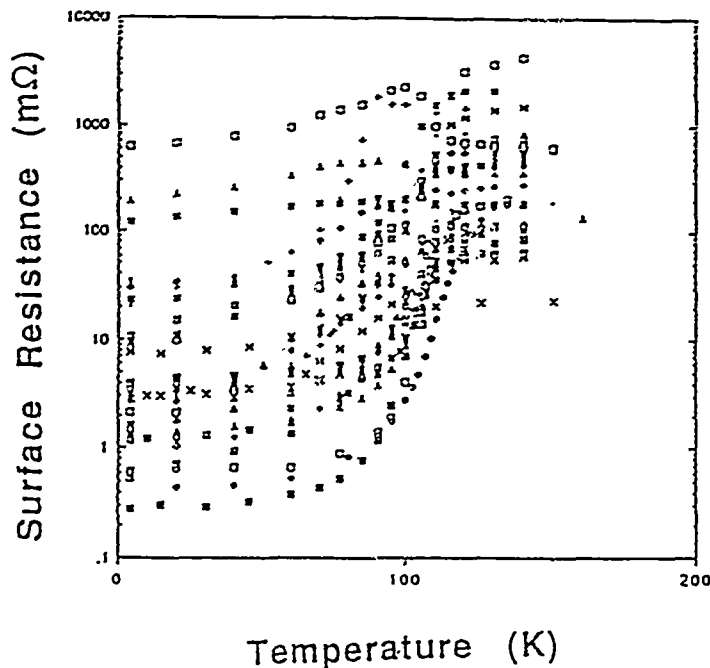
Figure 9. Surface resistance at 10 GHz for films produced up through February 1989.

The open gold pouch process could not be developed to handle substrates much larger than 1 square inch. Also, *independent* control of the thallous oxide overpressure above the film at high temperature is not possible with this approach. In the open gold pouch process, the thallous oxide verpressure above the film is "controlled" using a bulk sintered pellet. Ultimately we wanted to develop a process that would allow us to independently control the thallous oxide and oxygen overpressures.

In parallel with the initial thallium film production effort by OGP, advanced thermal processing techniques were developed using IR&D funding. The goal was to provide better control of the thallous oxide pressure during phase formation at high temperature and to provide a process which could easily be scaled for larger area deposits (i.e., >1" diameter).

The FTR utilized a two-zone furnace with a controlled thallous oxide vapor source and the as-deposited film placed in separate zones. By varying the oxygen partial pressure and make-up gas flow rates past the thallium source, a wide range of thallous oxide overpressures (0.05-50 torr) were provided above the film during firing. By programming the oxygen and thallous oxide partial pressures as a function of heating time and substrate temperature, it was possible to control the growth of the film under nearly equilibrium conditions.

The ELF process involves limiting the gas volume above the film to a *sufficiently low amount* that the film can serve as its own thallium source during thermal processing. Since the

12

atmospheric volume above the film is small, equilibration times can be very short, allowing the use of kinetically-controlled growth conditions (i.e., rapid evaporation, heating and cooling rates).

The ELF and FTR development projects both produced 2122 thallium thin films on single crystal $LaAlO_3$ substrates. The films had a more uniform (less terraced) surface morphology and were of better epitaxial quality than those produced by the OGP method. Although films were successfully produced on single crystal MgO, films with the best microwave properties and morphology were consistently obtained on $LaAlO_3$. These substrates give higher nucleation densities (i.e., improved epitaxy) and superior (melt) wetting characteristics (i.e., fewer pinholes) as compared to MgO. An added advantage of $LaAlO_3$ is its availability in 2" diameter wafers.

Epitaxial Low-loss Film (ELF) Process

The epitaxial quality of the ELF films was markedly superior to films grown by the open gold pouch process. Large area electron beam channeling patterns are observed for these films, indicating improved epitaxial film quality (see Figure 10). The films exhibit intense, sharp XRD patterns with <004> rocking curve widths ranging between 0.25-0.9 degrees. AC susceptibility measurements indicate the films to have very sharp transitions to the superconducting state--with T_cs exceeding 100K and transition curve widths less than 1 degrees being commonly obtained. A typical AC susceptibility curve is displayed in Figure 11. The 10-90% transition width of this film is a factor of two less than the best film obtained using the open gold pouch growth process.
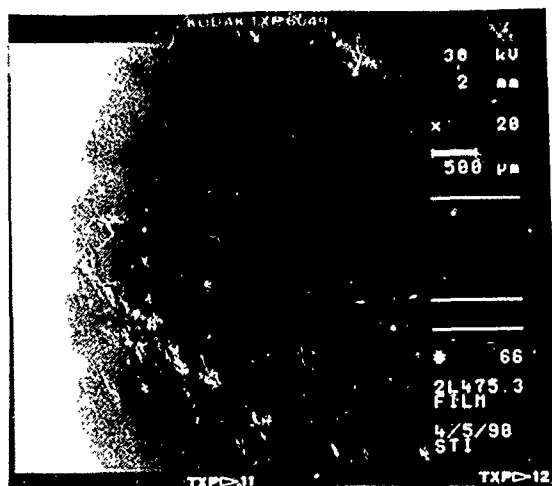
Figure 10. Large area electron beam channeling pattern for a new process film.

13

AC Susceptibility for ELF Film
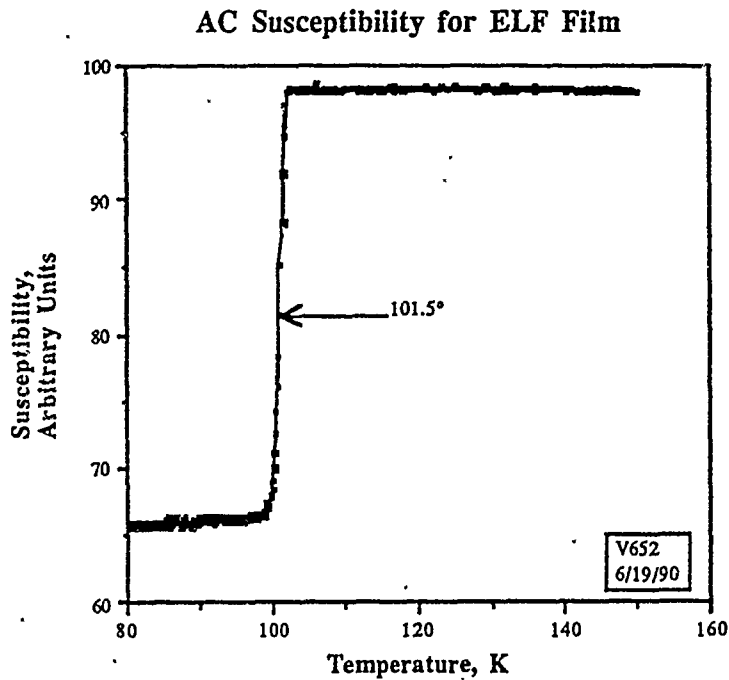
Figure 11. AC susceptibility for a 2122 Tl film grown by the new thermal process.

The transport properties of films produced using the ELF process were superior to the OGP grown materials in a number of other key areas. Critical current density measurements on 10 micron wide microbridges indicated 0.5-1 million amps/cm^2 at 77K: a factor of 10 higher than the highest quality OGP thallium films. In areas of obvious defects, the measured critical current densities are typically less than 50,000 A/cm^2 at 77K.

The microwave film properties also improved. A typical plot of surface resistance at 10 GHz is shown in Figure 12 below.

14

Surface Resistance at 9.55 GHz for SV366
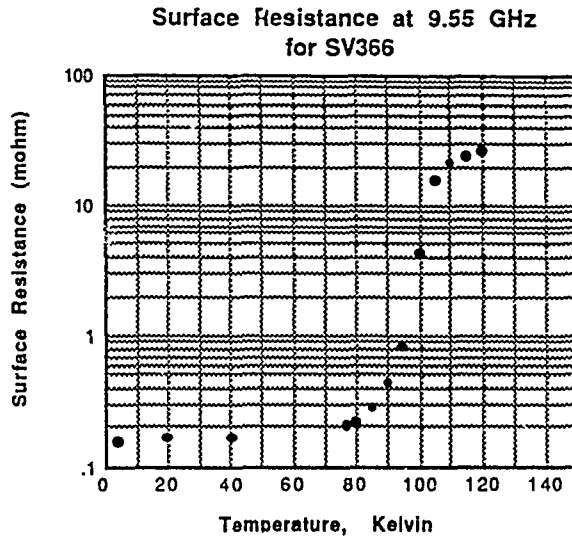
Figure 12. Surface Resistance of a 2122 Tl film grown by the new thermal process

ELF Film Production

In December 1989 an existence proof of high Q performance from a simple microwave device, a 2.6 GHz resonator, made from an ELF film was observed. Since that date continual improvements in control and reproducibility have led to the current production process. Over time, developments to increase the size and include double sided films have increased the range of products from the production process.

We continued to improve the process for fabricating microwave device quality thallium films by laser ablation followed by post deposition thermal processing (ELF process). We focused our resources upon improving the yield and consistency of ELF films on 1cm^2 lanthanum aluminate substrates using our production process. Production levels of single sided 2122 thallium films averaged 30 films/week. The superconducting properties of the films were consistent and uniform over the substrate surface. Figure 13 shows the transition temperatures of thallium production films produced over a 2 month period spanning August and September, 1990.

15
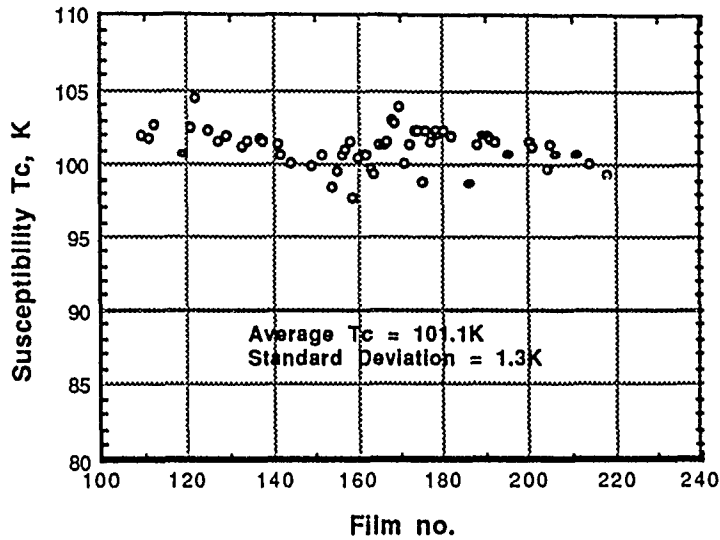
Figure 13. Production film T_c measured by AC susceptibility

We have found that the superconducting transition width of films measured by AC susceptibility to be an excellent indicator of HTS film uniformity/homogeneity. The superconducting transition width (90—10%) of these films averages 0.9 degrees (see Figure 14).
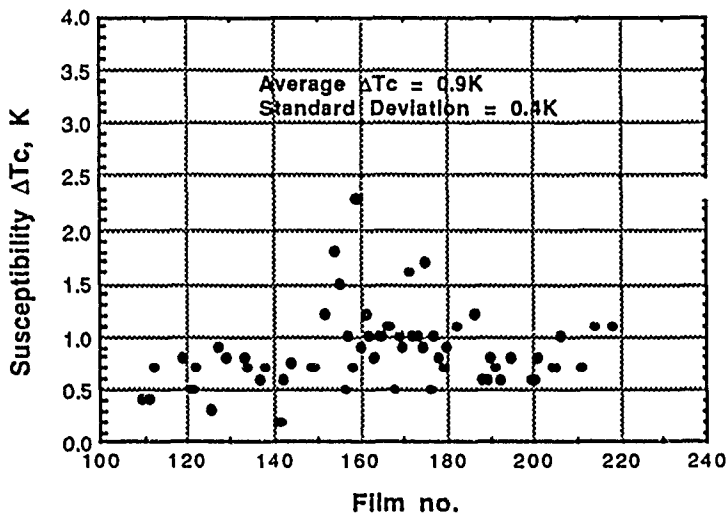
Figure 14. Production film ΔT_c measured by AC susceptibility.

Film microstructural uniformity was monitored using optical and electron microscopy. Defects relating to substrate nonuniformities, large end nucleated plates, or surface contamination of the precursor deposit often appear as holes in the film after firing at high temperature. In addition, several steps were taken to reduce contamination of the films including laminar flow

16

benches at all work stations, the required wearing of smocks, gloves and caps for all operators and improved wafer cleaning and handling. This was the first step toward the current protocol in the laboratory, where all production activities after target fabrication are carried out in class 100 environments.

Improvements to ELF

Two parallel development programs were started to expand our thallium film processing capabilities. The first program was to develop a production process for growing microwave quality double sided thallium films on lanthanum aluminate. Double sided films are desirable for building passive devices (e.g., filters, resonators) that operate at their design frequency. Also this structure is more mechanically robust than sandwich microstrip geometries using two single sided films. The second development program pertains to growing high quality thin film material on lanthanum aluminate substrates of 1 and 2 inches in diameter.

Double sided thallium films

Efforts to prepare double sided thallium films concentrated upon developing the substrate handling, cleaning and deposition techniques required to produce low defect density films on both sides of the substrate. Substrate cleaning and drying procedures developed for single sided films were modified to accommodate double sided substrates of 0.010 and 0.020" thicknesses.

Double sided amorphous deposits were fired in a specially designed reactor to prevent contact of the amorphous film with the reactor by holding the film horizontally by its corners. Process parameters were optimized to produce superconducting films with T_cs exceeding 100K and ΔT_cs of less than 2 degrees. A film exhibiting a low defect density and high T_c was selected for resonator testing at 2.3 GHz. Figure 15 shows the power dependent quality factor of this device.
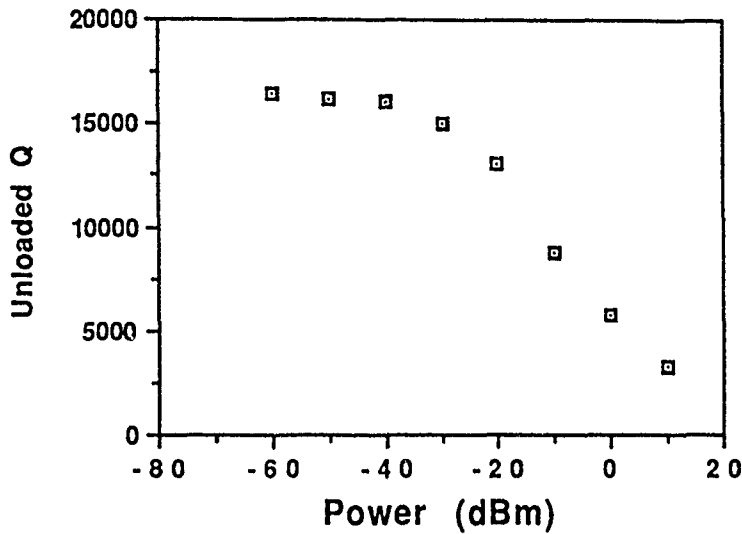
Figure 15. Power dependent unloaded quality factor for 2.3 GHz microstrip resonator at 77K fabricated from a 1cm^2 double sided thallium film on lanthanum aluminate.

The power dependent performance of this device is comparable to that observed for thallium films grown on single sided substrates by our standard production process.

Larger area thallium films:

The next step in large area development was to develop a process for 1" square lanthanum aluminate substrates using the ELF process. Annealing experiments were conducted to find the proper process parameters for producing thallium films on 1" substrates. Of key concern was that the films be uniform in morphology and superconducting properties over the entire wafer. We had expected that thermal gradients in the reactor could prove to be a major obstacle to progress. Fortunately, the reactor design and furnace configuration used, produced films that were uniform in appearance and morphology across the wafer (e.g., grain size, holes, defect distribution, reflectivity).

The superconducting properties of the films were determined to be comparable to the 1cm^2 process. AC susceptibility measurements were performed using a magnetometer designed to accept 1" square substrates. The transition curve of a representative film is shown in Figure 16. The film exhibited a T_c of 103K and a transition width of 0.9K.
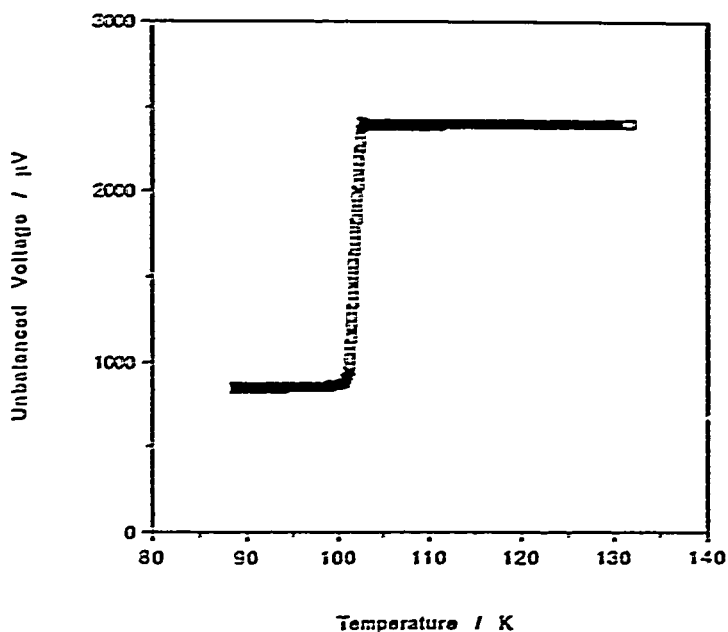
Figure 16. AC susceptibility curve of a 2122 thallium film grown on a 1 × 1 inch lanthanum aluminate substrate.

The success of the scale up is shown clearly by the results described below. The ease with which 1" square and 2" round films have been produced is a consequence of the simplicity of the ELF process, one of the original reasons for choosing this processing scheme. The microwave data shows excellent performance, comparable to that displayed on 1cm^2 films. Three 2.5 GHz resonators were patterned from the same 1" square film and the data is shown in Figure 17.
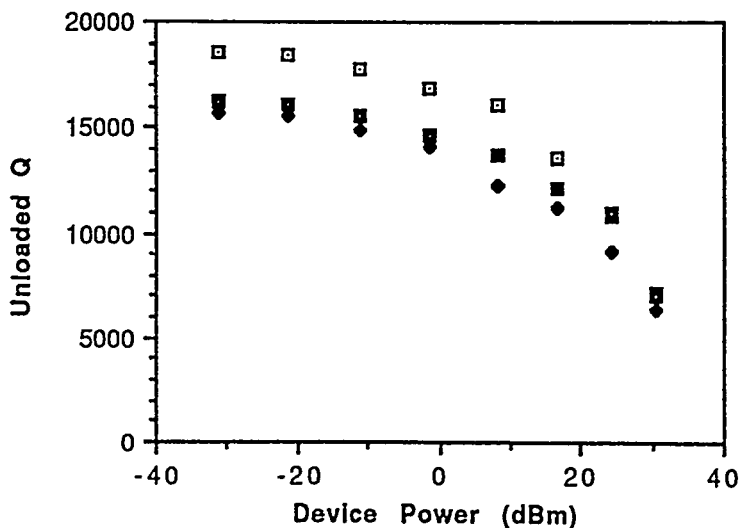
Figure 17. 2.5 GHz resonator performance for three films diced from the same 1" film.

19

In addition to the 1" square results, the data from 1cm^2 devices patterned and diced from a 2" round TBCCO film show outstanding performance as microwave devices. A 2" round film was patterned into twelve 5.6 GHz resonators and four 5 × 5 mm susceptibility test chips. The mask design is illustrated in Figure 18.

PLATE 39
12 X M10182
NO LAUNCH
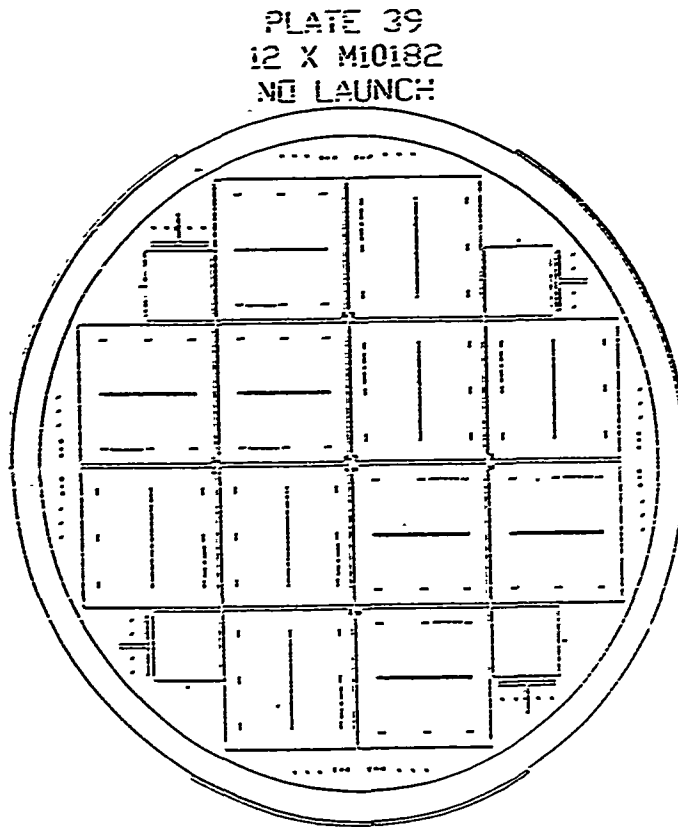
Figure 18. 2" test pattern

The susceptibility results are shown below:

Position	Tc$_0$, K	Mean	Range	Std dev.
1	104.2	104.2	0.3	0.1
4	104.5		(±0.1%)	(±0.1%)
13	104.3			
16	104.5			

Position	ΔTc, K	Mean	Range	Std dev.
1	1.3	1.4	0.3	0.1
4	1.3		(±11%)	(±10%)
13	1.4			
16	1.6			

Note that the range of T_{co} and ΔT_c are small. Note also in Figure 18 that the susceptibility test chips are all at the perimeter of the wafer where one would expect the lowest quality material. Resonator results are summarized below and are given for all resonators. Despite the larger number of samples in the outer ring, the differences in standard deviations at both frequencies show that the inside ring is more uniform.

Low power Q at 5.6 GHz:

All resonators		Outside ring (8)		Inside ring (4)	
Mean 15367		Mean 15684		Mean 14734	
Max 17508		Max 17508		Max 15269	
Min 13835		Min 13835		Min 13858	
Range 3673	± 12.0%	Range 3673	± 11.7%	Range 1411	± 4.8%
Std dev. 1304	± 8.5%	Std dev. 1472	± 9.4%	Std dev. 612	± 4.2%

Low power Q of 1L85? a, 16 GHz:

All resonators		Outside ring (8)		Inside ring (4)	
Mean 6196		Mean 6464		Mean 5659	
Max 8193		Max 8193		Max 6105	
Min 4488		Min 4488		Min 4826	
Range 3705	± 29.9%	Range 3705	± 28.7%	Range 1279	± 11.3%
Std dev. 1075	± 17.4%	Std dev. 1196	± 18.5%	Std dev. 569	± 10.1%

The 5.6 GHz resonators are 0.006" wide and represent the most demanding test of microwave performance for superconducting films. The distribution shown in Figure 19 is among the best seen from our 1cm^2 films.
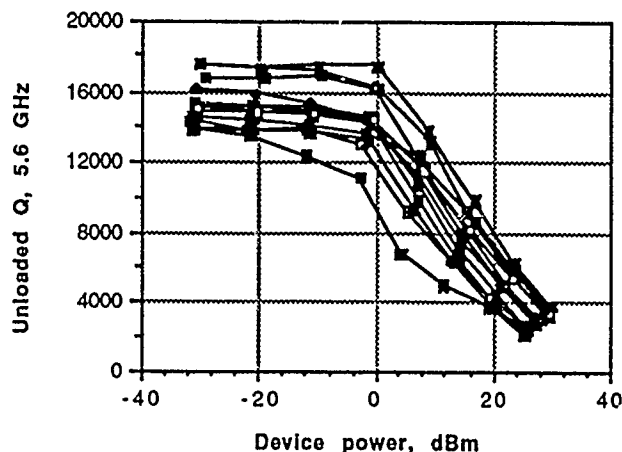
Figure 19. Power dependence of resonator Q at 5.6 GHz for all resonators from 2" round wafer.

To test the microwave performance of our films at extreme conditions we developed a test mask for evaluating the performance of narrow lines patterned on our 2" thallium films. Figure 20(a) shows the layout of the test mask. It contains fine lines for J_c testing and a variety of inductively coupled resonators to study the linewidth dependence of effective surface resistance. The test structure also contains resonators with linewidths that vary from 0.5 mils to 20 mils (12.5 microns to 500 microns). As the linewidth becomes narrower, Q shows the decrease calculated for a fixed surface resistance of approximately 0.6 mohms (Figure 20(b)).

PLATE: 82 STEP: HTSC ETCH
2X M10353 6X M10347 2X M10354

2X M10355

SET 15

5/10/91

BRF Data for 2L822

O -50 dBm

□ Predicted for
   0.6 milliohms
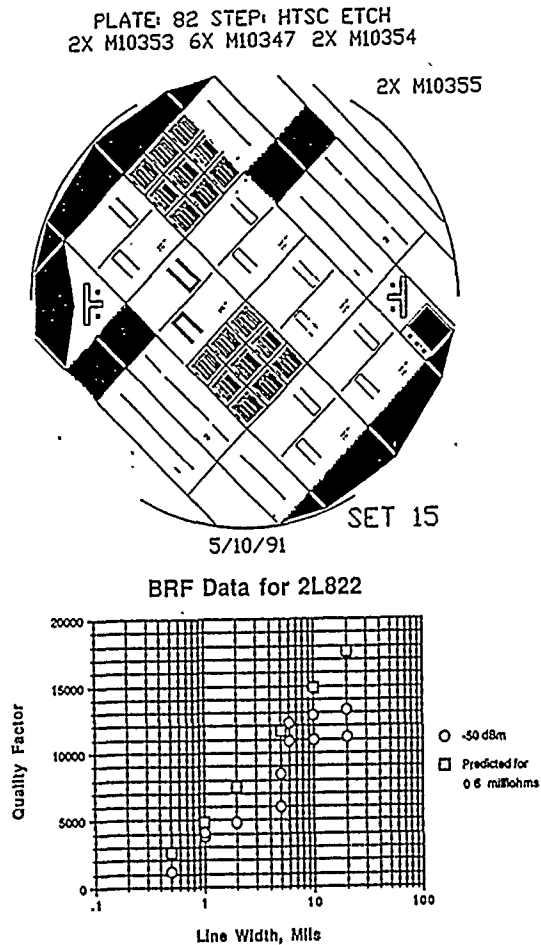
Line Width, Mils

Figure 20(a) Mask layout on 2" Tl wafer for fineline test structure, (b) plot of Q vs. linewidth for microstrip resonators. The various linewidths all yield R_s values near 0.6 ohms.

Summary

The progress made in developing a thin film, HTS manufacturing capability at STI is best illustrated by showing the films delivered on a recent sub-contract to Lockheed Sanders, under a DARPA contract. The actual deliveries are listed in Table 1. The films delivered were primarily 1" squared, both double and single sided on 0.010" thick substrates.

22

Table 1. Performance data for films delivered to Sanders for the technique development and building of the antenna feed network.

	Film No.	Tc	Delta Tc	5 GHz resonator Unloaded Q
2" Ø	2L1055/56			
	2L956/57			
	2L924			
	2L825			
	2L933			
	2L892			
1" square	2L1029/30	99.8	1	10300
	2L1044/45	99.4	1.3	11000
	2L1046/47	100.3	1.3	10820
	2L1048/49	99.1	2	12500
	2L951/52	100.7	1.9	10100
	2L989/90	100.8	1.2	12600
	2L994/95	100.5	1.3	13500
	2L1003/04	101.9	0.8	9100
	2L894	101.2	0.8	11800
	2L918/19	99.2	0.8	9800
	2L937/38	99.2	1.6	11100
	2L910/11	101.2	0.7	14700
	2L948/49	99.7	1.9	12400
	2L896/97	101.4	0.9	12300
	2L902/03	102.4	1.1	13300
	2L870	100	0.9	17800
	2L877	99.2	0.8	13900
	2L878	101.9	0.9	15700
	2L893/94	103.3	0.5	11800
	2L898/99	102.1	0.4	11300
	2L886/87	102.1	0.9	9915
	2L761	103.3	0.5	9300
	2L787	102.2	0.6	10600
	2L770	101.5	0.7	9500
	2L779	102.5	0.7	12100
	2L785	102.9	0.6	11400
		Total		
1 cm	Double sided	6		
	Single sided	78		

Totals			
	2"Ø	Single sided	4
	2"Ø	Double sided	2
	1" square	Single sided	16
	1" square	Double sided	19
	1x1 cm	Single sided	78
	1x1 cm	Double sided	6

23

All 1" square wafers were supplied with the device performance of a standard straight line, 0.006" wide 5.6 GHz resonator. Each deliverable 1" square wafer is diced from a 2" round wafer, and hence standard wafer qualification structures can be patterned onto the wafer for evaluation. Some of the later wafers were delivered undiced to allow for more area, and STI agreed to measure the 5.6 GHz device upon completion of the lithography and dicing at Sanders.

Figure 21 shows the distribution in device performance for all films supplied in the second year of the contract. The lowest unloaded Q measured on any wafer was 9100 which corresponds to a surface resistance of ~0.8mΩ at 10 GHz and 77K. An unloaded Q of 11,000 using a 0.010" thick substrate corresponds to an Rs of 0.5mΩ. Consequently, as can be seen from Figure 21, a significant number of films met the 0.5mΩ specification.
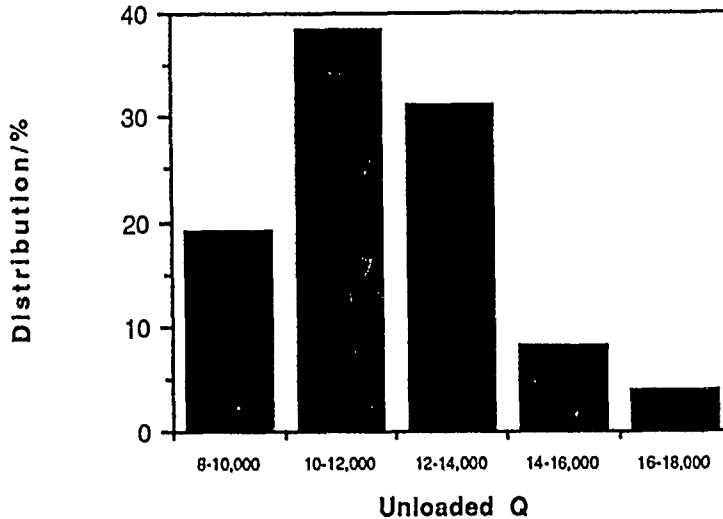
Figure 21. Distribution in the performance of films delivered on this sub-contract. The data set is listed in Table 1.

The capability demonstrated in delivering films for this program is a direct result of the funding provided on this contract.

Device Fabrication

Our device fabrication process has evolved from a simple one step process on single sided 1 cm^2 substrates to a 5 or more step process on double sided 2" diameter substrates. Initially substantial efforts were devoted towards identifying process chemicals, such as photoresists, etches and cleaning solutions, that are compatible with thallium HTS films. Generally the HTS films stand up well to most solvents but are relatively sensitive to most aqueous solutions. Most

positive photo resists appear to have little or no effect on HTS films, we found Shipley's 1800 series resist to work particularly well with our films. We also found that HTS films are generally incompatible with negative photoresists.

A more detailed description of the various processes developed as part of this program follows below.

HTS patterning

The first process that had to be developed was a patterning process for the HTS films. During the duration of the program, three different patterning processes were investigated in detail. The wet etching remains our standard process to date; it is simple, inexpensive and meets the relatively relaxed line width requirements of microwave devices. The other techniques investigated allow in principle for patterning to be very fine (1-2 μm) dimensions; however the surface roughness and the presence of second phases, particulates, etc. in current HTS films limits the useful line widths to ~25 μm. Substantial improvements in the quality of HTS films will be required before these processes can be fully utilized.

Wet chemical etch process

A relatively simple wet etch process was developed early in this program in order to fabricated simple test structures such as J_c bridges and microwave resonators. Several common acidic etches were evaluated: a very dilute $HCl:H_2O$ was found to work well. All etches have a severe undercutting due to the anisotropic nature of the HTS-film itself. We found that the undercutting is increased with the dilution of the acid. The dilution ratio was minimized while keeping the etch time from becoming impractically short. Our current etch process consists of $HCl:H_2O$ at 1:75-150 which results in an etch time of around 15-20 seconds. The average undercutting for this process is around 5 μm per edge. By carefully controlling the etch temperature and by minimizing over etching we have learned to reduce the variation in undercutting to approximately ± 2 μm. By correcting for the constant undercutting in the mask design stage, we have shown that line widths can be controlled to within $\pm$ 2 μm routinely (see Figure 22).
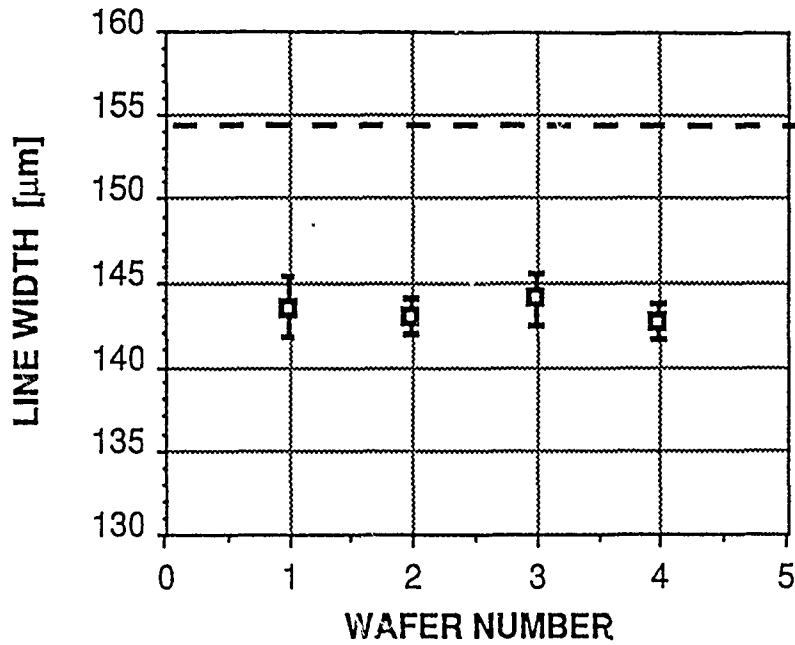
Figure 22. Line width of 5 GHz resonators on 4 sequential 2" diameter wafers. The design line width was 144 μm.

Dry etching

A small effort in evaluating various dry etching techniques was accomplished as part of this program. Dry etch techniques based on various reactive plasmas, such as Reactive Ion Etching (RIE), are known to have impractically low etch rates for oxide material, and are predicted to be of little use for patterning HTS films. The only practical dry etch technique at this point appears to be Ar ion-milling. Ion milling was evaluated, in collaboration with Sanders, as part of this program. We found that HTS films are very sensitive to the milling parameters, in particular to milling rate and acceleration voltage. By carefully optimizing the milling parameters, however, it is possible to use Ar ion-milling to successfully pattern thallium HTS films without any degradation in microwave properties as shown in Figure 24.
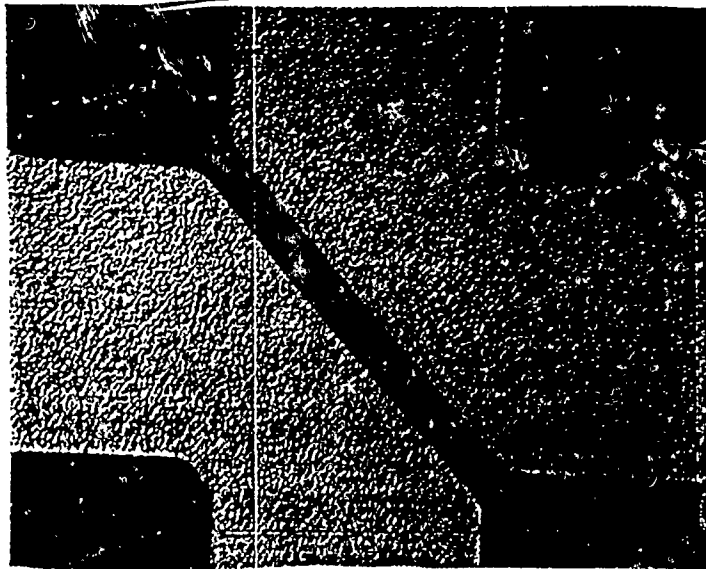
Figure 23. Micrograph of ion-milled Tl film using Ar ion beam milling.

2.4GHz Microstrip Resonators Fabricated by Ion Milling
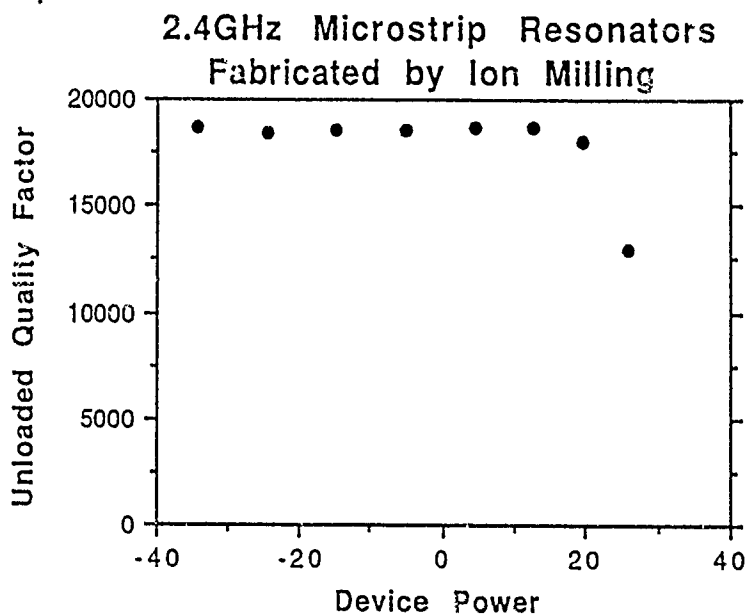
Figure 24. Unloaded quality factors for 2.3 GHz microstrip resonators fabricated by Ar ion milling.

Lift off

As an alternative patterning process, we investigated the possibility of using a lift off technique in order to improve our ability to pattern very fine lines out of the thallium superconductor. Our standard process described previously uses a dilute HCl etch to pattern the film. The etch undercuts the photoresist by approximately 5-10 μm because of the anisotropic nature of the etch, making it virtually impossible to pattern lines narrower than 10 μm or to control

27

the precise feature size to less than ±2-3 μm. Precise control of the feature size is crucial for many microwave devices in order to achieve the designed performance. Our ELF process allows us to employ a lift off technique, commonly used in the semiconductor industry, to define very narrow (<< 1 μm) lines. The photoresist is applied to the substrate prior to deposition of the precursor. The photoresist is treated with chlorobenzene so that the edge profile will have a certain shape to aid lift off (see Figure 25). After deposition the photoresist is removed together with the unwanted film. The film is heat-treated in our ELF process to form the superconducting phase. We have demonstrated, as shown in Figure 27, that this process has no detrimental effects on the microwave properties of the HTS film. Using the lift off process, we have demonstrated patterning of 5 μm lines, with a precision of less than ±1μm limited only by the photolithographic mask.
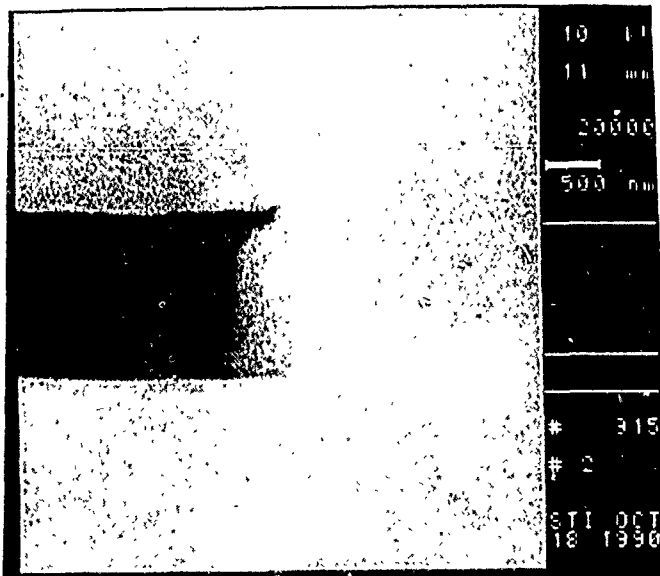
Figure 25. Photo of photoresist edge profile.
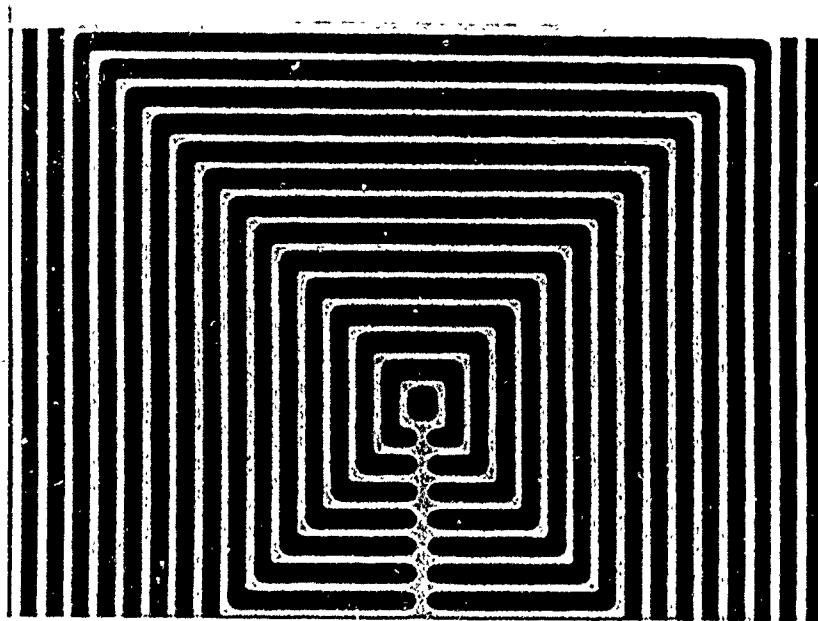
Figure 26. Photo of Narrow line pattern produced by lift off.

Film no. 2L663.3, 2.5GHz resonator
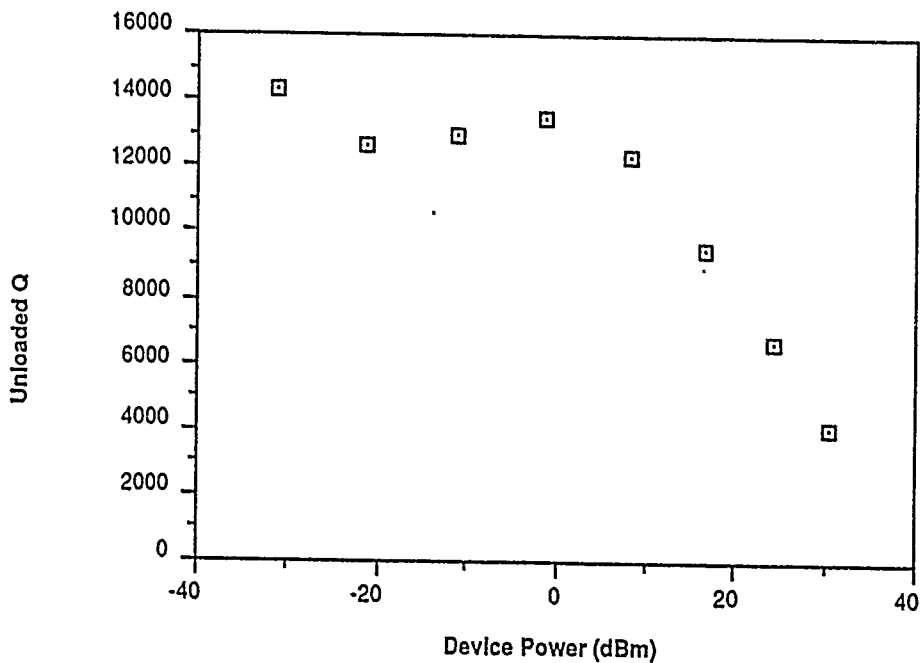
Figure 27. Q values as function of power for a 2.3 GHz resonator fabricated by lift off.

Ohmic contact process

A significant effort was spent on finding an ohmic contact process. A metal contact process is necessary in order to interface with any non-superconducting circuitry. Key requirements for a contact process are: (i) very low DC contact resistance to prevent heat generation at the contact pad , (ii) good adhesion so that conventional wire bonding apparatus can be utilized, (iii) low RF loss in order to take advantage of the low loss properties of the HTS circuitry, and (iv) use of a non corrosive metal scheme in order to prevent degradation of contact and/or HTS film.

Early in this program we demonstrated relatively low loss contacts by simply depositing a noble metal, such as Au, directly on to the HTS film. These contacts however had very poor adhesion, and it was essentially impossible to wirebond to these contacts. Adhesion could be dramatically improved by using an adhesion layer such as Ti or Cr. It was found, however, that these metals had a reducing effect on the thallium film surface forming a thin insulating layer between the metal and superconductor and thereby causing very high ($\approx$ 1-10 ohm*cm^2) contact resistance. Two processes were developed to overcome these problems. We are currently utilizing the single step process for most of our contact needs. Recently the two step process has been used for high power microwave applications where gap welding must be used in place of wire bonding.

Two step ohmic contact process

The first process we developed is based on a two-step metallization. Initially the thallium superconductor is coated with a thin (2000 Å) layer of gold; this contact has an excellent contact resistance, typically $\approx 1 \times 10^{-5}$ ohm*cm^2, but it has a relatively poor adhesion not as suitable for wire bonding. Secondly a layer of TiW followed by 5000 Å of gold is deposited over the first gold layer extended out over the LaAlO$_3$ substrate, assuring that the TiW/Au does not contact the superconductor (see Figure 28). The TiW/Au film has excellent adhesion to the LaAlO$_3$ substrate and can be wire bonded with excellent bond-pull strength (> 10 grams). The drawback of this process is, however, that it requires two separate mask levels, one to define the gold on the superconductor and the other to define the TiW/Au.
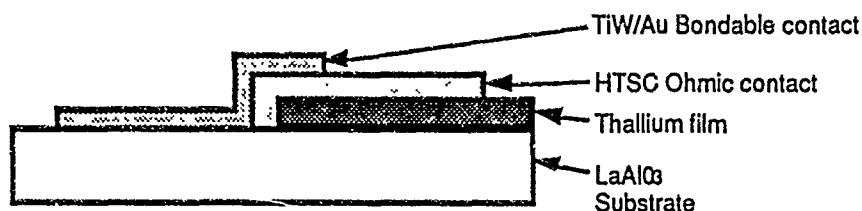
Figure 28. Cross-section of TiW/Au gold contact.

Single step Br-Au process

   The second approach that we investigated is a single step process directly on the superconductor. The superconductor is first treated with a Bromine etch to remove a few hundred Angstroms of material from the surface; immediately after this etch, a 7000 Å gold film is deposited by sputtering. The gold is patterned using conventional photoresist and a gold etch. We have demonstrated reproducible contact resistance $< 1 \times 10^{-5}$ ohm*cm^2 and bond-pull strengths > 5 grams using this process. We also demonstrated that this process has no detrimental effect on the microwave properties of the HTS films.

OHMIC CONTACT PROCESS

Bromine Etch

Thallium film
LaAlO3 Substrate

Sputter Deposit Au

Au film
Thallium film
LaAlO3 Substrate
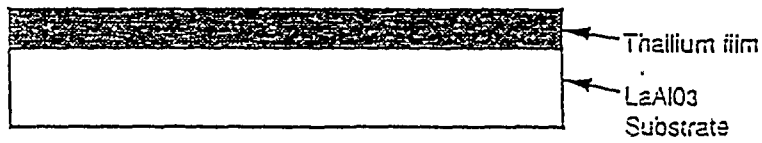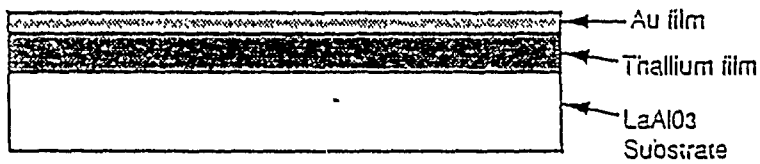
Define Contact with Photoresist

Au film
Thallium film
LaAlO3 Substrate
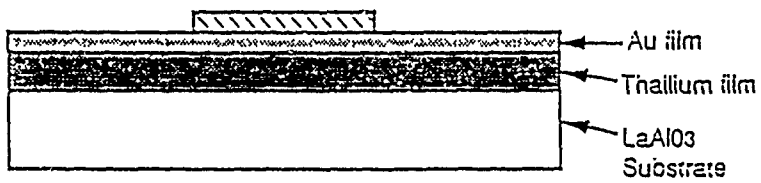
Etch Au and Remove Resist

Au contact
Thallium film
LaAlO3 Substrate
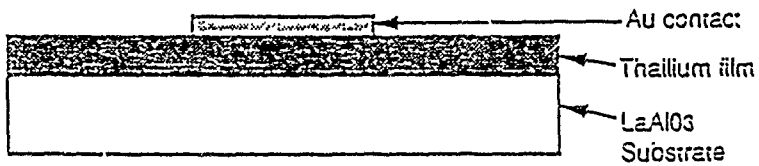
Figure 29. Process flow for single step ohmic contact process.
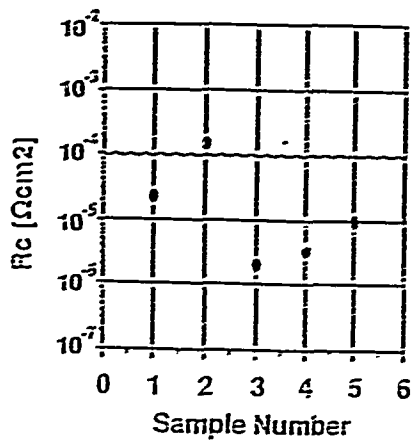
Figure 30. Contact resistance from five sequential 2" wafers.
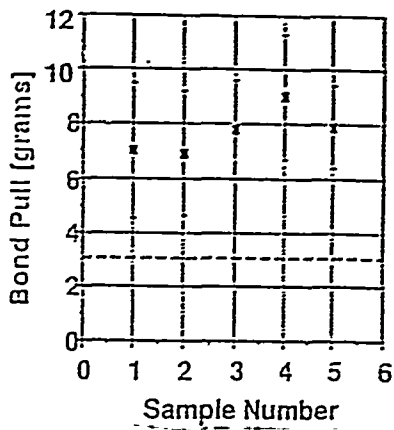
Figure 31. Bondpull strength measurement from five sequential 2" wafers.
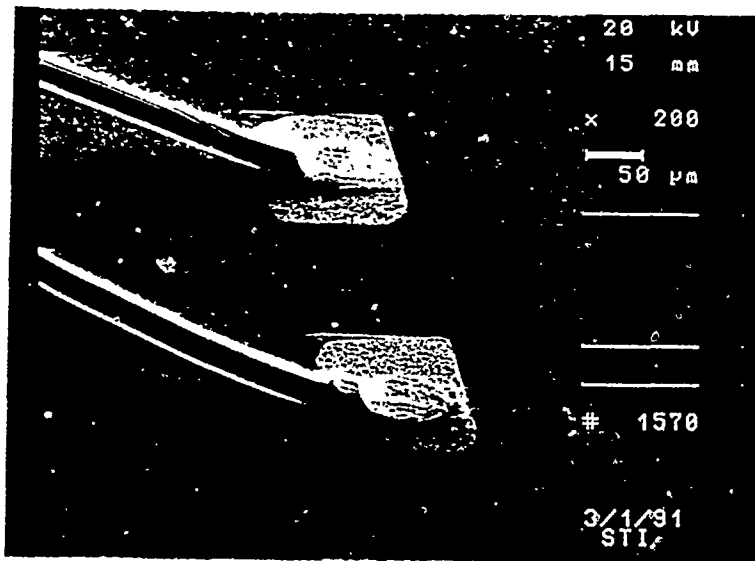
Figure 32. Photo of wire bonded contacts on HTS film.

33

In order to evaluate the RF loss of our contacts, a special test structure was developed. The structure was designed to have a measurement sensitivity of 0.01 dB per contact, which was the targeted loss for our contact process. The test structure consists of 125 series connected Au-to-HTS ohmic contacts (see Figure 33). Loss measurements were performed from 0.5 to 10 GHz. As seen in Figure 34, the RF loss was ≤ 0.01dB per contact at 77K.
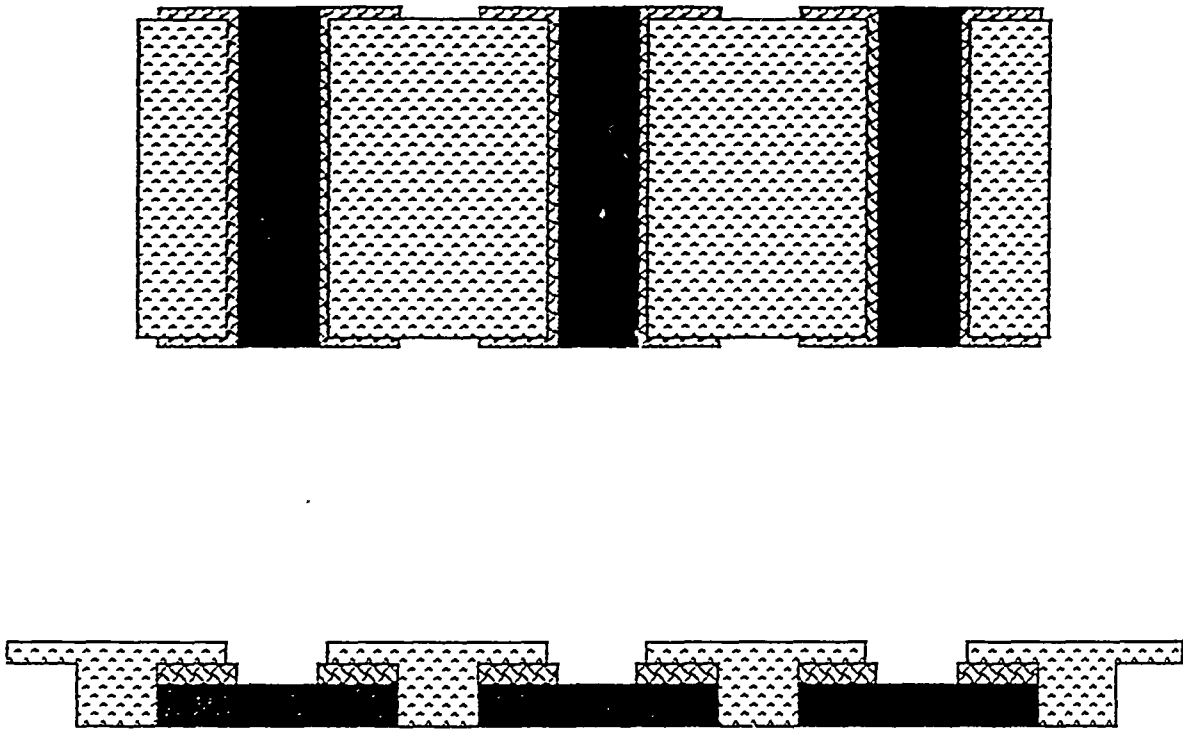
Throughline consists of 125 ohmic contacts
connected by gold bridges

Sputtered and etched 7000 A Au (ohmic contacts)

Bromine etched HTSC

Evaporated gold -- 3 microns

Figure 33. Schematic diagram of contact resistance test structure.
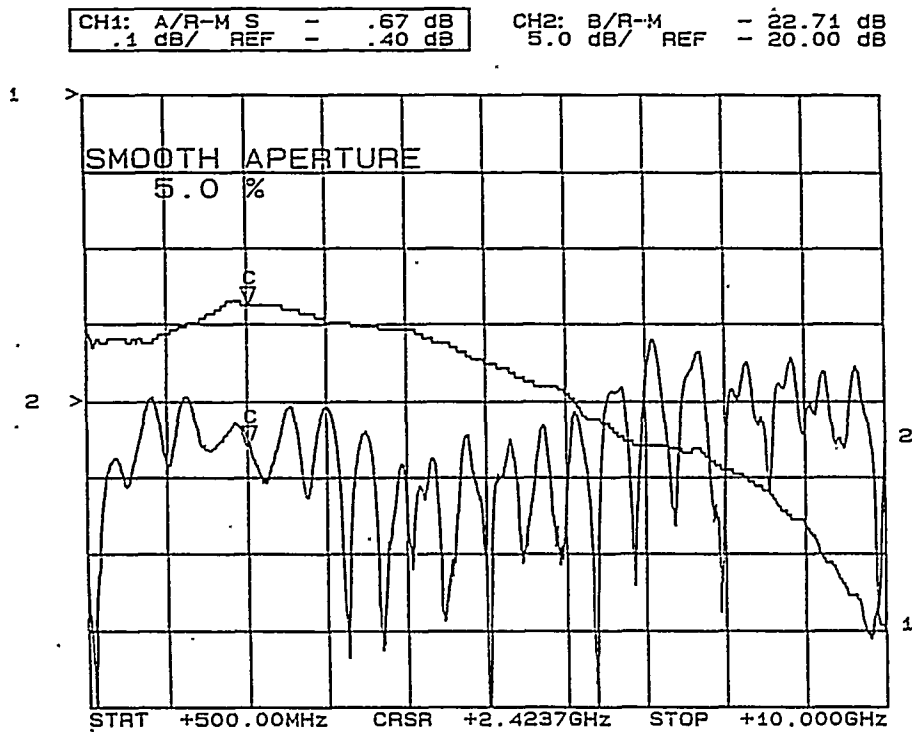
Figure 34. Plot of measured insertion loss on 125 HTS to Au contacts in series.

Ground plane metallization

Efforts to improve our ability to design passive microwave devices have emphasized the need for processing double sided films. This requires developing device fabrication processes for patterning and metallization on two sided HTS films. One key process we developed involves depositing 3μm thick gold metallizations on the back side of single sided films. The film is first cleaned by soaking in boiling toluene for 10 minutes followed by rinsing with acetone, methanol and isopropanol. This solvent clean serves to remove organic contamination from the surface. The films are then baked at 140°C for 30 minutes prior to metallization. Gold metallizations are deposited by thermal evaporation at a background pressure of $8*10^{-6}$ torr. A sputter deposited Ti/W buffer layer is used to attain excellent adhesion of the gold on $LaAlO_3$. Gold deposition rates are monitored *in-situ* using a quartz crystal.

Process development experiments have demonstrated our ability to deposit 3 microns of gold on the back and sides of thallium films in high yield. Measurement of the T_c, ΔT_c and microwave device performance of films before and after processing have shown no indication of degradation during processing.

35

Polyimide process

Another major emphasis in our device fabrication program was the development of a polyimide passivation and dielectric technology. We have developed a process based on pre-imidized photosensitive polyimide. The polyimide is applied by conventional spin on technology to a 0.5-10 μm thickness range. Figure 35 shows a SEM micrograph of an opening patterned in 3μm thick polyimide.
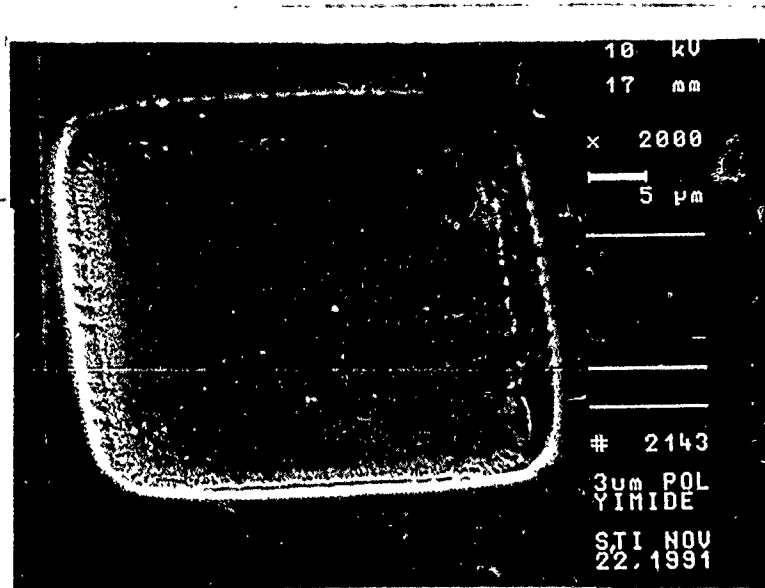
Figure 35. SEM micrograph of an opening patterned in 3μm thick polyimide.

We have made careful measurements of the microwave loss introduced by the polyimide process; as yet we have seen no additional losses. This data is summarized in Figure 36. No increase in loss is seen at 5.6 GHz or 16.5 GHz and 77K. We also performed a thermal stability study of polyimide-coated superconductors indicating that there is no degradation of the microwave surface resistance in the superconductor when heated at 200°C for 10 minutes and only a very slight degradation after 1 hour at 200°C. The data from these tests are summarized in Figure 37.

1L853.6 3µm Polyimide 15 min 110C
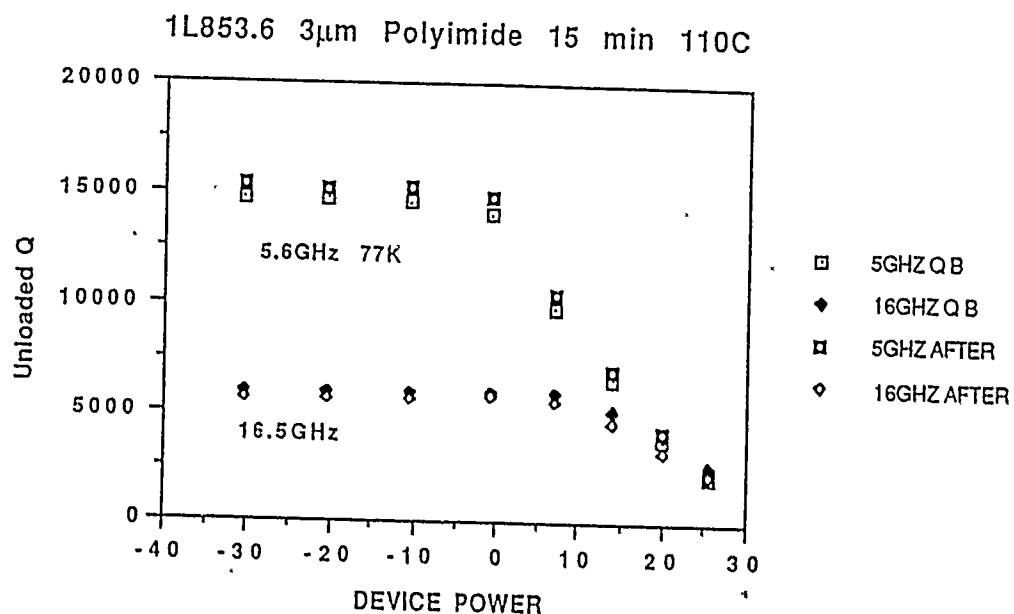
Figure 36. Resonator data before and after polyimide coating.

1L853.6   Polyimide Processing Expt
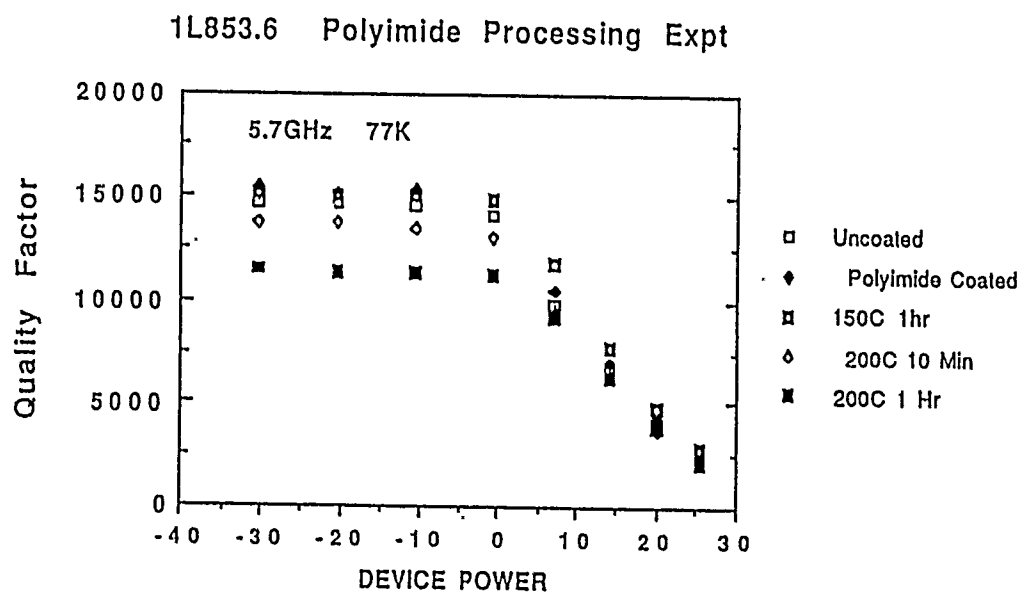
Figure 37. Thermal stability of resonator with polyimide coating.

The polyimide is very useful as passivation layer, protecting the underlying HTS film from degradation. We have tested the ability of polyimide coatings to survive repeated cycling to 77K by rapid immersion directly in liquid nitrogen followed by warming in ambient air. Data in Figure 38 show that a polyimide coated resonator suffered no degradation in Q after 50 temperature cycles

37

in liquid nitrogen. Also, the polyimide still p₁ ovided a hermetic seal for the superconducting film. This was demonstrated by dipping the device in HCl, an extremely effective HTS etch. The film was intact after exposure to the acid.
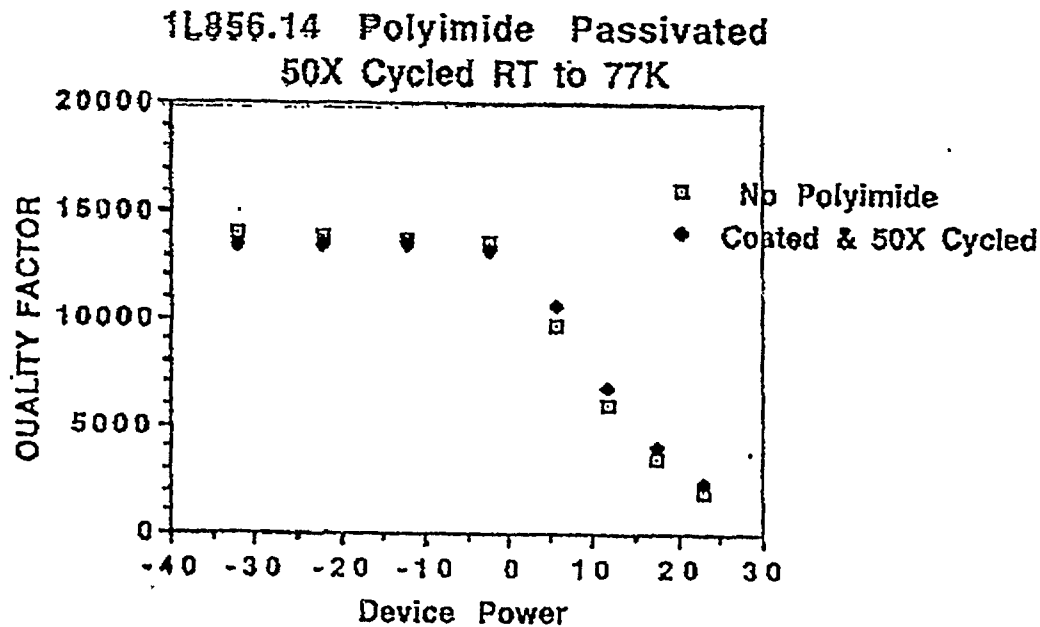
Figure 38. Polyimide coated resonator before and after 50× temperature cycling.

Polyimide can also be used in conjunction with our contact process and a second metal film (TiW/Au ≈3μm) to form cross overs. This is of particular importance for devices designed in a coplanar geometry where frequent ground connections are required. The process flow for the polyimide based cross over process is shown Figure 39. Early on we fabricated coplanar delay lines which contained more than 200 gold bridge crossings over superconducting lines without a single short (see Figure 40). This technology was later extended to a 29 ns delay line which contained in excess of 2000 cross overs without a single short between the ground plane and the center-conductor (see Figure 42). The polyimide/Au crossover allows excellent low resistance contact to the superconducting ground planes and low resistance connection between them. This process has been extensively utilized at STI in fabricating a wide variety of microwave devices; a few examples are shown in Figures 43-44.

38
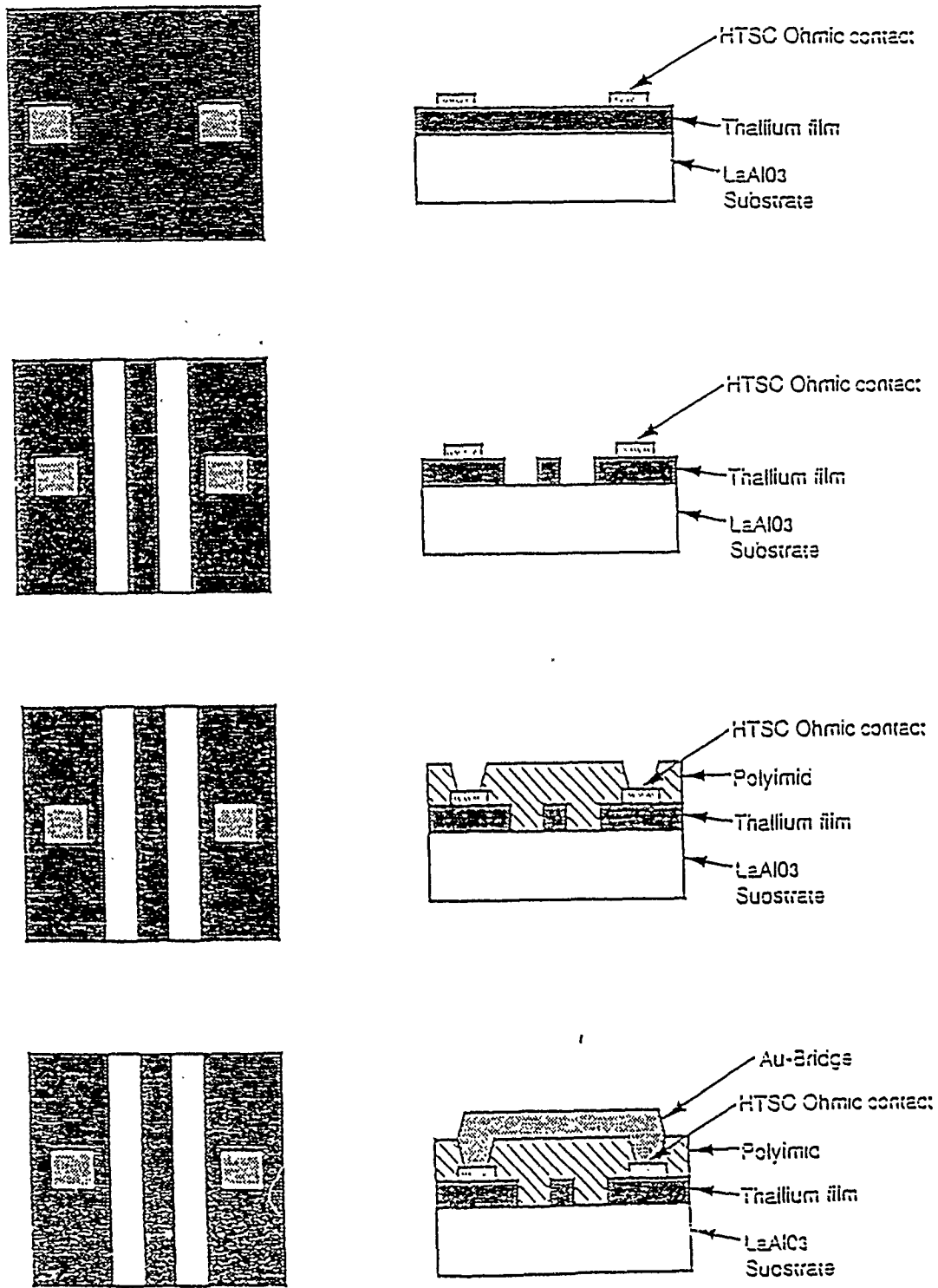
Figure 39. Process flow for Au cross over process.
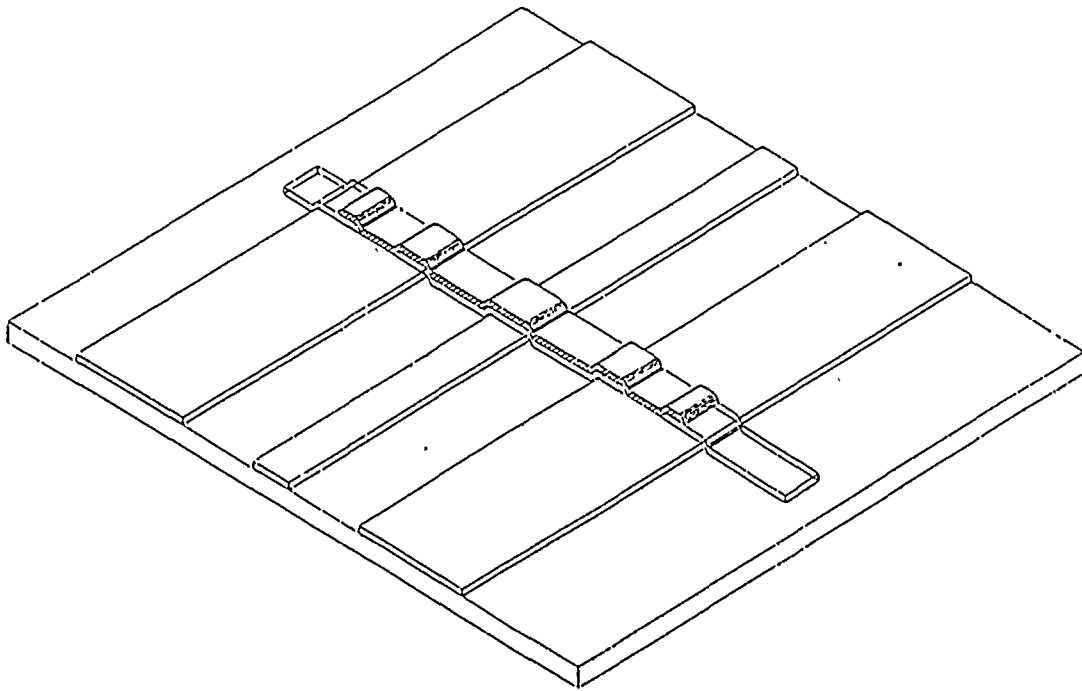
Figure 40. Conceptual drawing of single crossover.
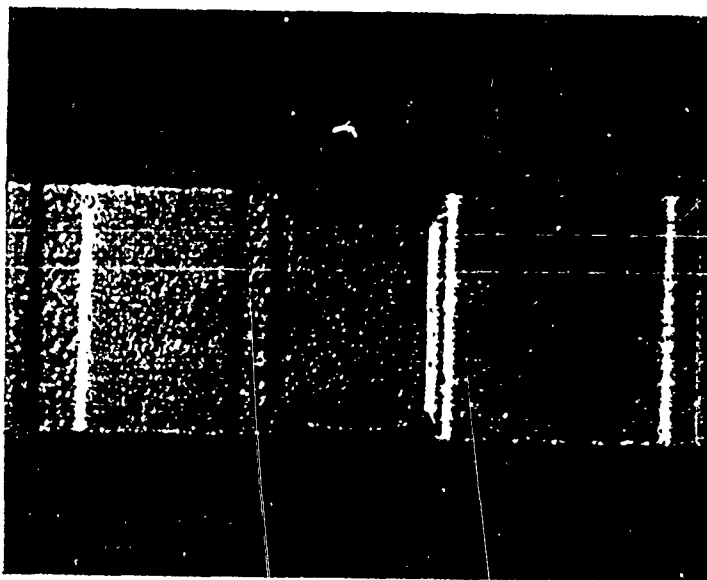
Figure 41. SEM micrograph of completed crossover.
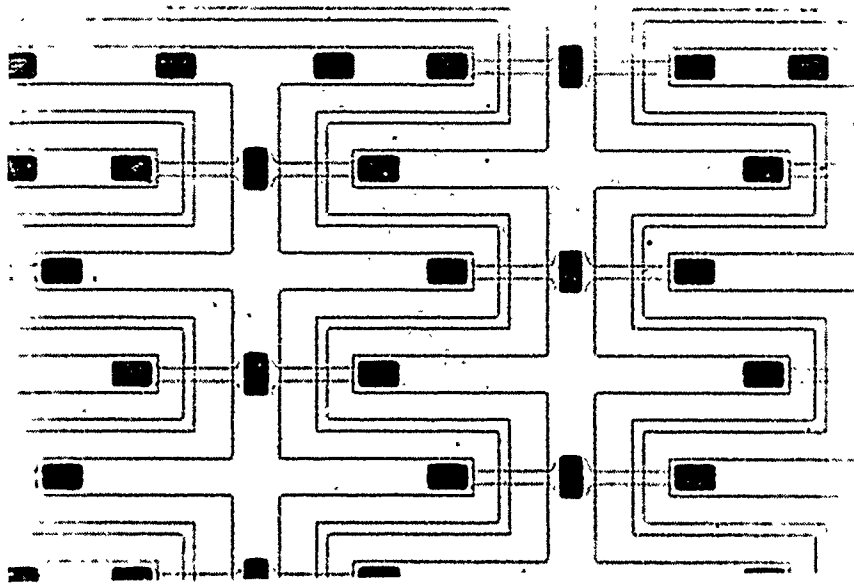
Figure 42. Detail of 29 ns co-planar delay line showing polyimide based Au cross overs.
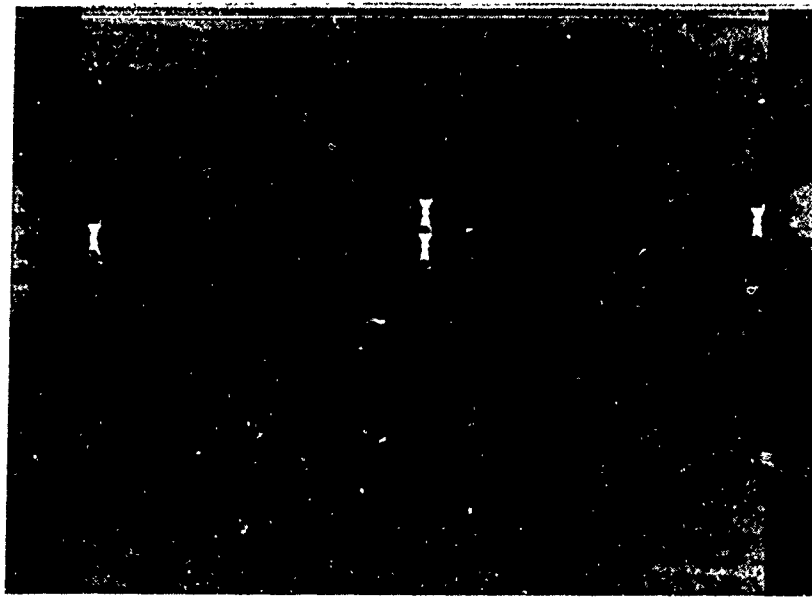
Figure 43. Photo of microwave Lang coupler utilizing polyimide/Au cross overs.
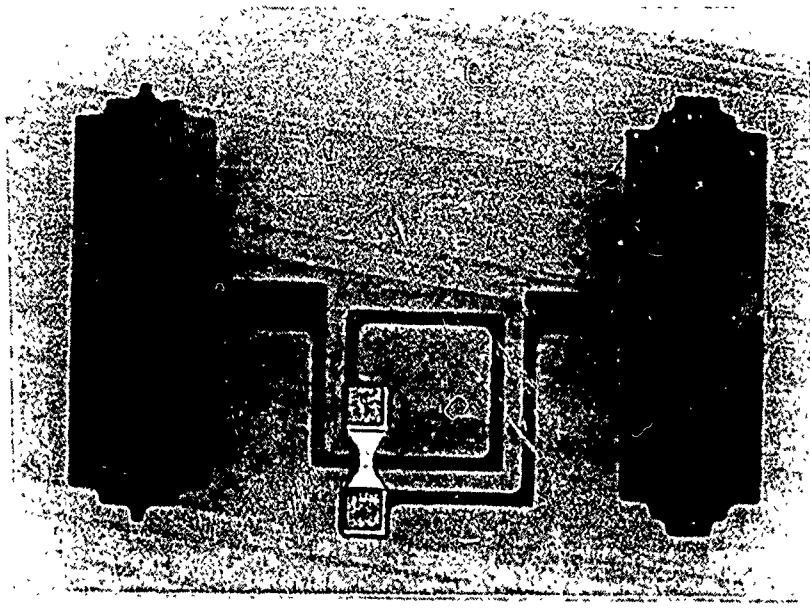
Figure 44. Photo of Lumped element filter with cross overs on the inductors.

Dicing process

In order to fabricate devices from our 2" diameter process, a dicing process for LaAlO₃ substrates had to be developed. We found that LaAlO₃ has a severe edge chipping problem when conventional diamond sawing is used. By mounting the HTS coated LaAlO₃ substrates to a larger Si-wafer during the dicing step the edge chipping was reduced to less than 100 μm from the edge.

Microwave Device Development

During the course of this program we developed a variety of thin film microwave devices utilizing our thallium thin films and fabrication processes. These devices included a number of different resonators, bandpass filters, bandreject filters, couplers, and a resonator stabilized oscillator.

Microwave Resonators

The basic resonator structure that we used during this program was based on the microstrip transmission line geometry. We have made devices with both single sided and double sided thin films. The double sided films have allowed us to use a conventional structure for these devices. Single sided films have been made into resonators using separate films for the center conductor and ground plane. Figure 45 shows a schematic diagram of the microstrip resonator structure used with single sided films. This structure was used for all the resonators discussed here except where specifically noted otherwise.

42

GOLD
CONTACT

PATTERNED
HTSC FILM

LaAlO3
SUBSTRATE

HTSC
GROUND
PLANE

WRAP-AROUND
GOLD
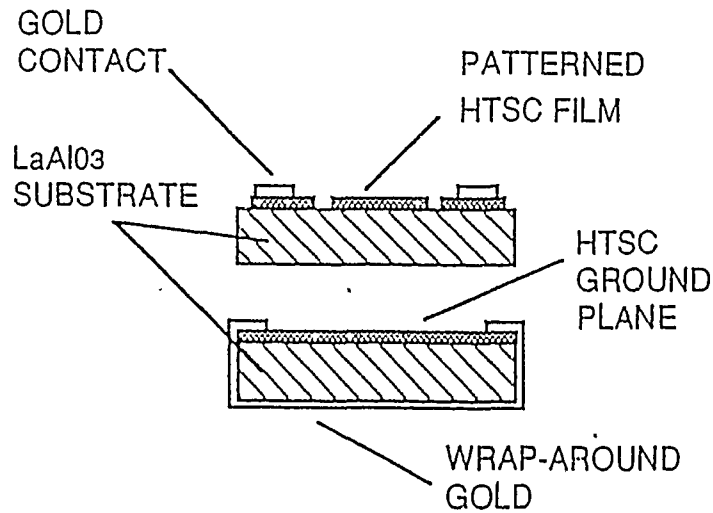
Figure 45. Schematic diagram of microstrip resonator structure. Two thallium films are used to form the resonant structure.

We developed a simple resonant structure that has yielded the highest Qs we are aware of in an all-thin-film device at 77K. This microstrip resonator was fabricated on 20-mil thick LaAlO3 substrates. The center conductor is a strip 1 mm × 7 mm. Figure 46 shows the measured unloaded Q as a function of device power at 77K of one of these devices. The device shows extremely high Q and also superior power handling. We have used a similar device to stabilize a very low noise oscillator. This is described in a later section.
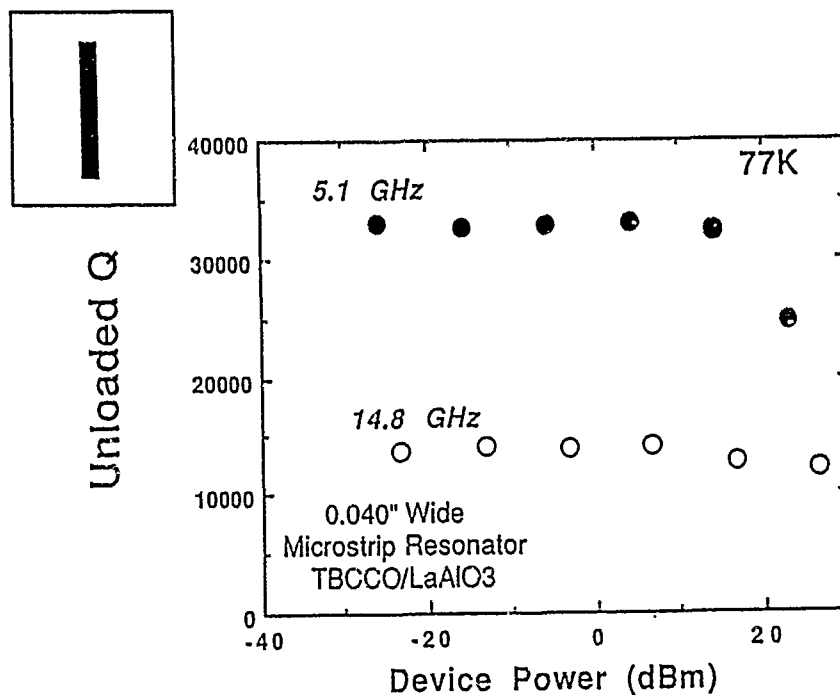
Figure 46. Unloaded Q vs. device power on a microstrip resonator made with two thallium films. The inset shows a schematic diagram of the resonator itself.

We developed another simple resonator to use primarily as a diagnostic of thin film surface resistance. The microstrip resonator is an ideal structure to determine thin film surface resistance because it has high sensitivity; power and temperature dependent measurements of surface resistance can be made easily. Furthermore, the structure is the same microwave structure that will be used in most applications. Using the same structure as described above, with a narrower center conductor line, we developed a sensitive and versatile thin film diagnostic structure. The resonator dimension used was 0.15 mm × 7 mm. Figure 47 shows the measured surface resistance plotted vs. peak power at 77K. The data are scaled to 10 GHz (assuming frequency squared dependence) for ease of comparison with other measurements. At the low power levels the surface resistance is 200 micro-ohms. This is the lowest surface resistance ever measured in a microwave resonator at 77K. In addition, the power handling is excellent for such a narrow center conductor. Figure 48 shows the surface resistance at low power inferred from the Q of the first three harmonic resonances of this resonator. The values measured follow the frequency squared dependence expected in a superconductor. Also they are dramatically lower than the best normal metal, OFHC Cu, as shown in the graph.
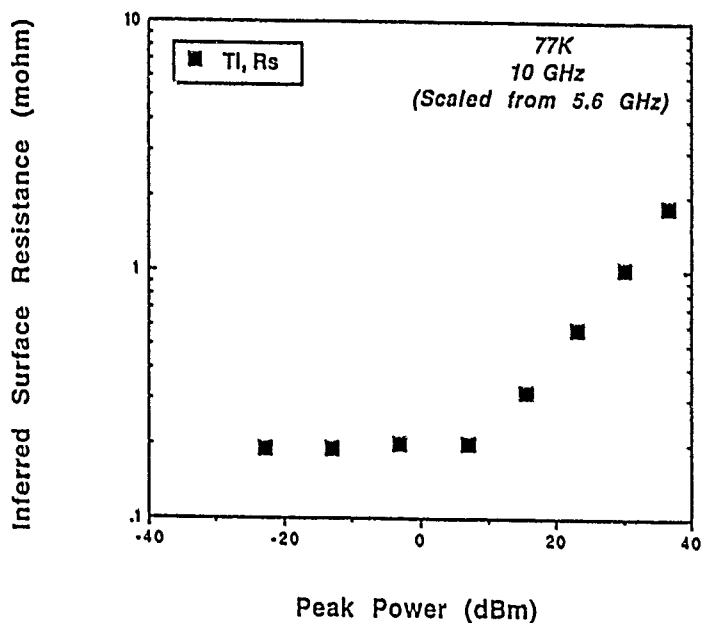
Figure 47. Surface resistance vs. peak device power at 77K in a thallium film microstrip resonator.
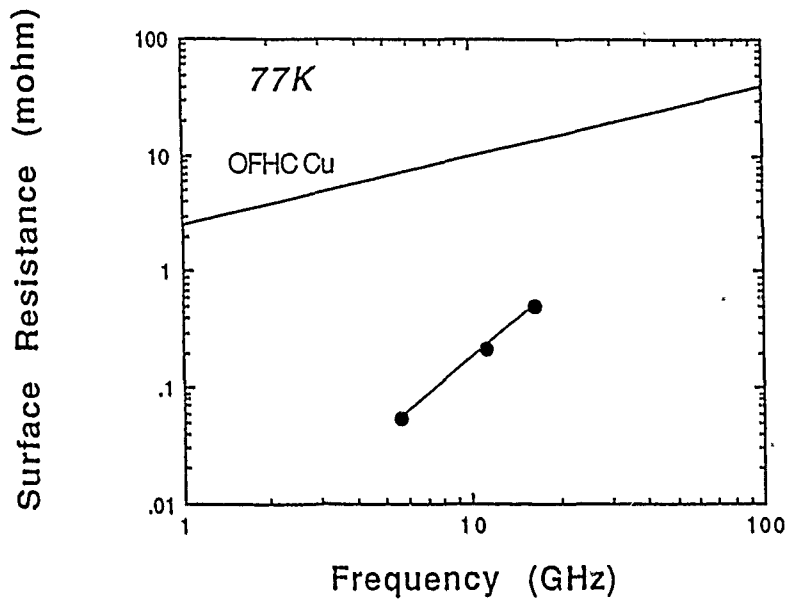
Figure 48. Surface resistance at low power as a function of frequency at 77K for the same microstrip resonator as described in Figure 47.

NRL HTSSE resonators

During the time period covered in this program we completed an effort producing microstrip resonators for the Naval Research Laboratory's High Temperature Superconductivity Space Experiment (HTSSE). This work, of course, was able to leverage on the work performed under this DARPA contract on thallium films and microwave devices. Figure 49 shows the layout of the microstrip resonator that we built for the NRL HTSSE program. It was an end-coupled device with a fundamental resonance at 4.8 GHz, and was designed to have a Q greater than 5,000 and an insertion loss of approximately 20 dB.
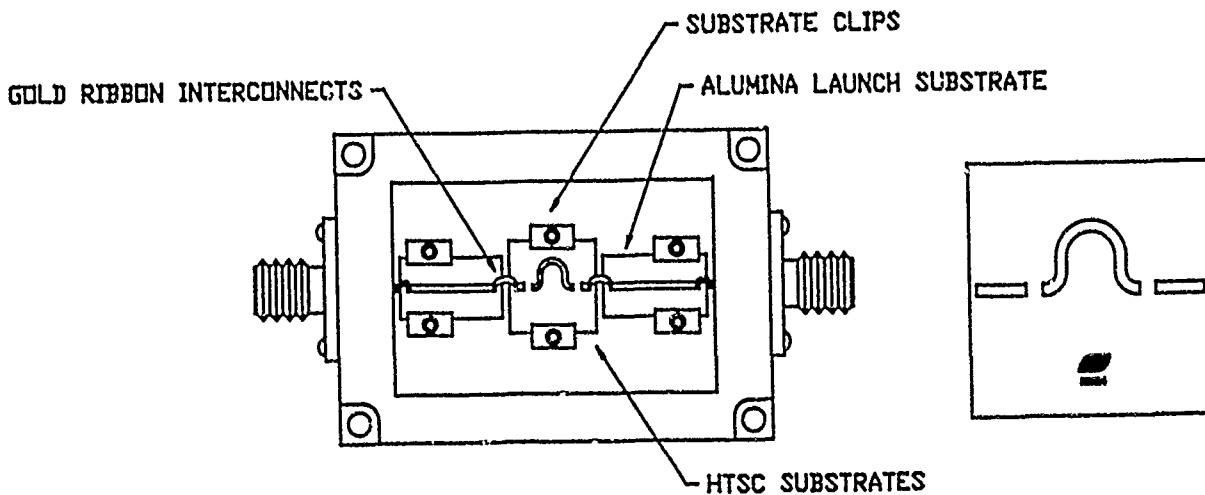
Figure 49. Layout of 4.8 GHz resonator and schematic diagram of the packaged device.

Since components for HTSSE had to be stored in uncontrolled environments for 1-2 years, we developed a hermetic package to protect the films for the required shelf life. The package, also shown in Figure 49, uses glass-to-metal seals for the microwave transitions into the package, and the top is laser welded. We delivered five of these devices to NRL. Each passed multiple temperature cycling tests and careful leak checking before shipment.

Figures 50 and 51 show the broad band insertion loss spectrum and the power dependent Qs at 77K measured on one of these devices. The device showed excellent performance at both its fundamental resonance at 4.8 GHz and its second resonance at 9.1 GHz, far surpassing an equivalent gold device. Figure 52 shows the data taken by NRL on this device after they received it. Their measurements agree very well with our measurements, and show the excellent performance of the device.
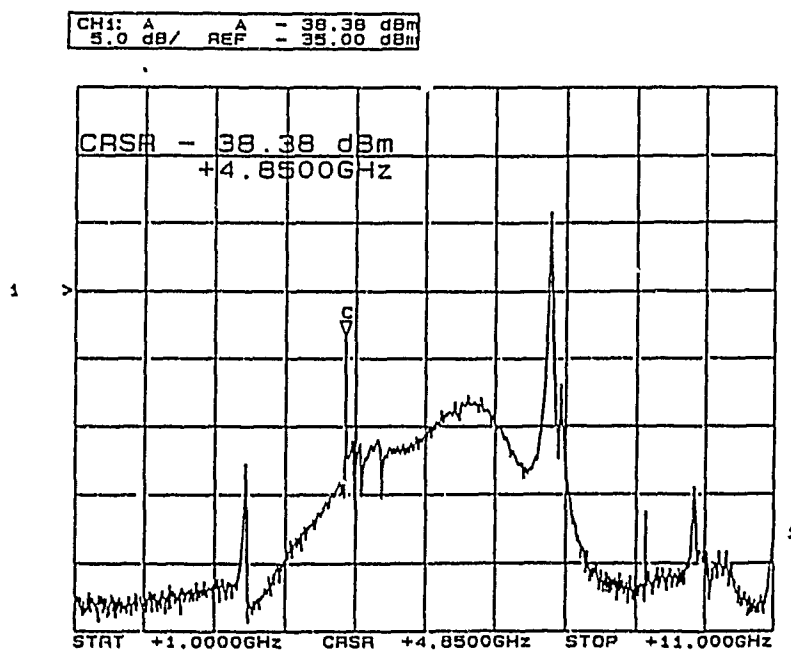
Figure 50. Broadband insertion loss measured on 4.8 GHz resonator.

MRG-1-01 S/N 006 (NRL HTSSE)
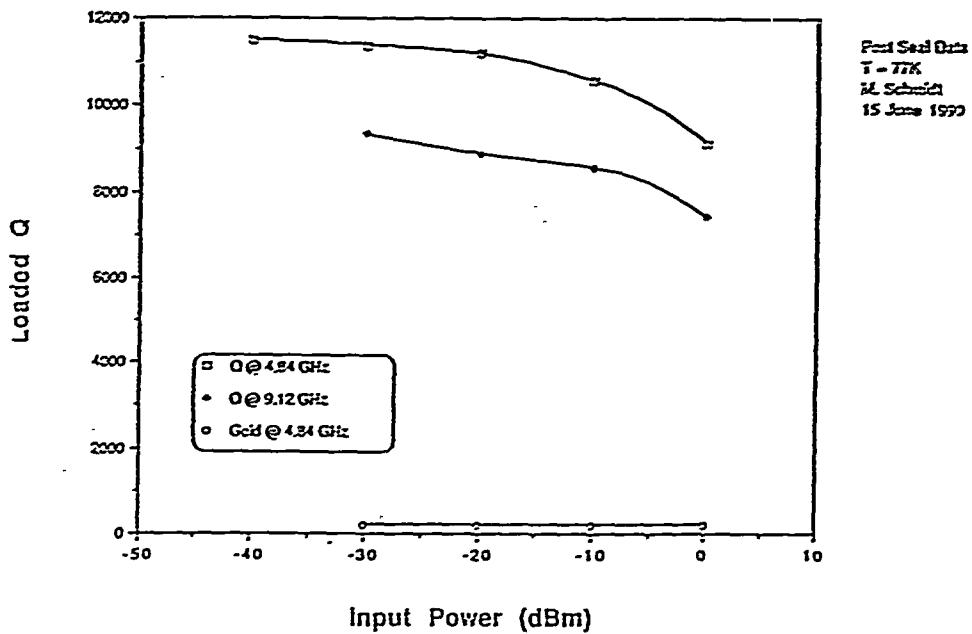
Figure 51. Power dependence of 4.8 GHz resonator.

STI - Model Number: MRG-1-01, S/N: 006
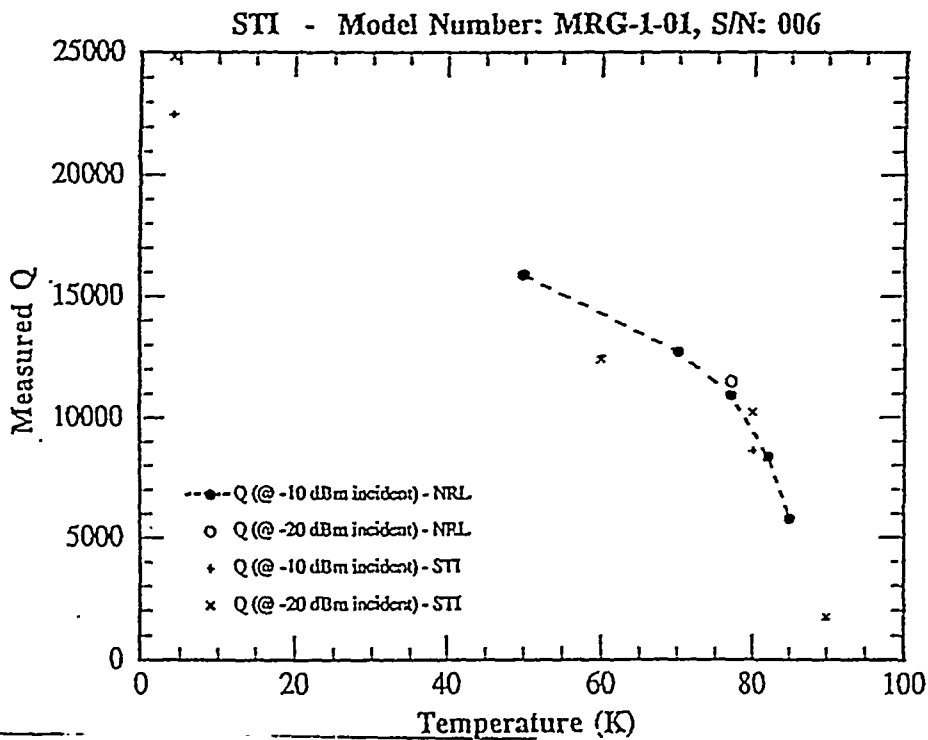
Figure 52. Power dependence measured by NRL on resonator shown in Figure 51.

47

To measure the microwave properties of HTS thin films at millimeter wave frequencies, we developed a microstrip ring resonator. The outer diameter of the ring was 0.044" and the linewidth was 0.006". We varied the input and output capacitive coupling gaps from 0.005 to 0.020", and performed measurements using the third harmonic response of the ring resonator at 35 GHz. The substrates were $LaAlO_3$, 1.0 cm × 1.0 cm × 0.010" thick. Three types of resonators were tested: an all gold resonator, an HTS center conductor with gold ground plane, and an all-HTS resonator. The resonators were mounted in a test package with APC-2.4 connectors. For the fully superconducting resonators, a patterned HTS resonator was stacked on top of an HTS ground plane, with gold wrap-arounds providing a ground connection to the package. Shown below are the test results at 77 K and -10 dBm input power for each of these 35 GHz resonators. Figure 53 shows the layout of the resonator and the insertion loss spectrum from 2 to 40 GHz.

Resonator Type	Insertion Loss	Loaded Q	Unloaded Q
All Gold	9.3 dB	360	550
HTS / Gold	8.6	900	1440
All HTS #1	18.8	2360	2670
All HTS #2	26.9	2610	2740
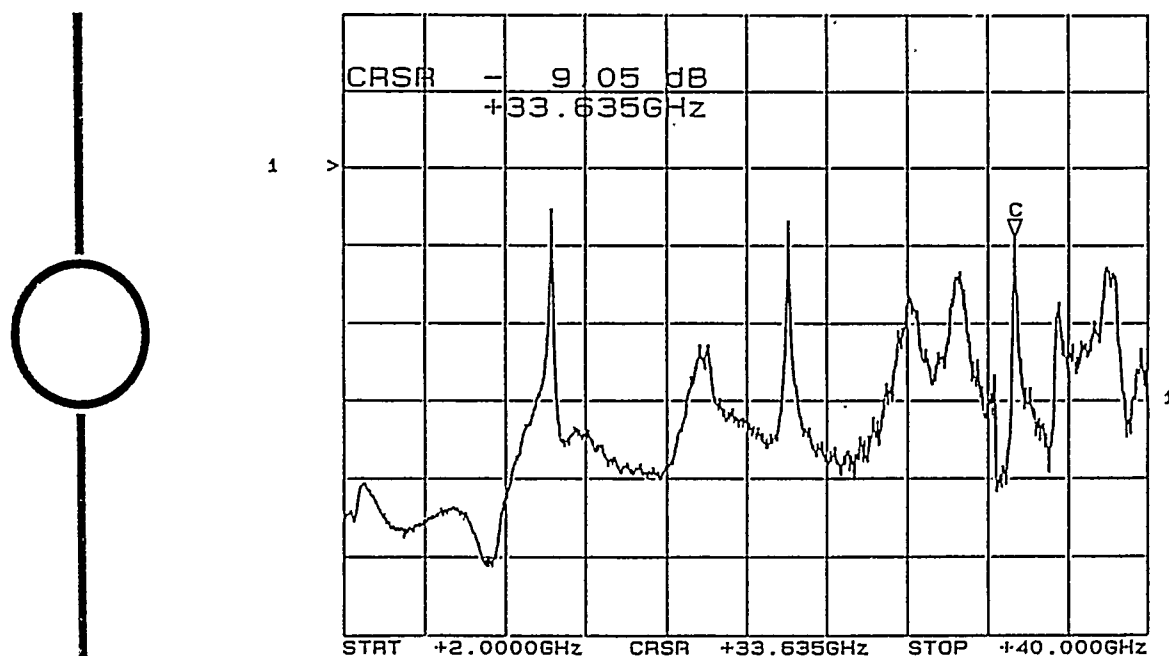
Figure 53. Diagram of layout and insertion loss spectrum for 33 GHz microstrip resonator.

The two all-HTS resonators were mounted in a cryostat and characterized over the 4K to 77K temperature range. Figure 54 shows the effect of temperature on the unloaded Q of the resonators. We extracted surface resistance of the superconducting films from the measured unloaded Qs using the Sonnet™ electromagnetic modeling program. We ignored the effect of loss in the substrate. At 77K the inferred surface resistance of the superconducting films was 6 mohms and at 4K it went down to 2 mohms. If we assume that the surface resistance of the superconductor is proportional to the square of the frequency, this extrapolates to $R_S = 0.5$ mohm at 10 GHz and 77K.

35 GHz Ring Resonator

•	2L653.3 / 1L843.2
o	2L657.7 / 1L843.3
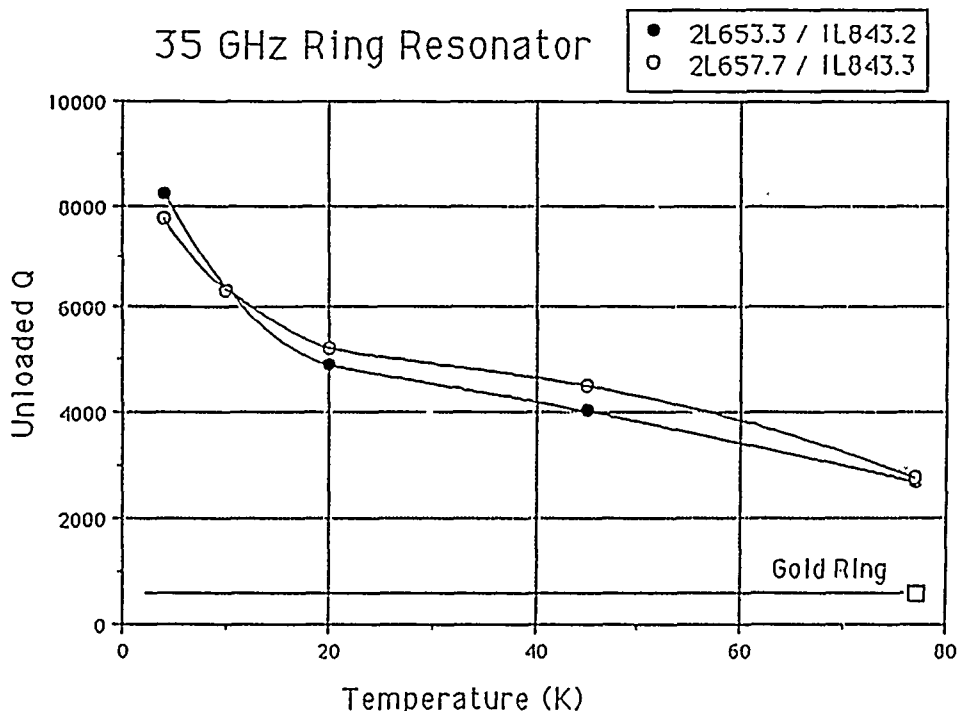
Figure 54. 35 GHz resonator Q vs. temperature.

Other resonator results

In a collaboration with Westinghouse Science and Technology Center in Pittsburgh, Pennsylvania, we demonstrated the highest resonator Q for an HTS thin film device. Figure 55 shows a schematic diagram of the sapphire/HTS resonator that has been developed by Westinghouse under a DARPA contract. The resonator uses a small cylinder of sapphire that is sandwiched between two large area thallium thin films. The fundamental resonance is at 10.5 GHz. This resonator produces a Q of 120,000 with Cu endplates at 77K. Westinghouse has measured Qs of 300,000 using YBCO films. Using STI Tl films they have achieved Qs of 660,000 at 77K, 10.5 GHz. This high Q has been their best result to date, and they believe that the Q is limited not by the HTS film, but rather by the styrofoam mounting material for the

49

sapphire puck. Tests have been completed to measure the ultimate noise reduction potential for resonators of this type used in stable oscillators for radar applications. Westinghouse has demonstrated the lowest noise ever measured at 10 GHz with this resonator employing STI thallium films.
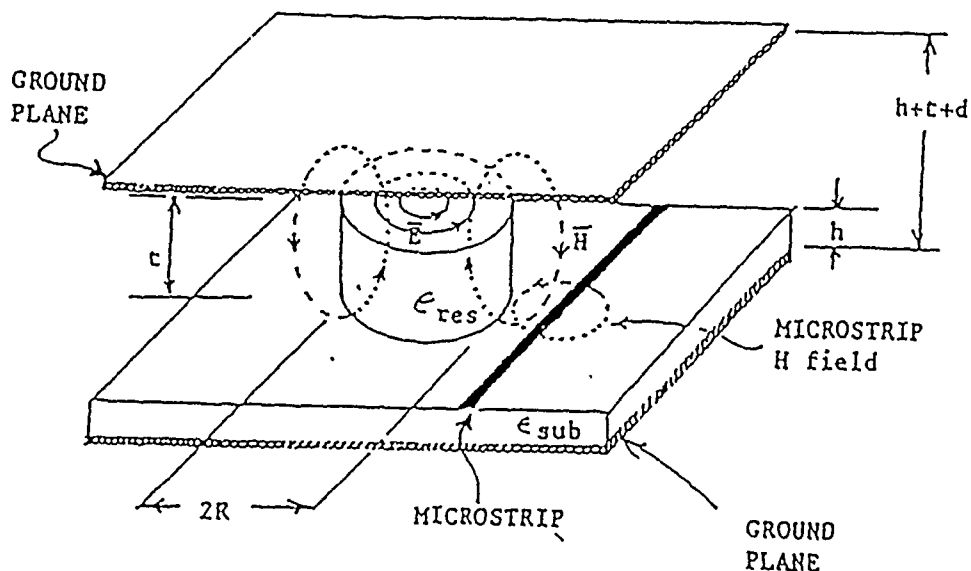
Figure 55. Schematic diagram of HTS/sapphire resonator designed by Westinghouse.

We have also developed novel lumped element resonant structure utilizing our thallium thin films. Figure 56 shows a schematic diagram of one such device. The resonator measures approximately 1 mm × 1 mm and is capacitively coupled as shown in the figure. It consists of two capacitative plates of thin film superconductor that are connected by a single inductive coil of thin film superconductor. This device produced a loaded Q of over 3,000 at 2.5 GHz at 77K. This structure fabricated in normal metal would have more than 100 times lower Q. These types of devices are forming the building blocks for extremely compact high performance filters as described in a later section.
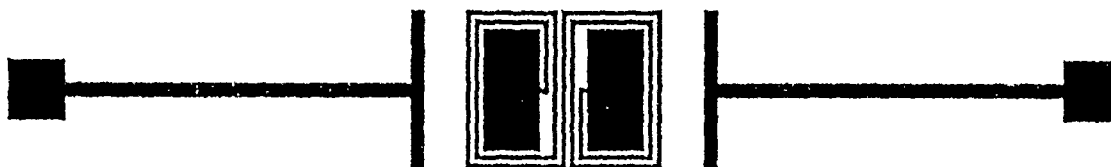
Figure 56. Schematic diagram of a thin film lumped element resonator.

Figure 57 shows unloaded Qs measured on a variety of STI microstrip resonators measured at 77K. The data span the frequency range from 2.3 to 33 GHz.

Microstrip Resonator Q's
Tl-Ca-Ba-Cu-O Thin Films
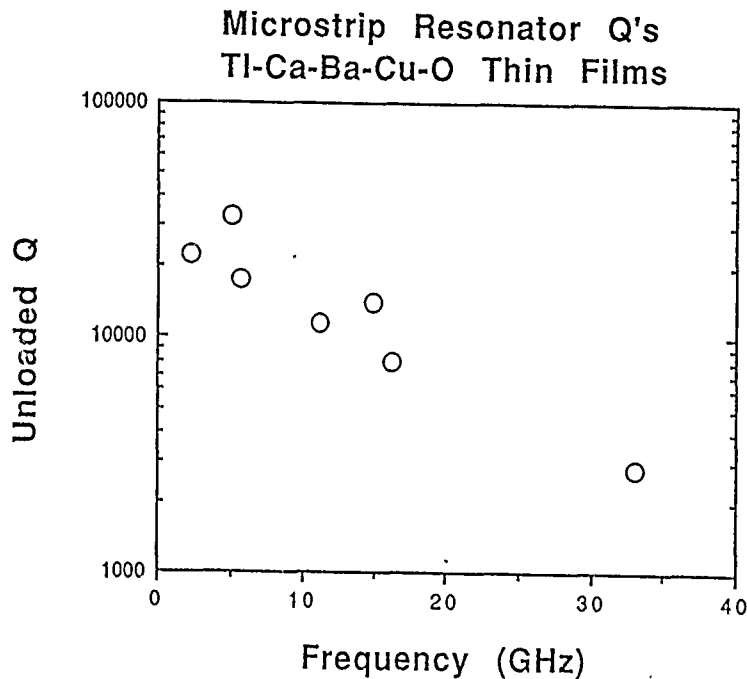
Figure 57. Measured unloaded Qs at 77K for a variety of microstrip resonators fabricated from thallium thin films.

10 GHz Bandpass Filters

During the course of this program we developed a number of thin film HTS bandpass filters. This is an important potential application for thin film high temperature superconductors. The promise of this technology is that filters can be developed that will meet and exceed the performance of waveguide filters that are bulky and expensive. Waveguide filters are currently used for the most demanding microwave filter requirements.

The first filter we developed was a straightforward coupled line microstrip geometry. The filter was designed to provide 10% bandpass at 10 GHz. It is a 4-pole design and implemented on a 1-cm square substrate. The layout of the filter is shown in Figure 58. Although designed to be centered at 10 GHz the filter actually had a center frequency of 9.1 GHz. This difference was due to the incorrect value of dielectric constant assumed for the lanthanum aluminate substrate. A dielectric constant of 20 was assumed using values found in the literature. Precise determination of the dielectric constant has given values of 23.4 at 10 GHz and 77K. Figure 59 shows the insertion loss spectrum of the filter measured at 77K. The filter shows a good shape, very close to the designed shape, with a midband insertion loss of 0.5 dB.
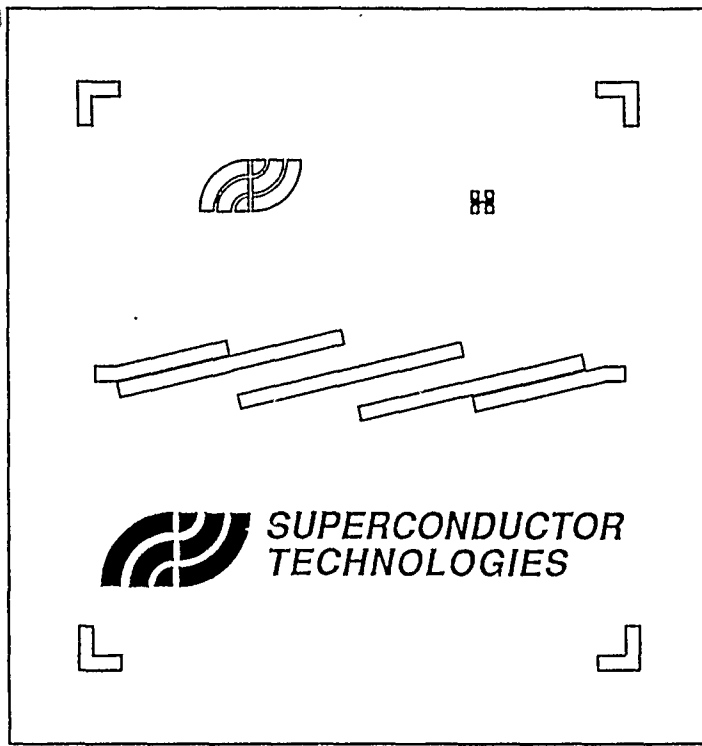
Figure 58. Layout for 10% bandpass filter at 10 GHz.
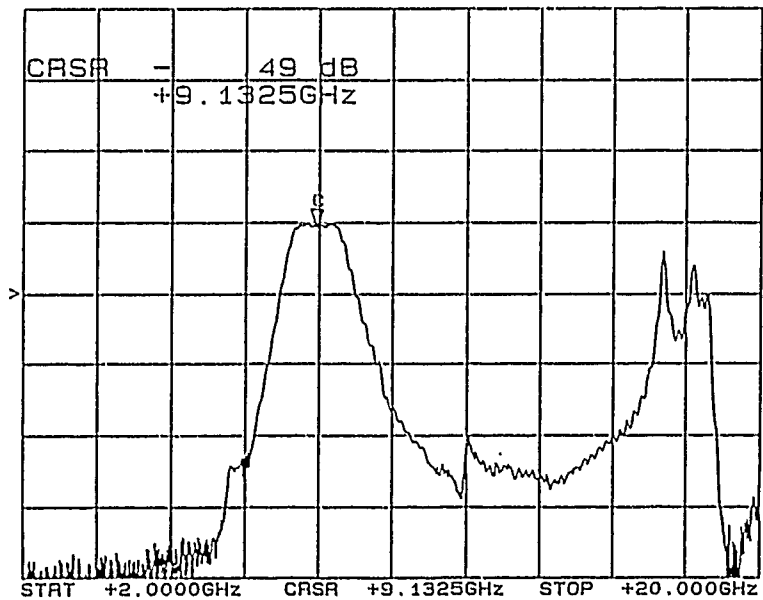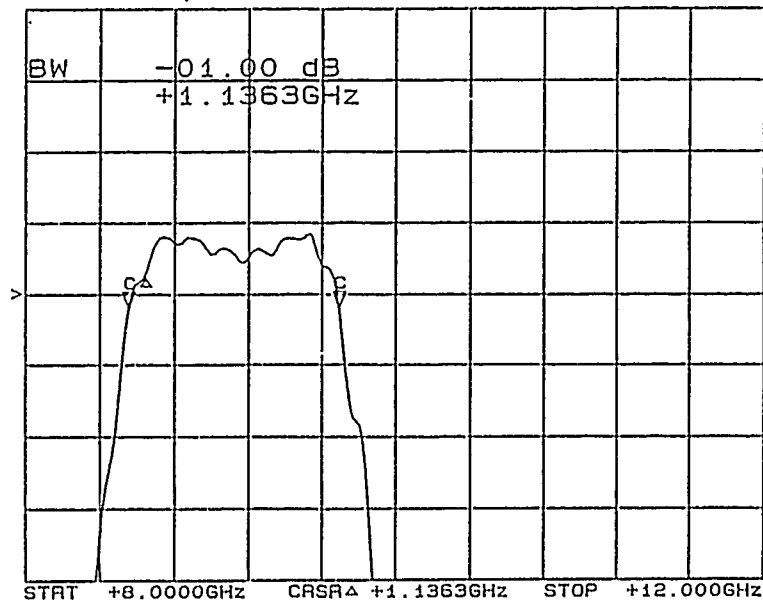
Figure 59. Narrowband and broadband insertion loss measurements at 77K on the filter shown in Figure 58.

A 5-pole interdigital HTS bandpass filter was designed and fabricated on a 1.00" × 0.25" LaAlO$_3$ substrate. The ground plane was 3.0 mm of sputtered gold, and the substrate thickness was 0.010". The filter was designed using proprietary software, and was verified by electromagnetic analysis using Sonnet Software's "em" program. The filter layout is a quasi-interdigital, parallel microstrip resonators.

53

Three filters were fabricated and mounted in aluminum housings with SMA connectors. The filters were fabricated simultaneously on the same 1" square LaAlO3 wafer. Each filter was tested separately at 82K and 0 dBm input power, using an HP8340 synthesized sweeper and an HP8757 Scalar Network Analyzer. Typical test results are summarized below.

Center Frequency:	10.10 GHz	1 dB Bandwidth:	430 MHz
Insertion Loss:	1.5 dB	Passband Ripple:	0.2 dB
VSWR:	< 2.0:1	Out of Band Rejection: at 500 MHz from CF	30 dB

Performance of the three filters tested was very consistent. Figure 60 compares passband response of the filters at 82K. Variations in bandwidth were less than 5%, and the center frequency error was less than 0.2%.

Comparision Of Filter Responses
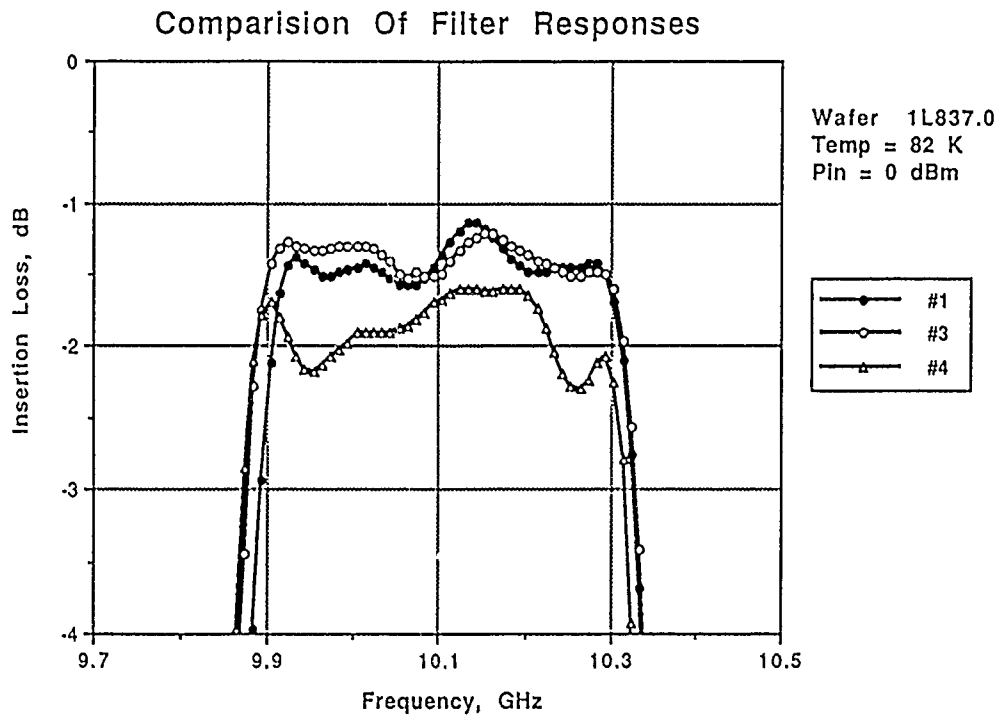
Figure 60. Repeatability of filters from single 2" wafer.

In addition, we developed other HTS microstrip filters. Figure 61 shows a 5-pole, 5 GHz bandpass filter. This filter shows excellent, flat in-band response with less than 1 dB insertion loss. Also the return loss in-band is greater than 15 dB. This is the cleanest HTS filter we have seen; however, since it is a 6% bandpass, it is not a particularly challenging demonstration for superconductor filters.
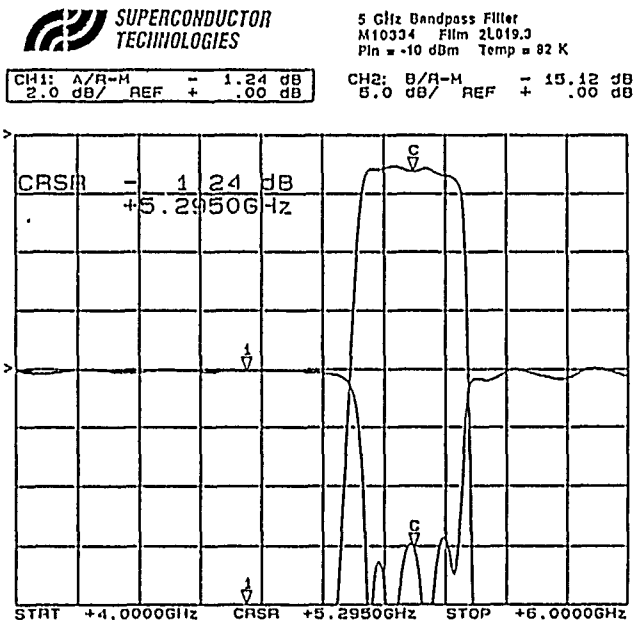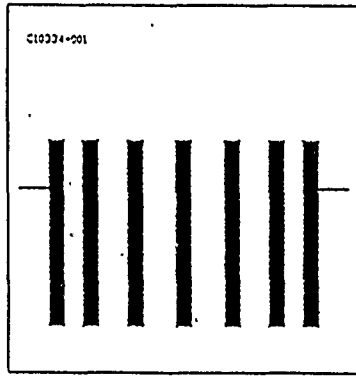
Figure 61. Structure and measured performance of 5 GHz pseudo-interdigital bandpass filter.

Figure 62 shows data on a 7-pole, 1.6% bandpass filter at 10 GHz. This filter also has less than 1 dB insertion loss. These data confirm the benefit of HTS for narrow passband filters with low insertion loss. However, the in-band ripple in both the insertion loss and the return loss prevent this from being useful for high performance applications. Accuracy of existing filter design tools and package interactions in the finished filter are two challenges we need to solve to produce practical HTS filters. These data show the excellent promise for HTS filters, but in-band ripple is unacceptable for high performance applications.
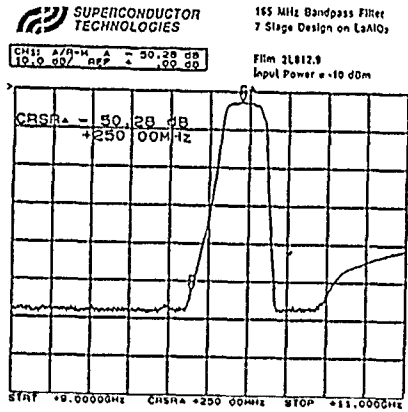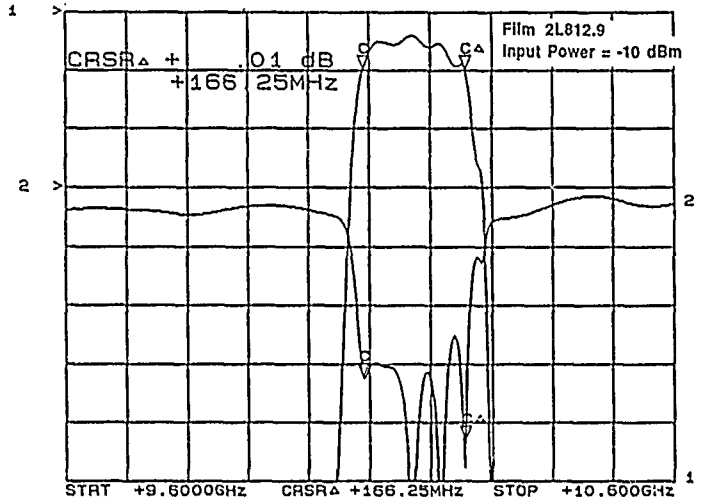
Figure 62. Structure and measured performance of 10 GHz pseudo-interdigital bandpass filter.

Using a conventional coupled-line microstrip geometry, we have also made attractive filters. Figure 63 shows the structure and measured insertion loss and return loss of a 9-pole 4% bandpass filter at 10 GHz. The filter performed as expected in the design simulation, both in terms of bandwidth and center frequency. It was designed for 10 GHz and had a center frequency of 10.075 GHz. The return loss was much improved over the filter in Figure 62; it was greater than 10 dB.

56
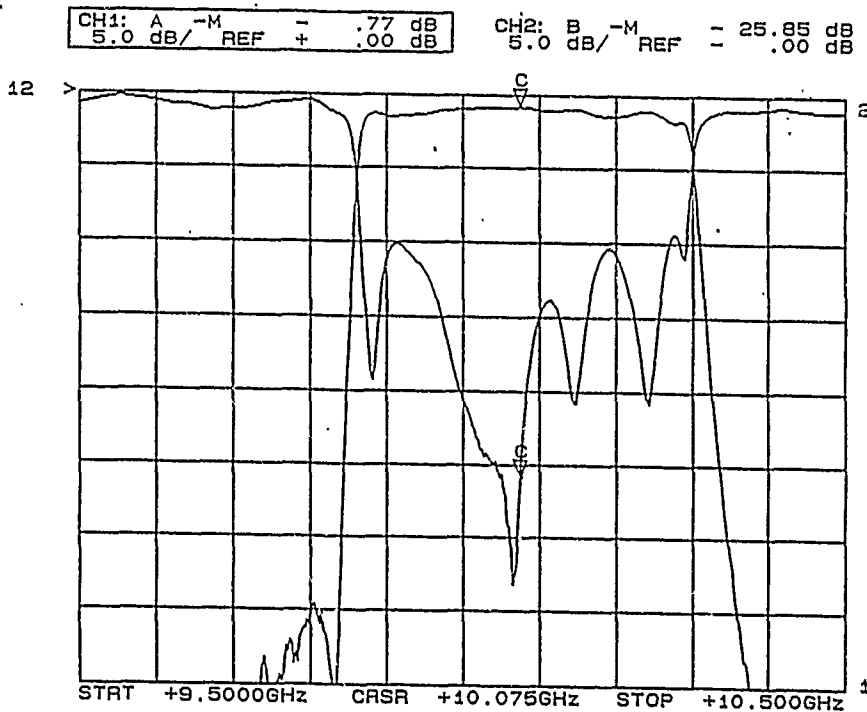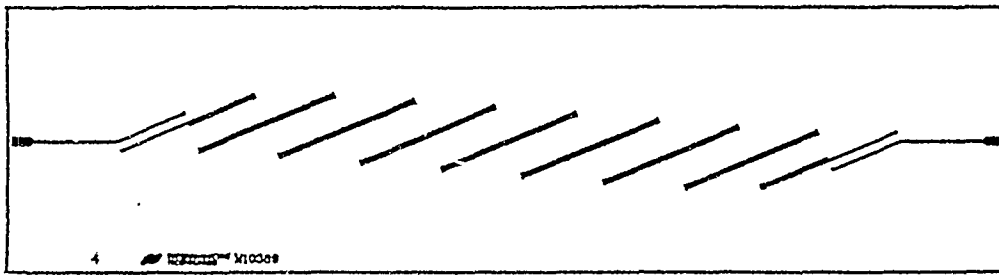
Figure 63. Microstrip filter layout and measured performance at 77K.

One of the most exciting potential approaches that is made possible by superconductors for high performance filter applications is thin film lumped-element designs. We have developed a dramatically new filter concept using this approach which is only possible using thin film superconductors. We designed, fabricated, and tested a narrow band thin film lumped element filter centered at 10 GHz. This filter does not suffer from the undesired spurious responses seen in thin film distributed filters using HTS technology. The measured filter has a 2.5 dB insertion loss at band center, 3% bandwidth and is within 50 MHz of the designed center frequency. Measurements were made to confirm spurious free stopbands from 1 GHz to 21 GHz. The measured performance of the filter is shown in Figure 64. The insertion loss is 2.5 dB which may improve as the processing of the dielectric cross-overs improves. The actual bandwidth is about 290 MHz which is greater that the desired 200 MHz bandwidth and may be due to coupling

between networks that were not modeled. The filter layout is shown is Figure 64 at the top. The structure consists of alternating capacitors and inductors. Crossovers for the printed spiral inductors were realized using a polyimide dielectric layer and conventional thin film gold. A broadband plot of the stopband performance is shown in the middle of Figure 64. Note the lack of spurious responses down to -30 dBc. This is due to the fact that the filter is truly semi-lumped over a broad frequency range; there are no resonant quarter-wave or half-wave distributed elements to launch energy into the substrate. The spurious performance demonstrated here may make it possible to place several of these filters on the same substrate in a microwave channelized receiver.
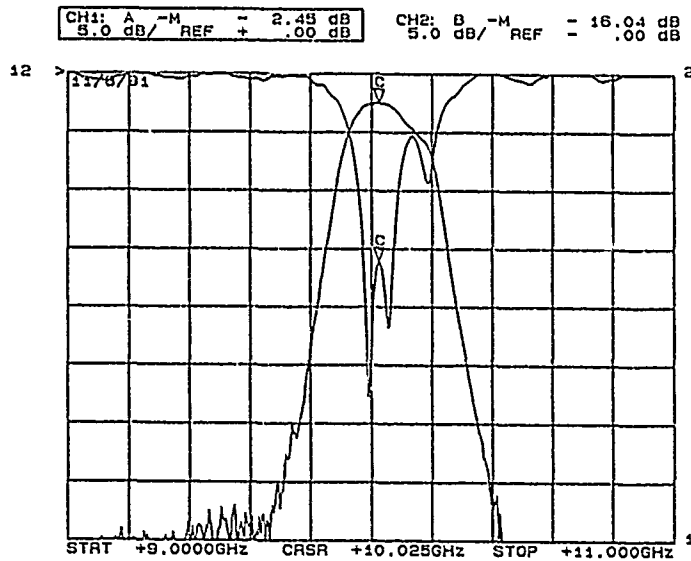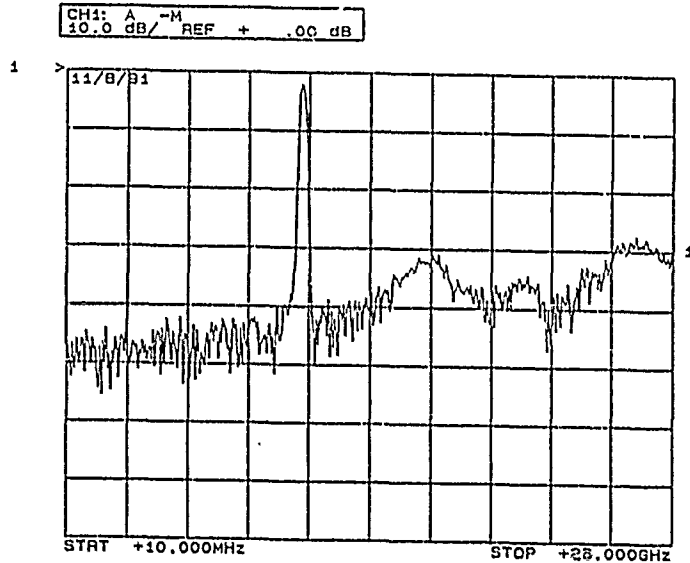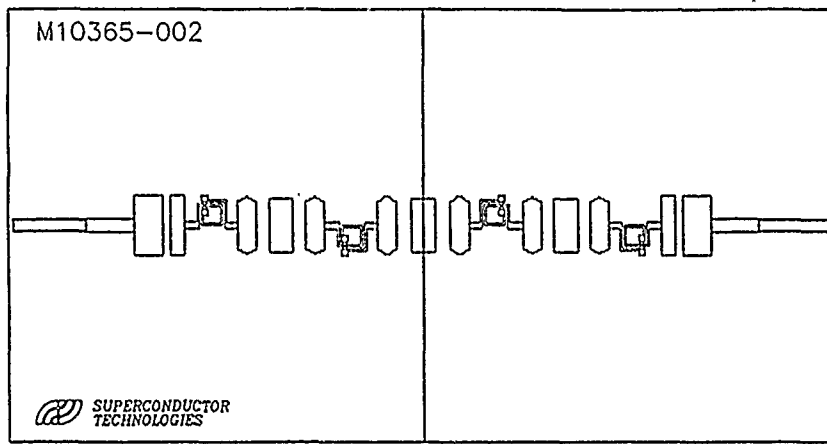
Figure 64. (top) Layout of lumped element 10 GHz filter; (middle) broadband insertion loss of lumped element filter at 77K; (bottom) narrowband insertion loss and return loss of lumped element filter.

Delay Lines

During the final year of this program, we scaled a 2 ns delay line HTS delay line that we developed under contract to the U. S. Air Force Avionics Lab to a length of 29 nsec. The delay line structure, which is a coplanar waveguide meander line, is shown in Figure 65. The center conductor is 25 microns wide, and the HTS ground planes on either side of the center conductor are connected together with Au crossover bridges at intervals of approximately 1 mm. Figure 65 shows the 2 nsec delay line structure which is fabricated on a 1-cm square LaAlO3 substrate. It is a broadband, 50 ohm structure. Figure 40 shows a close-up of the meander line structure with the Au crossovers. The delay line shown in Figure 65 was extended to a 1.2-inch square substrate and laid out in such a way as to provide a microwave signal delay of 29 nsec. The layout for this much longer delay line structure is shown at the top of Figure 66. The completed delay line on a 2-inch thallium-on-LaAlO3 wafer is shown before dicing at the bottom of Figure 66.
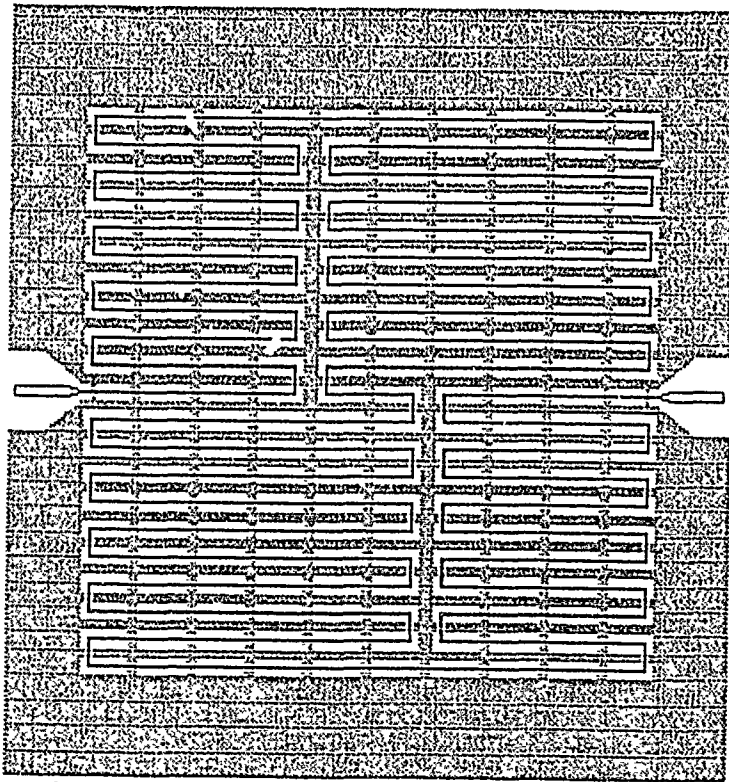
Figure 65. Layout of 2 nsec coplanar delay line.
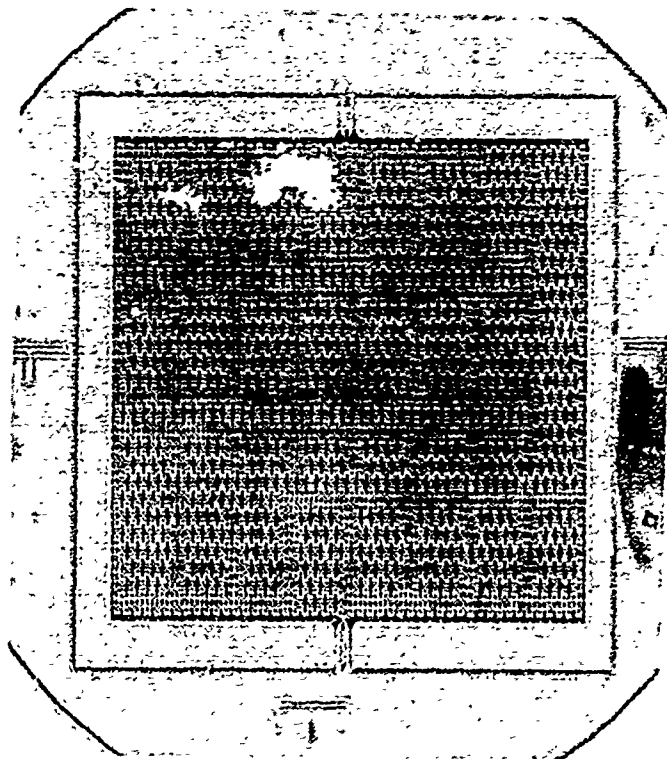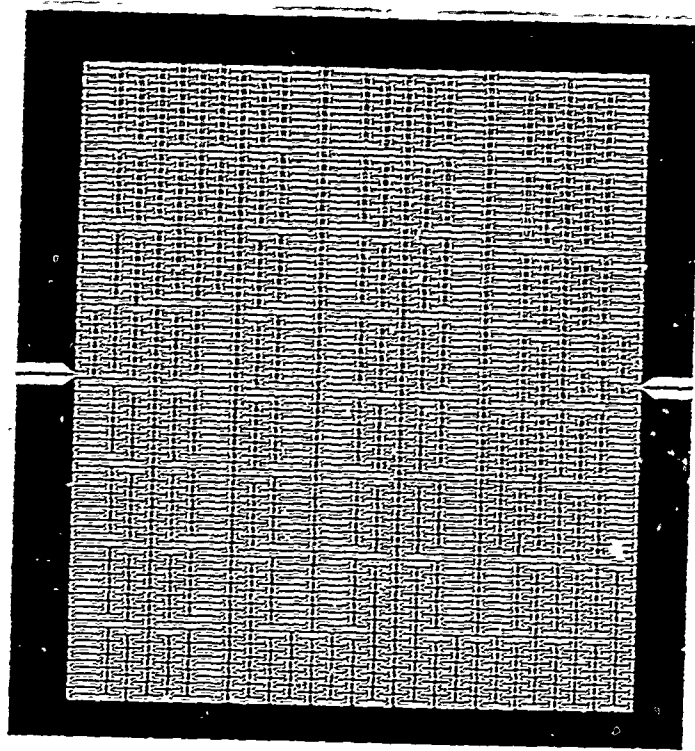
Figure 66. (top) layout of the 29 nsec coplanar delay, (bottom) photograph of the finished delay line fabricated on a 2-inch wafer.

The delay line performed very close to design expectations. The insertion loss was between 130 MHz and 6 GHz at 77K and is plotted at the top of Figure 67. The response shows a

slowly increasing loss at increasing frequency, as expected due to the loss of normal metal crossovers and the superconductor. It shows < 0.4 dB loss per nsec of delay at 6 GHz. The insertion loss is very clean, showing an almost monotonically increasing loss with increasing frequency. The feature at 3.5 GHz is due to a substrate mode in the 1.2" × 1.2" lanthanum aluminate substrate. For practical applications this must be engineered out by appropriate shaping of the substrate. This device is evidence that our thallium films can yield very long broadband delays in a very small volume. The bottom of Figure 67 shows a time domain reflectometry trace indicating the 29 nsec total delay in the delay line. The line shows a uniform 50 ohms over its entire length, and a clear reflection at the open end.
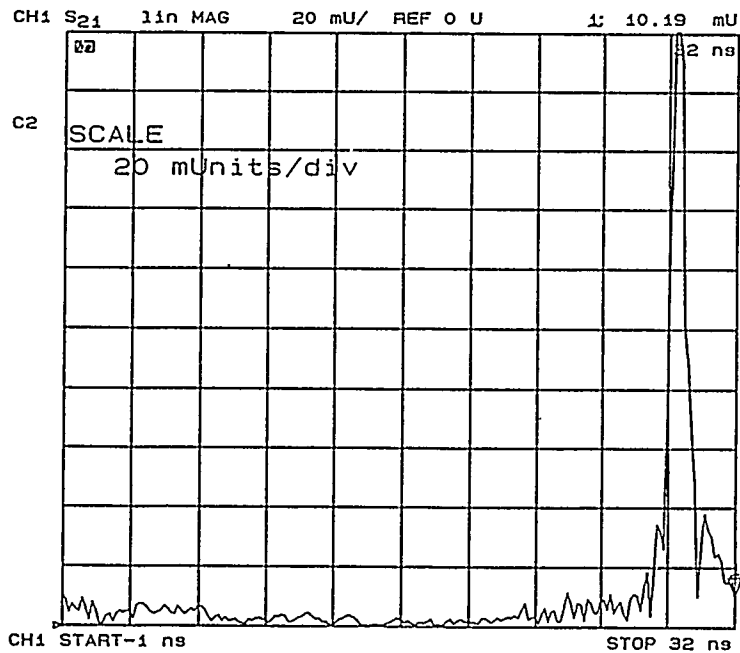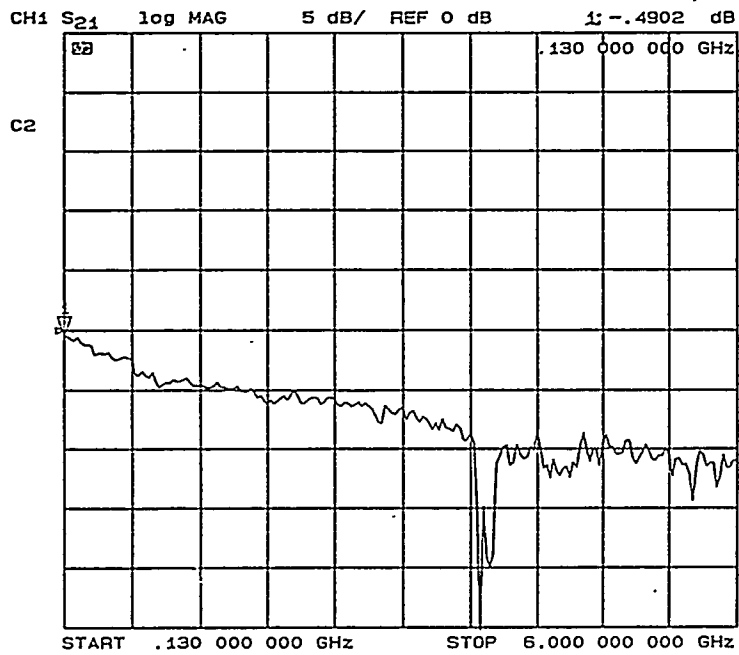
Figure 67. (top) Insertion loss of 29 nsec coplanar delay line at 77K; (bottom) time domain reflectometry trace of delay line showing clean end reflection at a delay of 29 nsec.

HTS Switched Band Reject Filter

In addition to our work on capacitively coupled resonators that perform as simple, single-pole bandpass filters, we have also developed inductively coupled resonators that perform as single-pole band reject filters. The device we report here is a single-resonator band-reject filter designed to be as steep as possible while maintaining low loss near the band edges. It is an inductively coupled half-wave-length resonator that provides a reflective short at its resonance, but has no effect off-resonance. The circuit is critically coupled to give it a large shape factor.

As seen in the device layout in Figure 68, the coupling length is a small percentage of the total resonator length and may be adjusted to raise or lower the bandwidth of the filter. It is inductively coupled in the middle of the resonator to make the analysis more accurate than would be possible with end coupled resonators. The real finite Q of the resonator gives a finite depth and width, which provides a useful measure of microwave loss in the superconducting film. The measured data (Figure 68) shows the good out-of-band performance and the sharp in-band rejection expected. The resonator loaded Q was 12,422 and it provided 17 dB of rejection 1% from the bandedge.
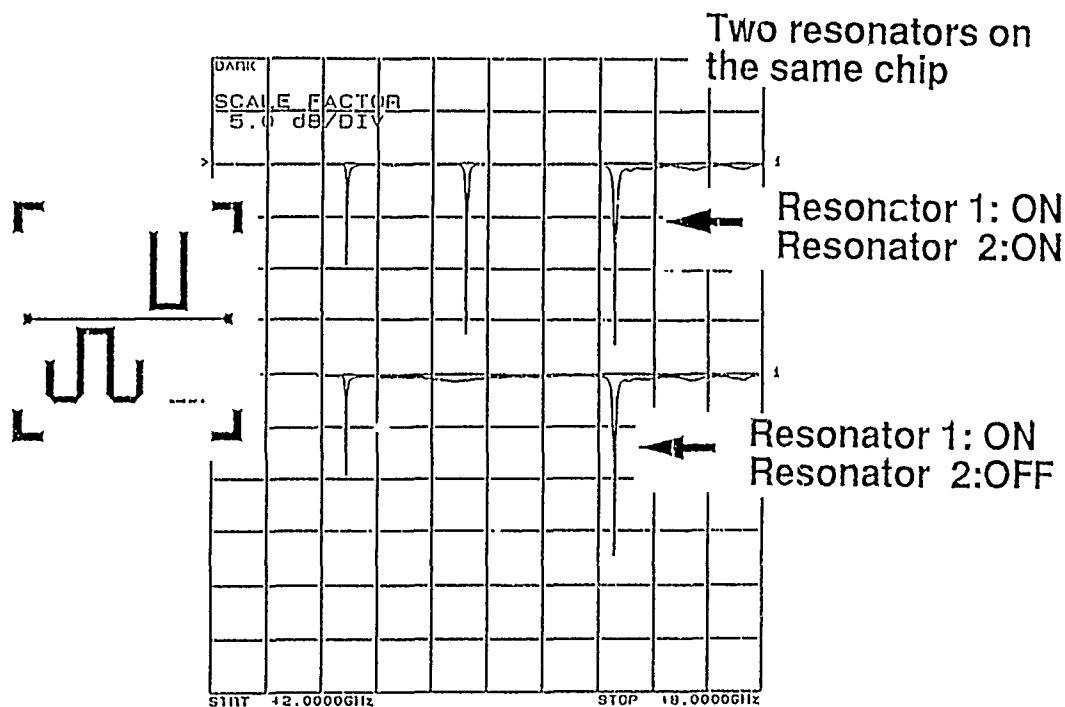
Figure 68. (inset) Mask layout of the 4.6 GHz inductively coupled band reject filter on a 1cm × 1 cm lanthanum aluminate substrate, along with a 3.3 GHz filter (lower left of inset).

The through line also gives a good measure of the interconnect and general connector losses of the package which is useful in troubleshooting as well as the measurement of the transition temperature and width of the HTS material. We used this structure to measure loss of our HTS material and have good agreement with the more traditional end-coupled resonator measurements. This topology would be ideal for filtering a strong interfering signal near the desired band or rejecting a fixed Local Oscillator from a frequency conversion device. To be able to cover a significant frequency range would require a large number of filters that could be switched in and out of the circuit as needed. Conventional switches are not practical because they would introduce too much loss.

We have developed a Q-switch that enables us to switch the Q of a resonator from above 10,000 to below 10 very rapidly. The technique uses optical excitation of a GaAs photoconductor in close proximity to the filter. Figure 68 shows the insertion loss of the double bandreject filter structure when the switch is on and when the switch is off. When the Q of the filter is very low, ~10 in this case, the resonance almost disappears. The insertion loss goes from 17 dB to 0.2 dB on resonance.

HTS Lange Couplers

We developed the first HTS Lange couplers, as shown in Figure 69. We designed these circuits for a passband of 9.5 to 10.5 GHz. They include Au crossovers to interconnect the HTS lines. Loss was less than 0.2 dB.
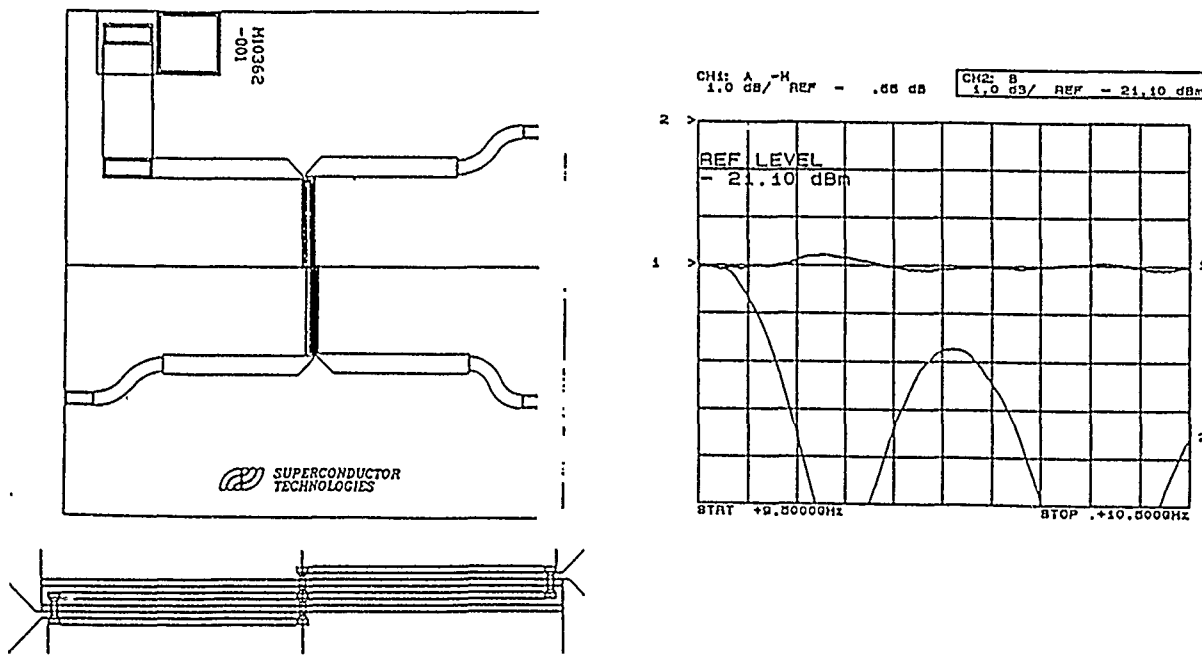
Figure 69. Structure and measured performance of HTS Lange Coupler.

65

Superconducting Resonator Stabilized Low Phase Noise Oscillator

An important application for high Q superconducting resonators is likely to be in low-phase noise oscillators. Here the resonator provides the stabilizing element for the oscillator. We have demonstrated low noise at 2.3 GHz and 10 GHz in a collaboration with our subcontractor on this program, Avantek Corp.

The amplifiers used in this work are GaAs FET low noise designs. The 2.3 GHz amplifier is a three-stage 0.5 micron gate device with small signal gain of 30 dB, nominal. The noise figure of the amplifier at 300 K is 1.2 dB, and output power at 1 dB compression is +13 dBm. The 10.2 GHz amplifier is a 5-stage design with 2.5 dB noise figure at 300K, small signal gain of 40 dB, nominal, and output power at 1 dB compression of +14 dBm.

Figure 70 (top left) shows the block diagram of the parallel feedback oscillator, using the transmission type high Q resonator and a GaAs FET low noise amplifier. In a parallel feedback design, the resonator is used as a bandpass filter and is connected across the terminals of an active device with forward gain greater than the insertion loss of the resonator. To oscillate, the electrical line length between the device input and output ports must provide a phase shift around the feedback loop equal to an integer multiple of 2π radians at the oscillation frequency. With the parallel feedback circuit, the use of a high gain amplifier can allow significant decoupling of the resonator. This results in a higher loaded Q with an associated reduction in phase noise.

For this experiment, the only cooled oscillator components are the superconducting resonators. The low noise amplifier, power splitter, phase shifter, and pads were maintained at room temperature for ease of operation. The resonators were immersed in a bath of liquid nitrogen at 77K, and their performance measured over a narrow range of RF input drive. The loaded Q for all superconducting resonators varies with applied RF power due to defects in the film structure. For high quality films, this power dependence is relatively minor, and high loaded Qs are still obtainable at 0 dBm and above. Figure 70 (bottom left) shows the measured Q_L vs. P_{in} performance for both resonators. In the oscillator circuit, the 2.3 GHz resonator was operated at a power level of 0 dBm and loaded Q of 13,800. The 10.2 GHz resonator was operated at a power level of +6 dBm and loaded Q of 6,000.

The oscillator circuits were assembled, with the packaged resonators mounted on a cold stage in the liquid nitrogen bath. After adjusting the phase shift for oscillation, data was taken on each circuit; this data is summarized below. Also included in the table are specifications for a dielectric resonator oscillator (DRO) operating in the same frequency ranges. Plots of phase noise

performance were taken, and are presented in Figure 70 (right) for the 2.3 GHz SCO and the 10.2 GHz SCO.

Test Parameter	SCO	DRO	SCO	DRO
Power Output (dBm)	+8.8	+13.0	+12.0	+13.0
2nd Harmonic (dBc)	-21	-20	-29	-20
Frequency Pulling (kHz) into 1.67:1 VSWR Load	100	460	50	2040
Frequency Pushing (kHz/V)	10	23	2	102
Phase Noise @ 10 kHz (dBc/Hz)	-110	-110	-100	-95
Phase Noise @ 100 kHz (dBc/Hz)	-148	-135	-126	-120
Phase Noise @ 1 MHz (dBc/Hz)	-155	---	-143	---

Improvements in performance over a conventional DRO are achieved at both 2.3 GHz and 10.2 GHz. Harmonic output, frequency pushing, and frequency pulling data for the SCO outperforms the DRO specifications in both oscillators. Phase noise performance at 2.3 GHz meets or exceeds the DRO specification. At 10.2 GHz, the SCO demonstrates a 5 dB improvement in phase noise at 10 kHz from the carrier, and a 6 dB improvement at 100 kHz. In addition, an SCO maintained at 77K has a significant advantage in frequency stability over temperature.
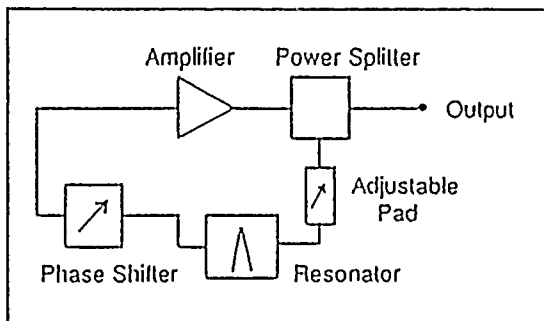
HTSC OSCILLATOR
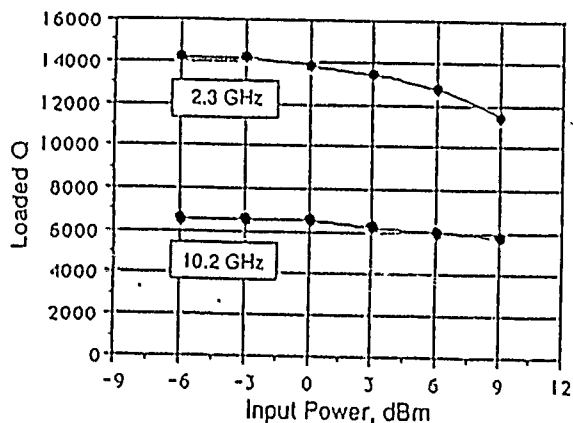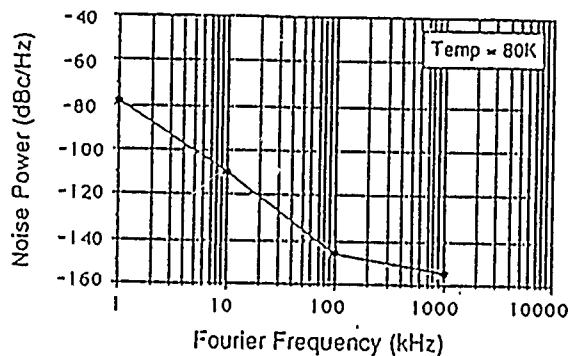
2.3 GHz Phase Noise
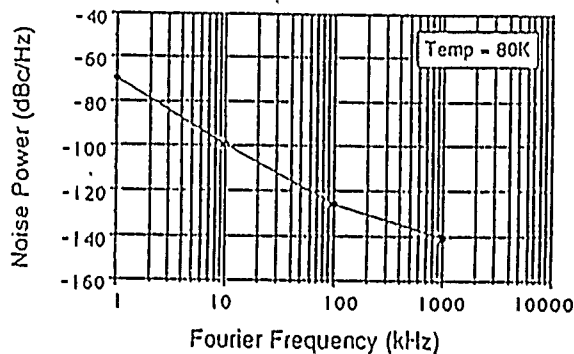
HTSC Resonator Q's

10.2 GHz Phase Noise

Figure 70. (top left) Block diagram of oscillator circuit; (bottom left) measured resonator Qs at 2.3 and 10.2 GHz as a function of input power at 77K; (right) measured phase noise for the 2.3 and 10.2 GHz oscillators.

We have demonstrated superconducting resonator stabilized oscillators at 2.3 GHz and 10.2 GHz. The performance of these devices is equal to or better than currently available dielectric resonator oscillators.

Further improvements in SCO performance will result from optimization of the oscillator circuitry. Resonators with higher loaded Qs are now available; Q_L approaching 50,000 at 5.0 GHz has been demonstrated at 77K. We are currently evaluating experimentally the effect of resonator loaded Q on phase noise performance. The low noise GaAs FET amplifiers will be replaced with very low noise GaAs or Si bipolar designs, optimized for the specific oscillation frequencies.

As phase noise performance improves, we are approaching the noise floor of our measurement equipment. More sophisticated and sensitive measurement techniques will be required to properly characterize the extremely low noise levels of these devices.

Development of Thin Film Characterization Measurements

During the course of this three-year research and development program we developed a variety of both conventional and unique measurement techniques for characterizing the electrical performance of our high temperature superconductor thin films. These included the most common diagnostic measurements: resistivity vs. temperature and critical current density, as well as more powerful measurements: AC magnetic susceptibility vs. temperature and AC field, remanent magnetization, and temperature and power dependent surface resistance. Our emphasis has been to develop diagnostics that would give us fast and accurate measures of thin film performance to feedback to film development. The following discussion describes the measurements we developed.

Resistivity

The standard method of determining transition temperature in a superconductor is to measure the resistivity of the material vs. temperature. The highest temperature at which the material has zero resistance is inferred to be the superconducting transition temperature. Quality of the superconducting film is inferred from the T_c, the width of the transition, and the normal state resistivity.

We developed a simple and rapid technique to measure thin film resistivity vs. temperature. Four-probe pressure contact is made to the thin film. The sample is inserted into an already cooled cryostat. Resistivity is measured as the sample cools below room temperature. Figure 71 shows the measured resistivity of an early thallium film made by our open-gold-pouch process. The transition temperature is 106K, where the measured resistivity becomes zero. The normal state resistivity at the transition temperature, 100 micro-ohms, places it among the lowest measured in thallium films. The measured width of the transition is 5K.
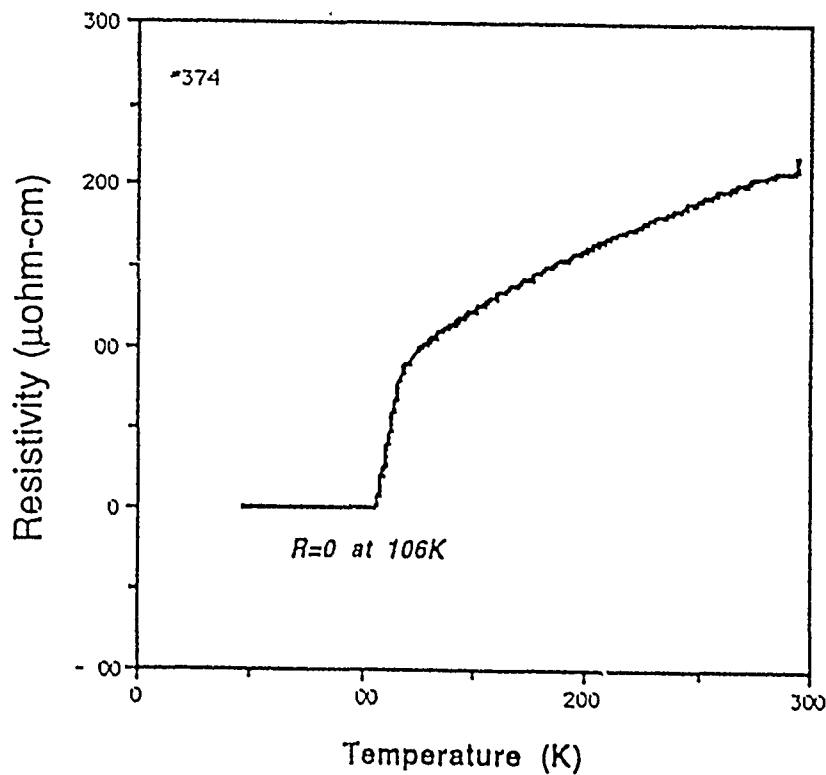
Figure 71. Resistivity vs. temperature for thallium thin film.

Critical current density

Critical current density is also a common measure of quality in thin film superconductors. We developed a technique to measure the critical current density in our films at temperatures down to 4K. A four-point measurement is used, and the criterion of 1 micro-volt per millimeter is used to determine critical current. This is the criterion established for the DARPA HTS program. Figure 72 shows the measured current-voltage characteristic of a 4-point bridge on one of our production thallium thin films. The inset in the figure shows the outline of the bridge. The linewidth is 25 microns, and the length of the bridge is 200 microns. The critical current density at 77K of the sample shown is 1.1×10^6 A/cm^2. This is determined from the measured thickness of the film.
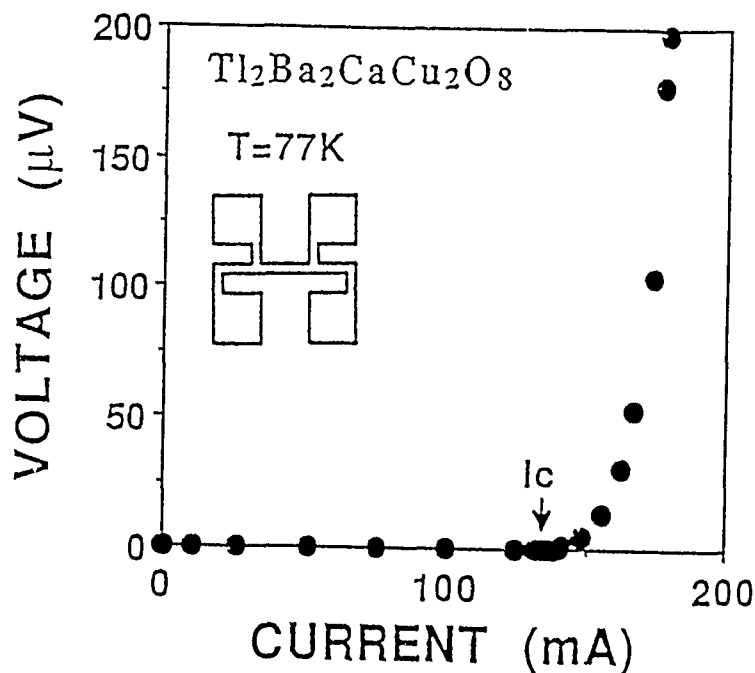
Figure 72. Voltage vs. current for J_c determination on thallium thin film.

AC magnetic susceptibility

In the process of our development of thin film superconductors we found that AC magnetic susceptibility offered a more demanding diagnostic than resistivity, while being equally as fast a measurement and also nondestructive. We developed an AC magnetic susceptibility measurement that we have used routinely on our production thin films. Figure 73 shows a diagram of the basic setup. The sample is placed inside a large solenoid. This solenoid provides the AC magnetic field that excites the sample. Two pick up coils, one close to the sample and one removed from the sample, are used to determine the electromagnetic response of the sample to the applied AC magnetic field. The difference in response of the two pick up coils is used to determine this response. The differential nature of the measurement gives it great sensitivity. The magnetic transition of the superconductor which can be measured with this apparatus is a much more critical measure of film quality than resistivity. Figure 74 shows the measured AC magnetic susceptibility vs. temperature for a production thallium film. The transition is less than 1K.

71

pick-up coils

Hac

Sample

ac magnetic field coils
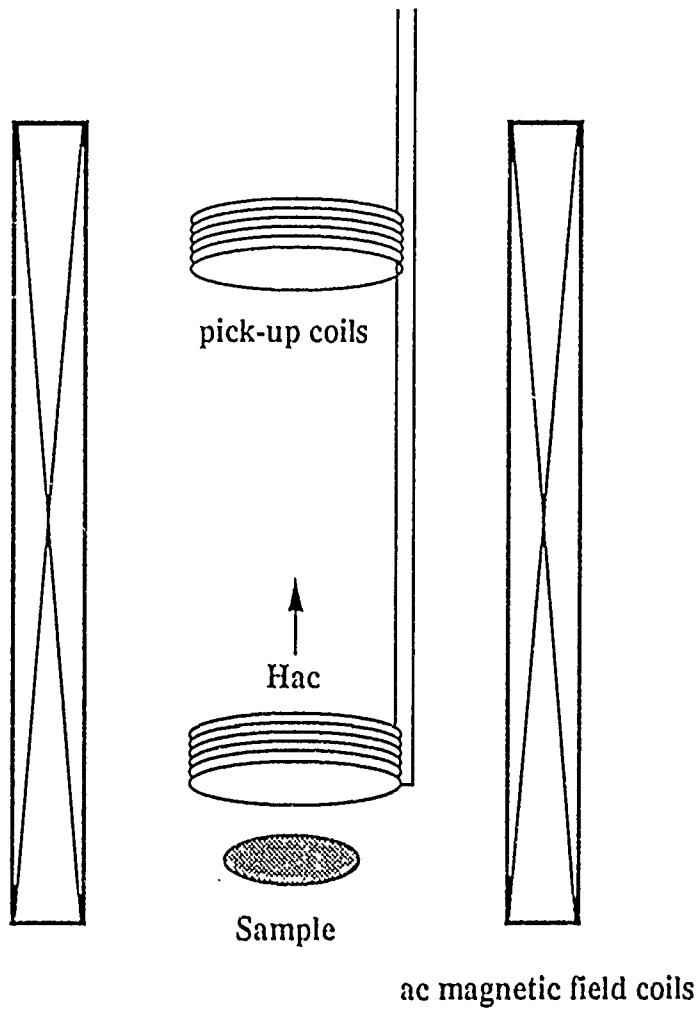
Figure 73. Schematic diagram of AC magnetic susceptibility measurement.
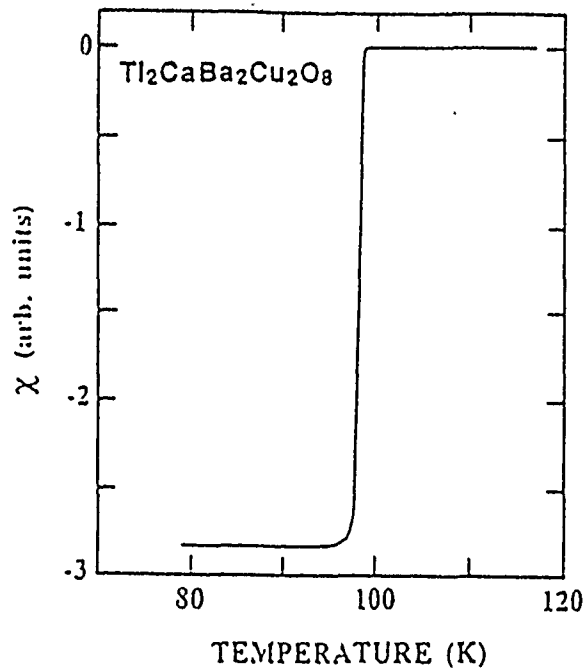
Figure 74. AC magnetic susceptibility vs. temperature on thallium thin film.

We implemented several production susceptibility measurements at STI. The first apparata were for 1 cm × 1 cm films. Following this we successively developed measurements for 1" square and 2" square films. We also developed a precision instrument that permitted measurement of both the real and imaginary parts of the electromagnetic response of the film as a function of temperature. It also permits precise measurements at various amplitudes of AC magnetic field excitation. Figure 75 shows the temperature-dependent magnetic response of a production thallium film to varying values of applied AC magnetic field. The real part, X', is the normal magnetic susceptibility. The imaginary part, X", is the loss. We took this measurement technique a step further and developed a novel method of determining thin film critical current density. Figure 76 shows a measurement of the temperature dependent critical current of a superconducting thin film inferred from our precision AC magnetic susceptibility measurement.

X (Hac) vs T
Tl film SVCP 301
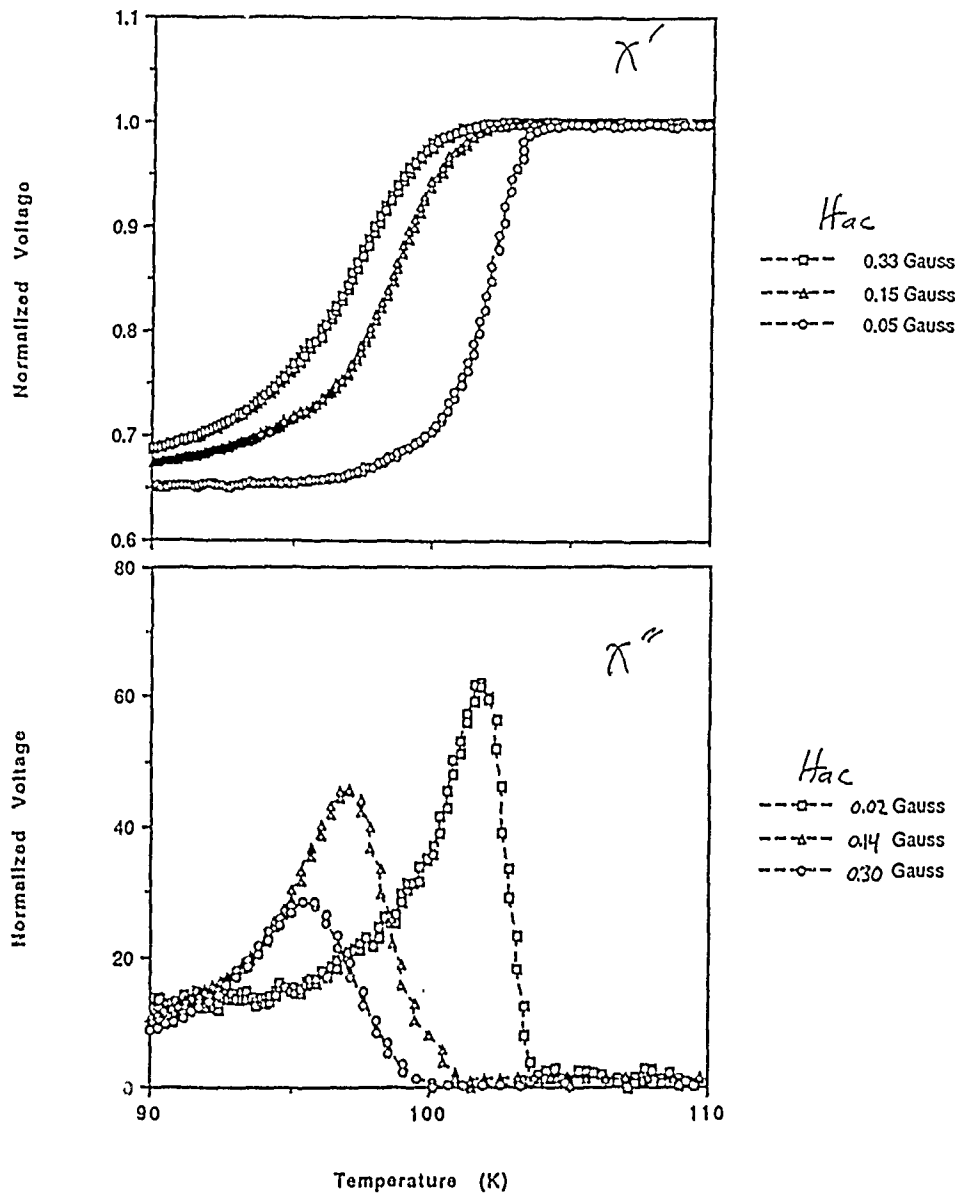
Figure 75. AC magnetic field dependence of the AC magnetic susceptibility transition on a thallium thin film.
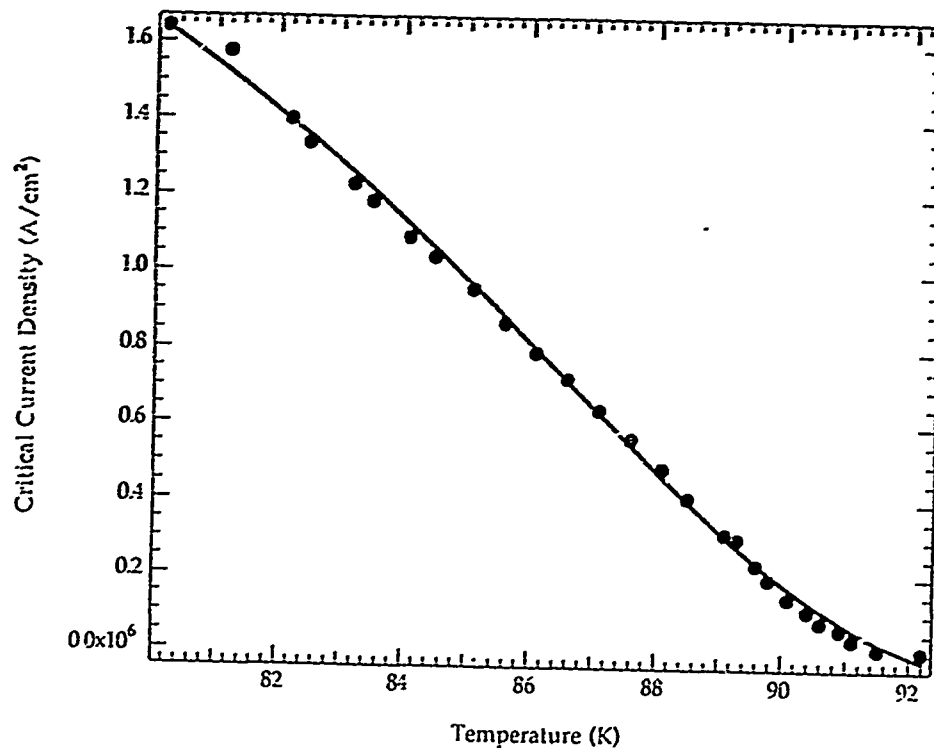
Figure 76. Critical current density vs. temperature inferred from AC magnetic susceptibility on an HTS thin film.

Remanent magnetization

In the quest for more rapid and accurate thin film diagnostics, we developed another technique, remanent magnetization. In this measurement the sample is cooled from room temperature down to the temperature of interest while exposed to a static magnetic field. The magnetic field strength is chosen so that it will be too large to be shielded by the film when it becomes superconducting. When the desired temperature is reached the static magnetic field is removed and the magnetic field generated by the superconducting thin film is measured as a function of time. The remanent field, that is, the field ʻremains after the initial transient decay, is a measure of critical current density. The remanent field represents the field due to currents flowing at the critical current density throughout the entire thin film. Figure 77 shows a schematic diagram of the experimental setup. Figure 78 shows the transient measurement of the remanent field after an applied field of 100 Gauss is removed. The inferred critical current density in this sample, at 77K, is 1.6×10^6 A/cm^2.

VOLTMETER
(HALL VOLTAGE)

D.C. CURRENT SOURCE
(HALL CURRENT)

VACUUM CAN

DEWAR

HELIUM EXCHANGE GAS

LIQUID NITROGEN
BATH

SUPPORT ASSEMBLY

MAGNET COIL
CROSS-SECTION

HALL PROBE

THIN FILM SAMPLE

SAPPHIRE PLATE

TEMPERATURE
SENSOR

D.C. POWER
SUPPLY
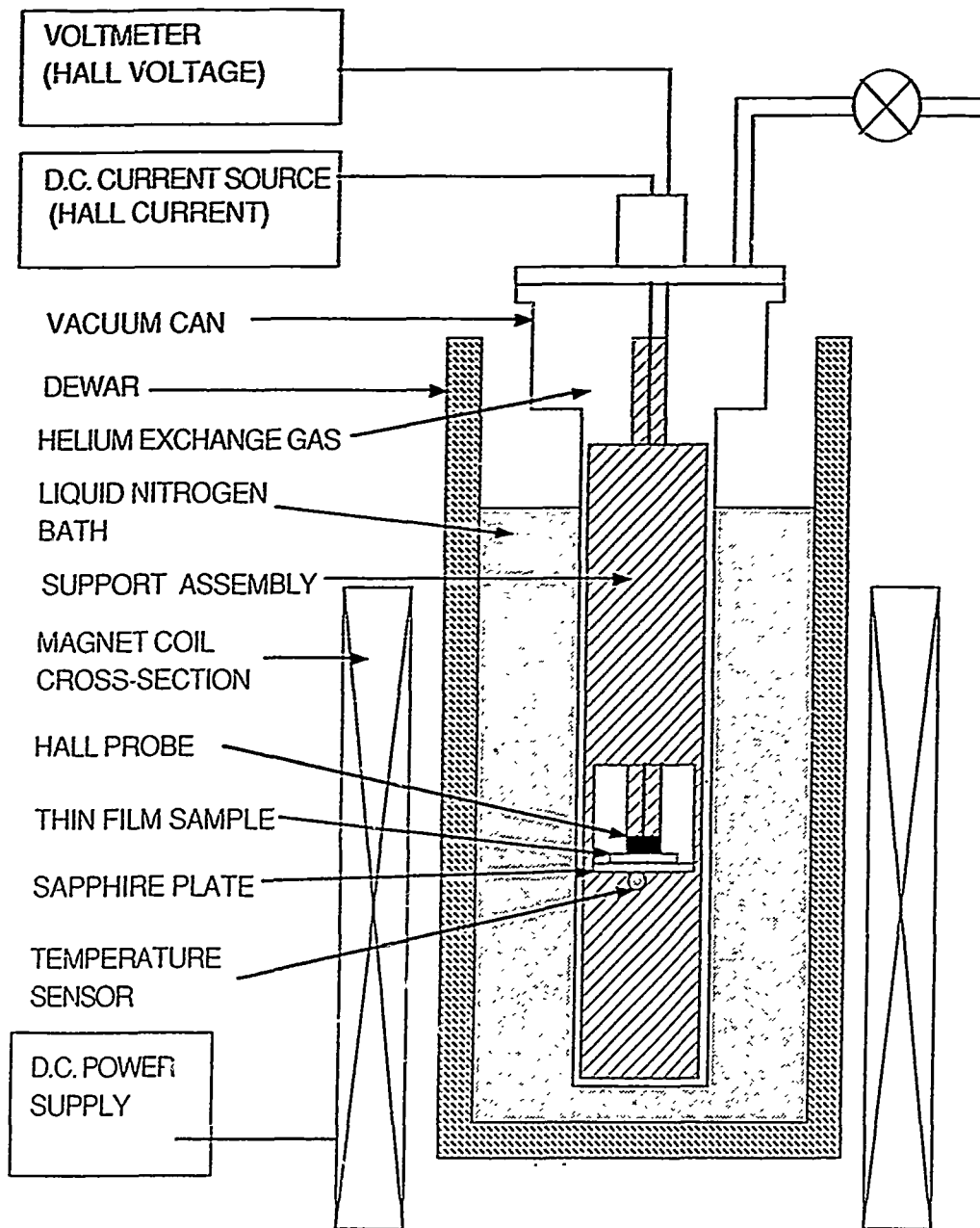
Figure 77. Cross-sectional diagram of the remanent magnetization instrument.
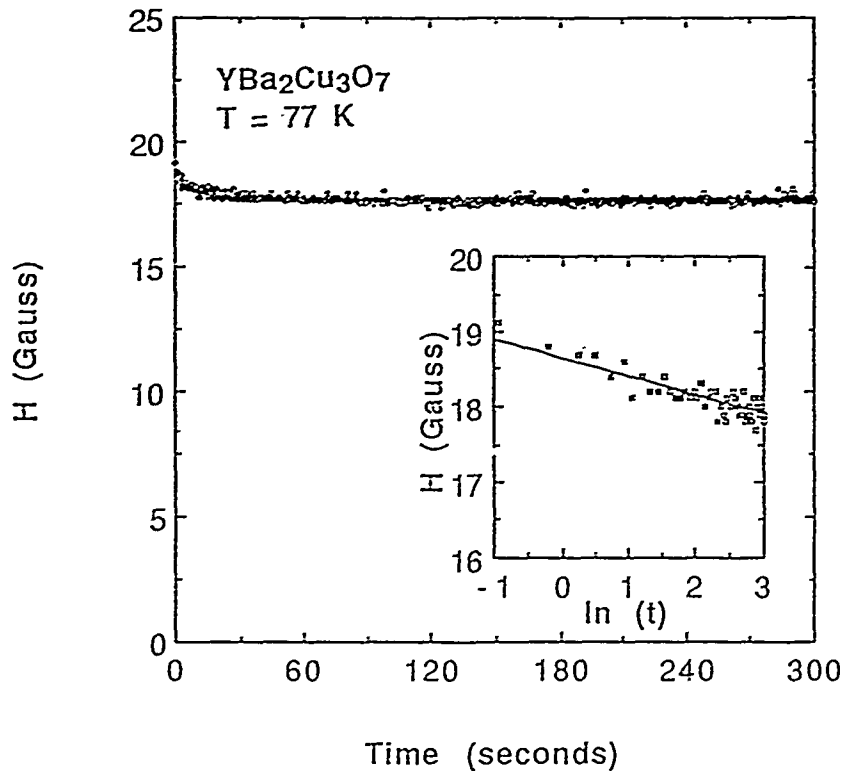
Figure 78. Time dependence of the remanent field of a YBCO film. An applied field of 100 Gauss was turned off at t=0. The inset shows a least squares fit to the remanent field as a function of the logarithm of the time for the first 20 seconds.

Surface resistance

Nb cavity perturbation at 9.6 GHz

In this program we developed a technique to measure the surface resistance of HTS thin films as a function of temperature and microwave magnetic field at 9.6 GHz. The technique was first developed by Sridhar at Northeastern University and Padamsee at Cornell. We took it to a more refined state to permit routine and accurate measurements. Figure 79 shows a schematic diagram of the measurement apparatus. A TE011-mode superconducting niobium cavity is employed. The sample is held in intimate thermal contact to a sapphire rod in the geometric center of the cavity. Coupling of the microwave signal is controlled to be either in the weak coupling limit (for low field R_S measurement) or at critical coupling (for field dependent R_S measurement). The niobium cavity is immersed in liquid helium at 4K, and has a Q of 21,000,000 at 9.6 GHz. The temperature of the sapphire rod and sample is controlled between 300K and 4K. The Q of the cavity with the sample is measured as a function of sample temperature and the sample surface resistance is inferred. Figure 80 shows a measurement of the temperature dependent surface resistance of one of our early thallium thin films made by the open-gold-pouch process.
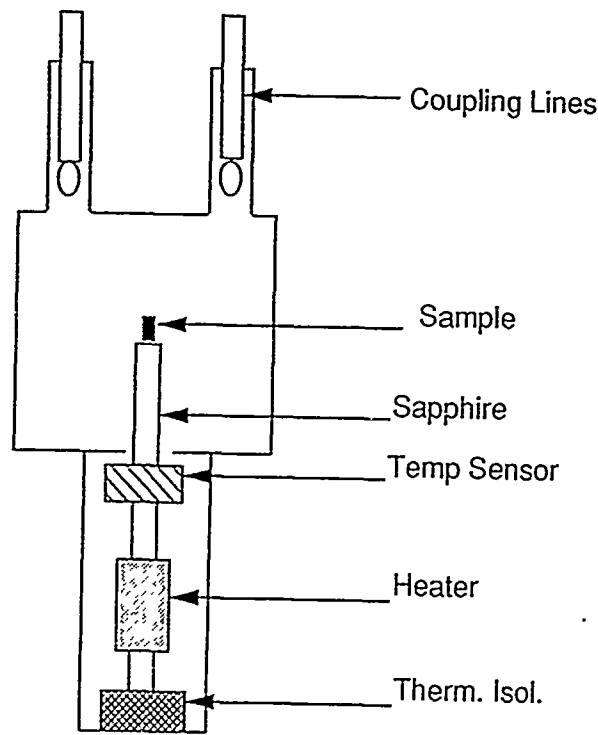
Figure 79. Schematic diagram of the 9.6 GHz niobium cavity used to measure surface resistance of HTS thin films.
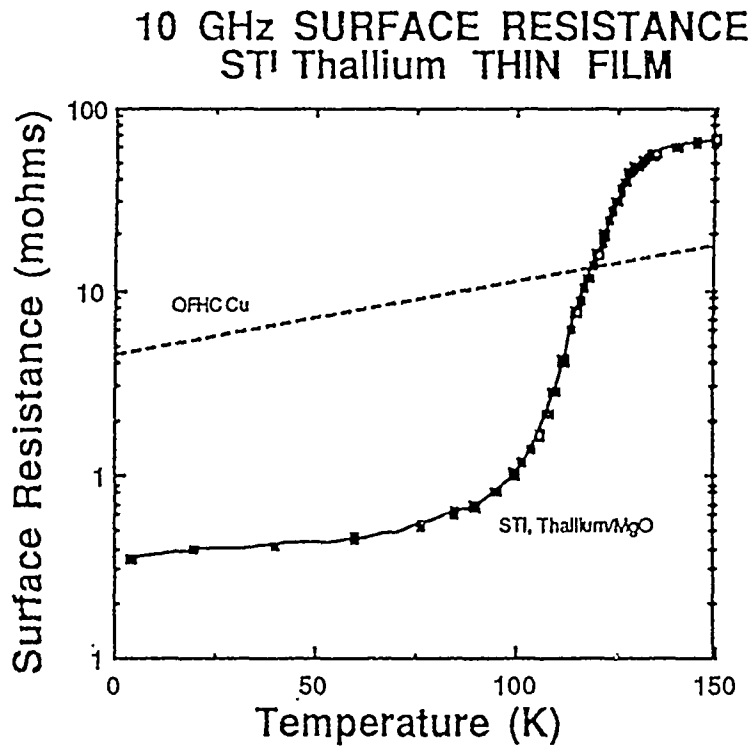
Figure 80. Surface resistance vs. temperature of a thallium thin film made by the open-gold-pouch process.

By changing the coupling of the input signal to the cavity for each measurement of Q, we are able to make a quantitative determination of the microwave magnetic field at the sample under test. In this way we can make a measurement of the surface resistance of the sample at various values of microwave magnetic field. This is a very demanding test of film quality. Figure 81 shows measurements of the field dependent surface resistance at 77K, 9.6 GHz of three thallium thin films. The old process referred to in the figure is the open-gold-pouch process. The new process is our ELF process that is our standard production process. The film with the best performance in the figure (the film made in February, 1990) was measured at several temperatures above 77K Figure 82 shows the field dependent surface resistance of this film at 77K, 90K, and 95K.
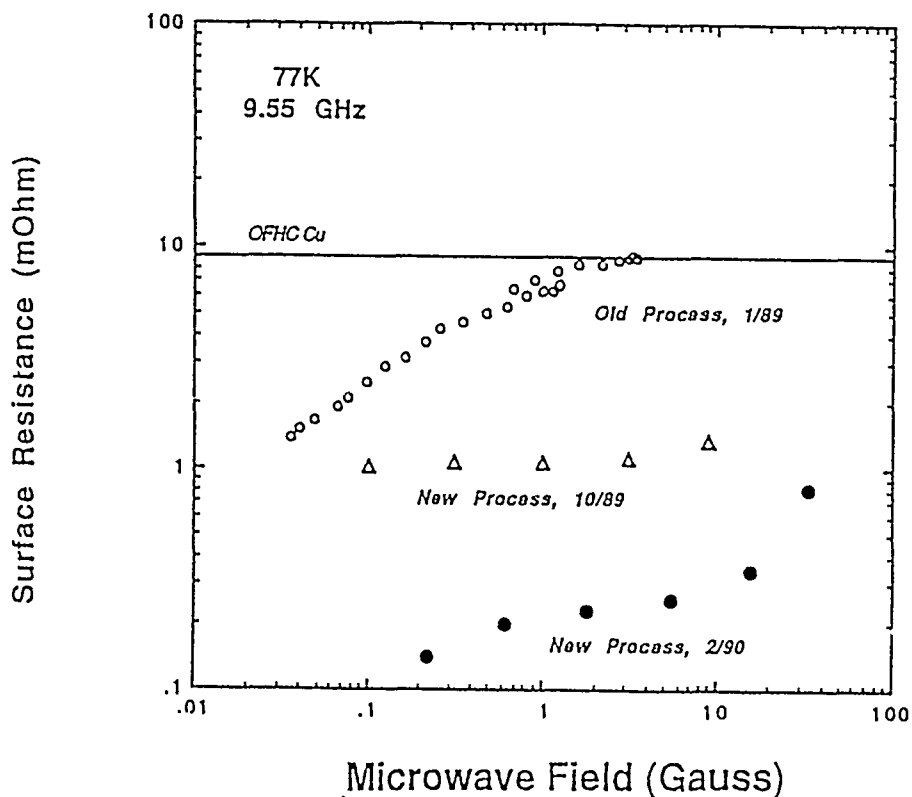
Figure 81. Surface resistance vs. microwave magnetic field for three thallium thin films made by two different processes, open-gold-pouch (Old Process) and ELF (New Process).
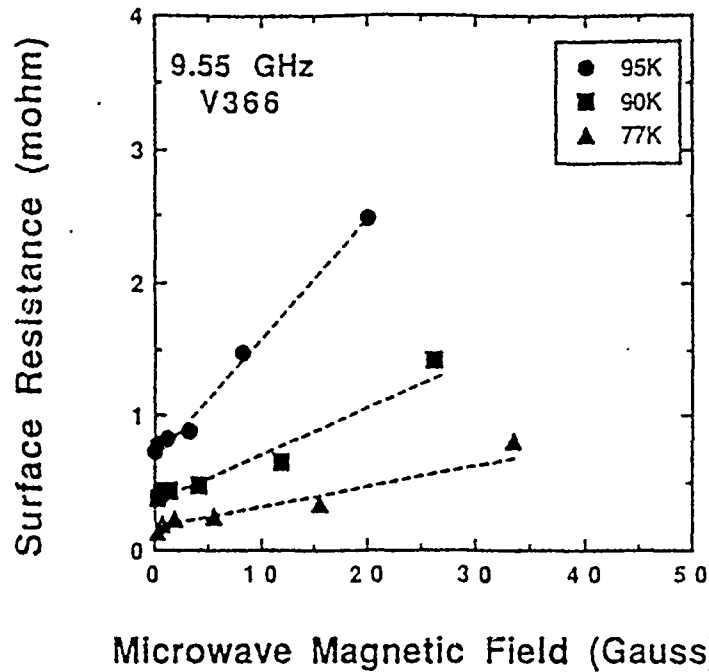
Figure 82. Surface resistance vs. microwave magnetic field for a thallium thin film at three temperatures.

102 GHz cavity end wall replacement

In the interest of developing a more rapid measurement of thin film microwave performance, we implemented a measurement at 102 GHz. This technique was first developed by Gruner at UCLA. We have refined the technique to permit rapid and accurate measurement of production thin films. This measurement involves a TE011-mode Cu cavity at 102 GHz. The Q is determined by measuring the width of the resonance. The temperature of the entire cavity is varied from room temperature down to 4K. The superconducting thin film sample replaces the end wall of the cavity. The Q measured with a Cu endwall vs. temperature is compared with Q measured with the HTS film as endwall. The superconducting thin film surface resistance at 102 GHz as a function of temperature is inferred from these measurements. Figure 83 shows a schematic diagram of the measurement apparatus. Figure 84 shows measured surface resistance on three samples. The open squares are from a high quality YBCO film, the closed diamonds are from a degraded thallium film, and the closed squares are data from a standard production thallium film. This measurement allows a direct, nondestructive determination of surface resistance vs. temperature on production thin films up to 2 inches in size. The time for complete measurement is less than 2 hours.

DIGITAL SCOPE	NICOLET 370
PULSE GEN	HP 8012B
GUNN OSC	WJ W3911-020P
RF ISO	AEROWAVE 10-5821
RF ATTN	HUGHES 45726H-1000
RF COUP	HUGHES 45326H-1310
HTR PS	TOPWARD TPS-2000
DC PS	TOPWARD TPS-2000
FREQ MTR	HUGHES 45716H-1000
DET	HUGHES 47326H-1111
ISO AMP	HUGHES 47500H-5000
DC AMP	EG & G 113
TEMP CONTRL	LAKESHORE CRYOTRONICS 805
LEAK DETECTOR & PUMP	DUPONT 120SSA
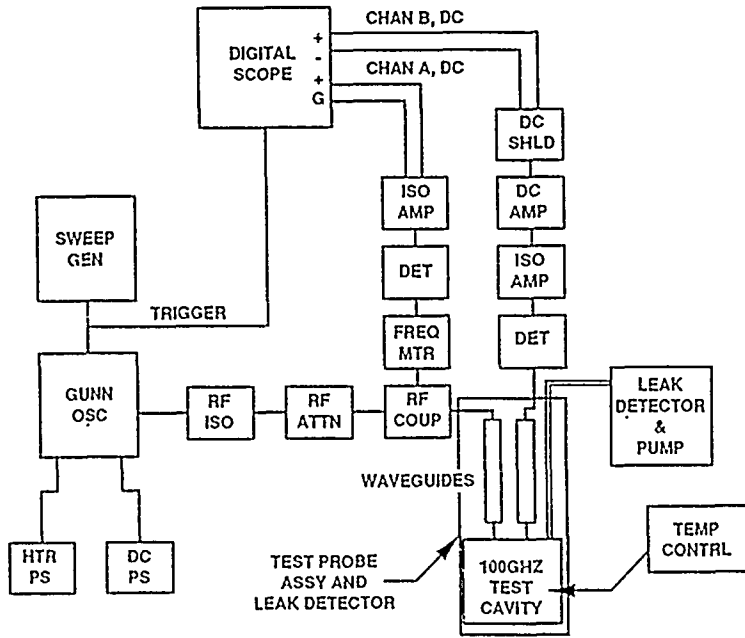
Figure 83. Block diagram of the 102 GHz surface resistance measurement.
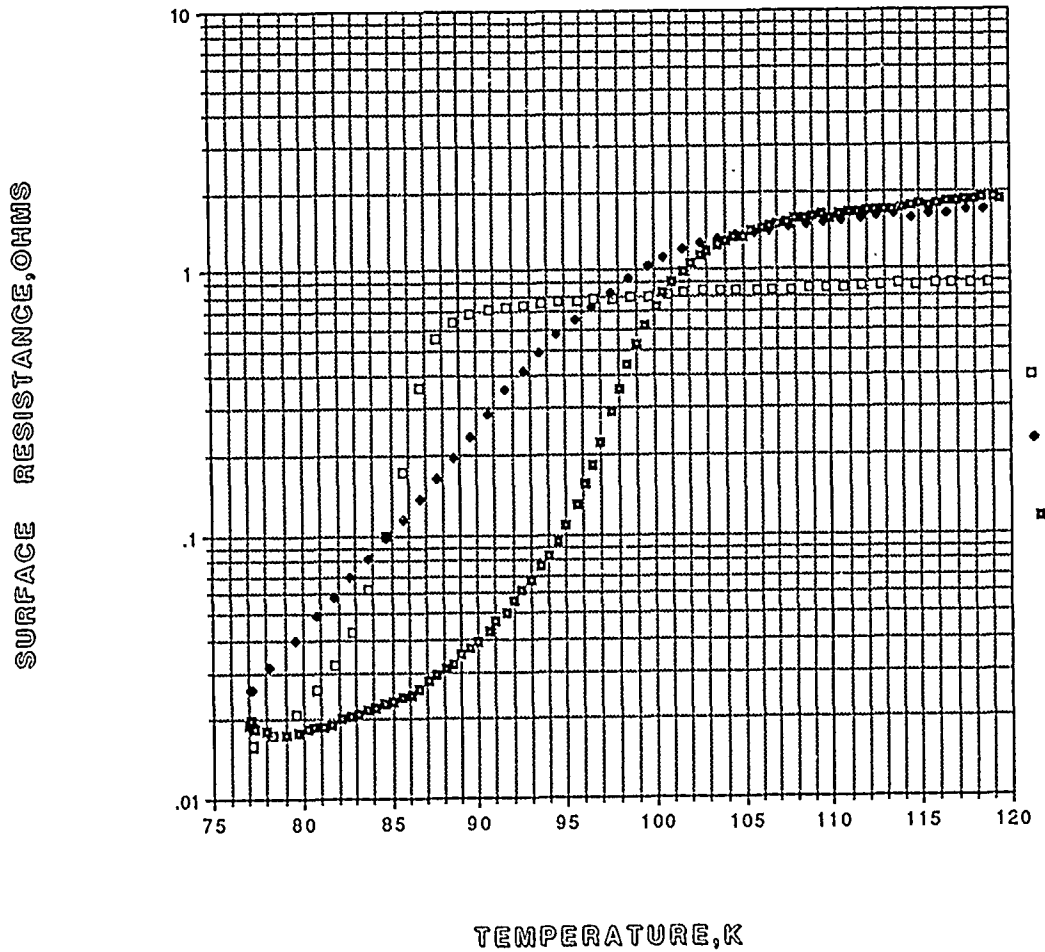
Figure 84. Surface resistance vs. temperature for three HTS thin films. The open squares are for a state of the art YBCO film. The closed squares are for a production thallium thin film. The closed diamonds are for a degraded thallium thin film.

Cryocooling/Packaging Development

Cryocooling

We recognized early that: (i) the success of HTS electronics depends upon the development of suitable cryocoolers, and that (ii) HTS electronics represents a major new market opportunity for cryocooler manufacturers. These two facts were the motivation for the recent "Workshop on Cryogenic Cooling for High Temperature Superconducting Electronics," hosted by STI at the Upham Hotel in Santa Barbara on the 27th and 28th of June, 1991.

The performance advantage of the new superconductors has been well demonstrated and is becoming widely accepted. Unfortunately, the major hurdle to rapid adoption of HTS devices is the need for cryogenic cooling. The situation is aggravated by the fact that the initial users of HTS electronics are generally unfamiliar with cooling and the wide range of cooling technology that exists. The perception of microwave engineers and systems designers is that cryocooling is rare, exotic and incompatible with most practical systems, and certainly not suitable for military systems.

The reality is that cryocooling is a well-developed and mature technology that is widely used, especially in military systems. There are a large number of varied techniques and coolers, and a relatively large number of manufacturers with many years of experience. Nearly all of this cryo technology has been developed for IR detector or industrial applications. Despite the large body of cryogenics expertise and knowledge that is available, there has not been an awareness of the needs and characteristics of the emerging HTS electronics market.

This workshop was the first large scale effort to bring together the HTS manufacturers and users with the cryocooler manufacturers. The goal was to accelerate the dialog that will help each group reach its objectives.

HTS materials and components offer the electronic system manufacturers a large performance advantage; this is particularly true in the microwave frequency range. This performance advantage is established at the component level. Resonators, filters, oscillators, and other components exhibit superior performance.

The main hurdle to wide spread acceptance of HTS components is the need for cooling. The traditional microwave market is a military market. Microwave components find many applications in planes, missiles and other vehicles. Systems quantities run from a few hundred to tens of thousands. Environmental conditions are usually severe with ambient operating temperatures up to 85, 95 or even 125°C. Systems designers are under constant pressure to minimize size, weight, power consumption, and improve reliability.

The use of HTSs and cryocoolers will grow rapidly if we can help the microwave systems manufacturers achieve their goals. Currently the combination of HTS components and available cryocoolers is not viewed favorably by most system manufacturers. The cooler is the primary source of problems: the cost of closed cycle coolers, the logistics of open cycle systems, the availability of coolers for heat loads in the 5 to 10 watt range, reliability, etc.

There is a considerable body of knowledge and expertise in the cryocooling field. A large variety of 1/4 to 2 watt open and closed cycle refrigerators are available for cooling small (a few mm^2) IR detectors. Recently a 250 watt, 77K cooler has been developed for the semiconductor industry. The cooling and packaging requirements for HTS devices are different. Our goal was to bring the considerable talent in refrigeration to focus on the HTS needs and to highlight the methods and products that will make HTS devices easy and beneficial to use.

Twenty-one experts in cryogenic cooling research and development attended this workshop. Key technologists from STI and E-Systems represented the HTS electronics industry since both STI and E-Systems are respected leaders in the introduction of HTS circuitry in high performance microwave and millimeter wave systems.

The approach to this workshop was fivefold.

1.   Evaluate and identify currently available cooling technologies appropriate for HTS electronics.

2.   Evaluate current development efforts and encourage acceleration of those that will help HTS cooling.

3.   Identify promising new approaches enabled by the requirements unique to HTS electronics.

4.   Identify other technologies with similar cooling requirements and encourage joint development of coolers to accelerate and justify developments.

5.   Prepare a summary of the workshop.

This workshop focused on coolers for airborne and surface applications where cost and reliability are major issues. We did not cover coolers for space applications where cooling is usually part of a much larger system issue. Small working groups evaluated both open and closed cycle technologies. Open cycle technologies covered were stored-cryogen and Joule-Thomson coolers; closed cycle technologies covered were Gifford-McMahon, Stirling, and closed circuit Joule-Thomson. A final session reviewed other new approaches.

This workshop was the first meeting between technologists in HTS electronics and in cryogenics. The atmosphere was very positive and constructive. Uncertainties for both groups concerning the present state of the art and the rate of evolution of the "other" technology at first impeded communication. However, each made significant progress toward understanding the others' problems and needs. Clearly, cryogenic solutions for HTS needs can only oe arrived at interactively, and this workshop represented the first step in that interaction. The written comments (requested from all participants) were positive and stated the workshop was definitely valuable.

The workshop consisted of five separate sessions that focused on specific cooling technology types. Sessions for each technology type focused on identifying key technological issues, significant strengths and weaknesses, and applications particularly well suited to that cooling technology. These evaluations included current and developing cooler technology.

Some technical limitations to current cooling technology are of a fundamental nature and others are the result of HTS cooling being different from IR and other established areas. Two of the most significant technical limitations for HTS applications are circuit size and, in some applications, a hot ambient. Table 2 summarizes the key technological issues that we identified and potential courses of action to address these issues. This list is inclusive for all the cooling types considered.

Table 2. Key technological cooler issues.

SIGNIFICANT COOLER ISSUES	POTENTIAL SOLUTIONS/COMMENTS
• Hot ambient (~85°C)	• Minimize parasitic heat load • Reject heat remotely
• Large (relative to IR) circuits (≥ several cm^2)	• Minimize thermal mass • Minimize parasitic heat load • Redesign cooling head
• Cooler cost (particularly closed-cycle)	• Don't over specify • Design around few standard coolers • "Piggyback" on other technologies
• Closed-cycle microphonics / EMI	• Evaluate magnitude of problem • Continue pulse tube R&D
• Closed-cycle reliability	• Continue current development • Introduce pulse tube expander
• Open-cycle gas/LN2 reliability and logistics for multiple use systems	• Choose appropriate applications • Utilize trained personnel

The workshop's assessment of the relative strengths and weaknesses of each cooling technology is summarized in Tables 3(a), (b) and (c). Basically, open cycle cooling technologies typically are the most reliable and the least expensive, but they have a finite mission time limitation,

85

typically minutes to a few hours. Closed cycle cooling technologies offer extended mission time capability but are typically expensive and have less than desired reliability or undesirably large size. Of the new technologies discussed, the pulse tube refrigerator offers the potential of reduced cost and increased reliability by reducing the number of moving parts in a closed cycle system. But this system is still in the research and development stage.

Table 3(a). Open cycle.

JOULE-THOMSON

STRENGTHS	WEAKNESSES
• Reliable for one shot applications • Rapid cool down capability • Low vibration / EMI • Simple interface with dewar • Adaptable to large cold heads • Low cost $500-$1000 (1W/2hrs) • Small cold head, gimbal-able • No Airborne power required • Infinite storage life (compared to LN2)	• Multiple use involves logistics problems • Multiple use means reduced reliability • Finite mission time

STORED CRYOGENS

STRENGTHS	WEAKNESSES
• Predictable hold time • Mature technology (low risk) • Reliable (no moving parts) • Low vibration • No Airborne power required • Low cost • Adaptable to large cold heads • Low vibration / EMI	• Finite mission time • Finite storage time (storage time subtracts from mission time) • Logistical support required for refill

Table 3(b). Closed cycle.

JOULE-THOMSON

STRENGTHS	WEAKNESSES

• Remotely locatable compressor
• Low vibration at cold head
• Simple interface with dewar
• Adaptable to large cold heads
• Rapid cool down
• Multiple cold heads / compressor
	• High pressures in compressor
	  (adversely affects reliability and cost)
	• Lower efficiency than Stirling
	  (2 to 5 times)
	• Under development

STIRLING

STRENGTHS	WEAKNESSES
• Highest thermodynamic efficiency • Available units to 2 watts • Demonstrated MTTF >4000 hrs.	• 2 to 100 watt not available • Small cooled area • Difficulty with >85°C ambient (lowered efficiency and reliability)

Gifford-McMahon

STRENGTHS	WEAKNESSES
• Remotely locatable compressor • >50,000 Hrs MTBF demonstrated • Generic compressor • Multiple cold heads / compressor	• Lower efficiency than Stirling • Larger than Stirling • No matched compressor/cold head systems available

Table 3(c). Other emerging technologies.

PULSE TUBE EXPANDER

STRENGTHS	WEAKNESSES

• Low vibration
 	
• No moving cold parts
 	
• Compatible with existing Stirling
  compressors
	• <30 watt units lower efficiency than
	  moving displacer Stirling (<2X at
	  5 watt)
	
	• Not currently available;
	  in R&D at NIST

The wide range in strengths and weaknesses of each cooling technology clearly makes the proper choice of a cooler technology dependant on the particular HTS application. Each cooling technology will be most suited to a particular set of HTS applications (the converse is also true). Unfortunately not all HTS applications will have a good match to a presently available cooling technology. Table 4 summarizes the current thinking on best match applications to cooling types.

Table 4. Example good match microwave applications and cooler technology.

• STORED CRYOGENS	• Circuit demonstrations and laboratory tests
• OPEN CYCLE JOULE-THOMSON	• Dual mode IR and milimeter wave seekers for missles
• CLOSED-CYCLE JOULE-THOMSON	• Airborne applications with hot ambients requiring remote heat rejection
• STIRLING	• ≤ 2 watts; Airborne applications • ≥ 100 watts; Ground and shipboard • Mid range under development
• GIFFORD-McMAHON	• Ground and shipboard applications with multiple HTSC components and multiple cold heads

We identified cost and reliability at the outset of the workshop as the two primary issues to be resolved with coolers for HTS applications. For at least the next three years no new cooling systems are likely to be commercially available, so that the choices of refrigeration are fixed both in type and cost. This workshop concluded that closed cycle cooler cost will not come down soon from the current $5K to $20K level.   Reductions in this cost to a target of ~$1K will require quantities of >100,000 units a year and significant capital investment. Such growth in the cooler market is unlikely if only HTS is driving the market. It is possible that cooled semiconductor processors will be installed in desktop work stations and this could provide the market to drive the cost down. Low cost also could be achieved by keeping cooler specs to a minimum and standardizing the cooler to one or two designs. Reliability in closed cycle coolers is steadily improving with 4,000 hrs. MTTF now and 15,000 hrs. expected soon in 1 watt systems. Carrier's 250 watt cooler is designed to a 50,000 hr. specification. We concluded that these latter values are acceptable for the vast majority of HTS applications.

Packaging development

As with cryogenic cooling, we recognized early that there are significant problems inherent with the required cryogenic packaging, as well as the availability of components for microwave/cryogenic packaging. Off the shelf vacuum dewars were not practical for HTS device packaging. Two years ago we initiated an IR&D project to solve these packaging problems. During this time, we have designed, fabricated, and tested dewars with HTS components.

Our efforts began with conventional cylindrical dewars cooled by stored liquid nitrogen. These dewars, though readily available, always required modifications for use with HTS devices. Examples of cylindrical liquid nitrogen(LN_2)wars are shown in Figure 85. These dewars utilize a repumpable port for occasional vacuum maintenance.
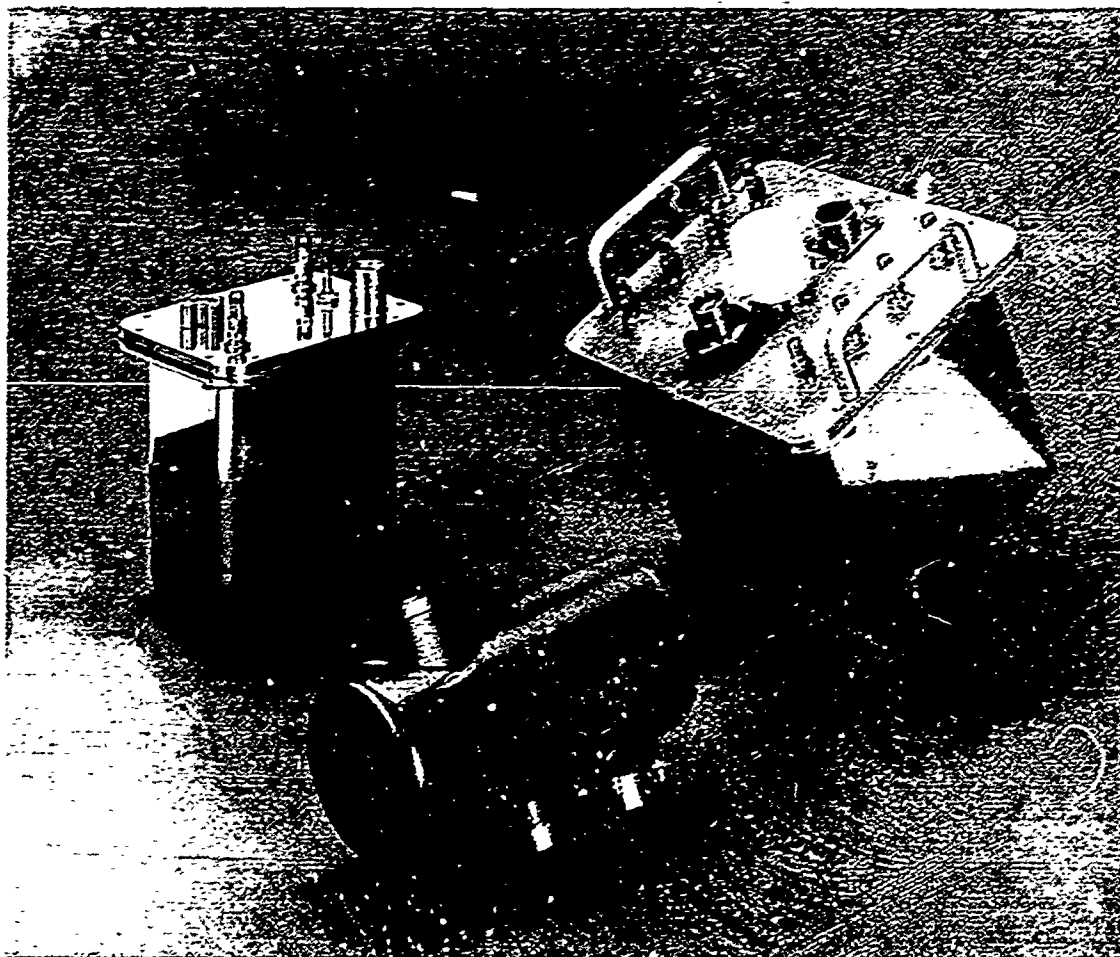
Figure 85. Typical STI developed LN_2 dewars.

Cylindrical dewars are not readily adaptable to packaging HTS devices mounted in rectangular housings. To solve this problem we designed, fabricated, and tested several versions of rectangular shaped dewars. These dewars were developed under IR&D funds to evaluate insulation efficiency, types of getters, coaxial cables, vacuum feed throughs, hold times, etc. Figure 85 shows examples of these rectangular dewars. These dewars (although more difficult to fabricate and somewhat less thermally efficient than cylindrical) significantly simplified the installation of the HTS devices and interconnection cables into the dewars. These LN_2 pour-filled dewars met design requirements to cool the HTS devices to cryogenic temperatures, have hold

times in excess of eight hours, and have a minimum of one month vacuum life time between re-evacuations. Vacuum maintenance is provided by a repumpable port.

We have also be en developing permanently sealed long life closed cycle cooled packages. The delay line in the FMCW radar demonstrator is the first HTS device both successfully packaged in a permanently sealed long life dewar and cooled using a closed cycle cryogenic refrigerator. This package is described in more detail in the next section on the FMCW radar demonstration unit. A cutaway of this dewar is shown in Figure 86.
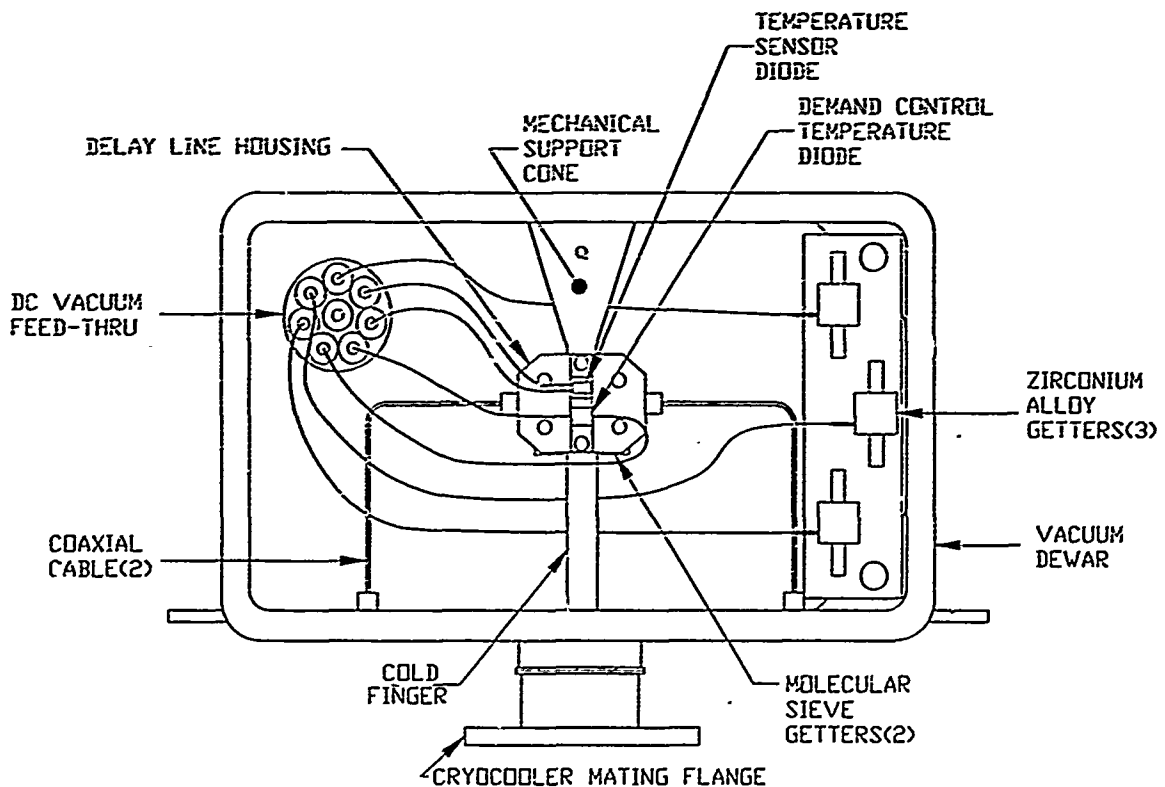
Figure 86. FMCW radar demonstrator dewar.

Key to the development of permanently sealed dewars is availability of "Off the shelf" standard microwave components such as coaxial cables and coaxial vacuum feedthrus. Current standard components are not compatible for systems requirements or for long life cryogenic vacuum packaging of HTS devices.

STI further recognized that there is an urgent need for these components. Based on experience from the infrared industry, the growth of fielding systems utilizing HTS devices will greatly depend on the availability of "universally " acceptable components that are low in cost. The military nearly 15 years ago recognized that IR detector vacuum dewars and their associated

cryogenic cryocoolers were very costly. Only after "common modules" were established, did the IR systems get built in production quantities at affordable costs.

Thus, STI is now developing, under a company funded IR&D project, cryogenic packaging modules that will help make the packaging of HTS devices a routine operation. The "common modules" under development are depicted in Figure 87 and will provide for:

- low loss transition
- standard circuit enclosure
- cold plate module

- insulation package
- cold plate suspension
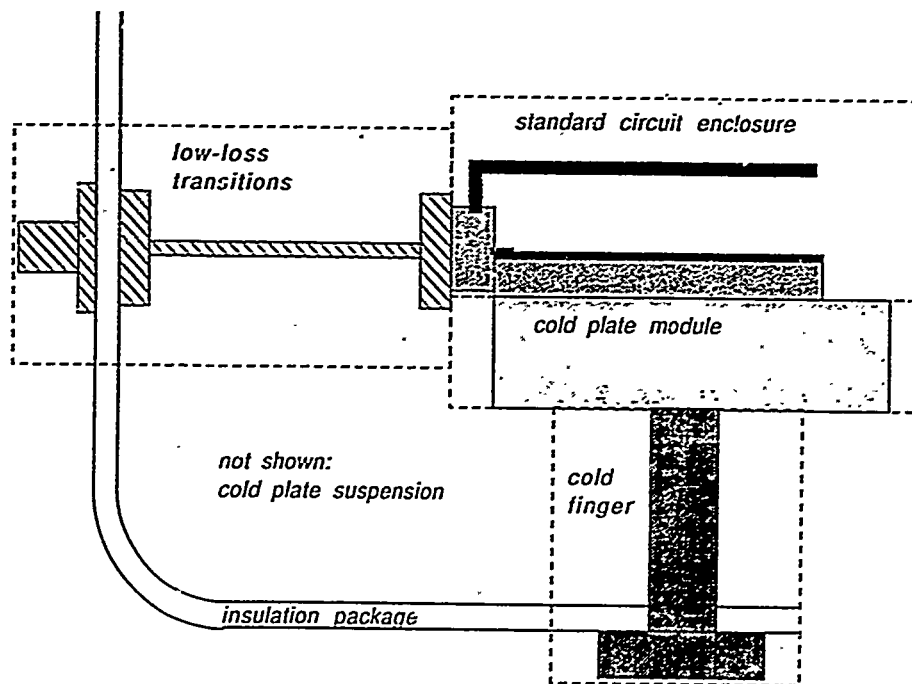
Figure 87. STI packaging modules under development.

STI's goals are to develop "common modules" which are produced at low cost, reliable, industry standardized, flexible, and universally accepted for vacuum packaging cryogenically cooled HTS devices.

FMCW RADAR PROTOTYPE

We chose a FMCW radar with an HTS delay line to demonstrate that we can produce functioning cryogenically cooled HTS circuits in a compact package requiring only power. We

chose the FMCW radar because it is interactive and does not require any additional test equipment to demonstrate its function. A detailed description of the demonstration unit is given in the following sections.

Basic FMCW Radar Principle

Figure 88 shows a functional block diagram of the RADAR.
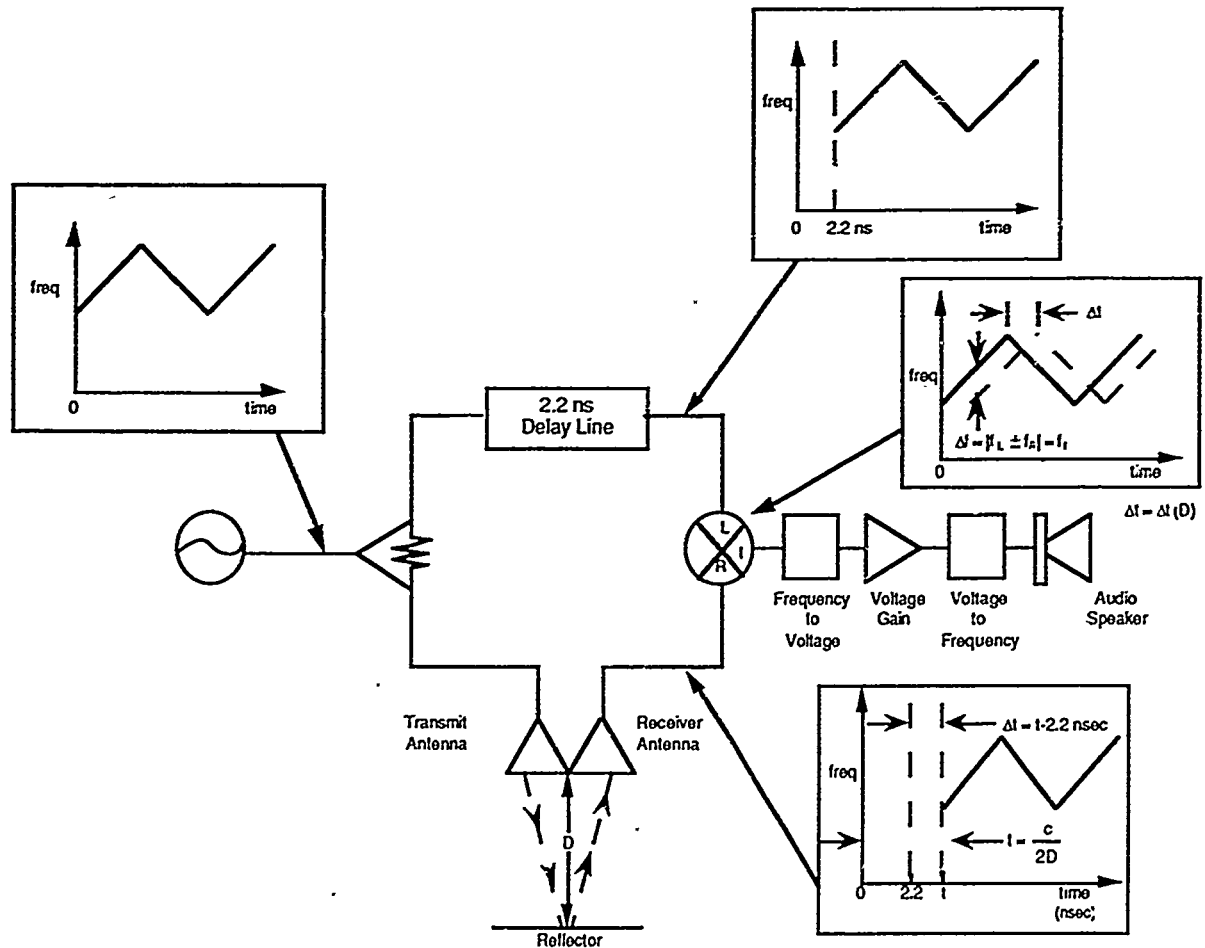
Figure 88. Block diagram of the FMCW radar demonstration unit. Plots indicate timing relationships of the signals.

A YIG voltage controlled oscillator, continuously swept in time from 8 to 12.4 GHz is used to produce a RF signal. The signal is then split into two parts. One half is sent through the HTS delay line where it is delayed by 2.2 ns. The other half is transmitted out one of the wave guide horn antenna, bounces off a reflector, and is received by the other antenna. This latter path has a variable delay time related to the distance D that separates the reflector from the antenna.

Since the frequency of the RF oscillator is changing with time, a different delay in time means that different frequency is present. The two signals are then recombined in a mixer that outputs the difference in its input frequencies. This output frequency is converted to a voltage, processed and used to drive a voltage controlled audio oscillator. The output of the audio oscillator is then sent directly to the speaker. The LEDs on the front panel are driven by the voltage which controls the audio oscillator.

The audio output frequency is proportional to the delay of the antenna path less the delay of the HTS delay line. The antenna path delay is easily varied by moving the location of the reflector. If the delay time in the two signal paths is the same, there is a 0 Hz output from the mixer and hence no audio output. The reflector distance (from the antenna) where this occurs is called the "null point". As the reflector distance is changed from the "null point" the audio frequency increases. See Figure 89 for the relation between frequency output and distance from the antenna.
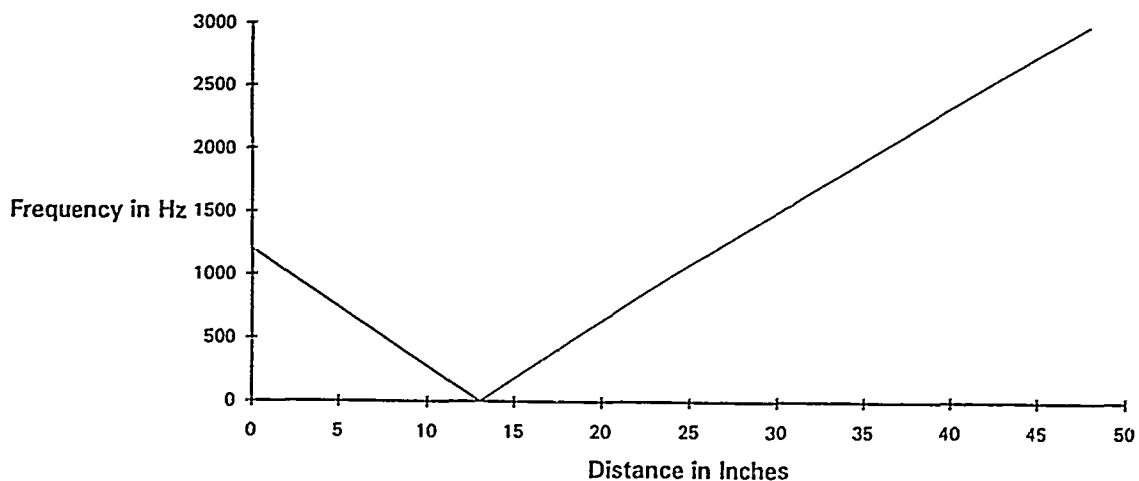
Figure 89. Frequency vs. distance.

HTS Delay Line

• Broad Band

• Compact 2.2 ns

• Can Be Made Much Longer (1 cm$^2 \geq$ 2.2 ns, 1.2" Square $\geq$ 30 ns)

The HTS delay line used in this demonstration measures 0.390 × 0.390 × 0.020" and weighs 0.33 grams. The time delay and insertion loss performance of the delay line are similar to

that of an RG141 coax cable with 90 times the volume and 50 times the weight of the delay line. Figure 90 shows the delay line and a comparable coax cable.

Figure 90. 2 nsec HTS delay line with a comparable coax cable.

The electrical performance of the delay line is shown in Figures 91 and 92. Figure 91 shows the time delay of the 2.2 ns delay line and Figure 92 gives the loss vs. frequency.

```
                                                  2.352 ns
C2
Del  MARKER 1
       2.352 ns
     705.11 mm
```

CH1 START 0 s   STOP 4 ns
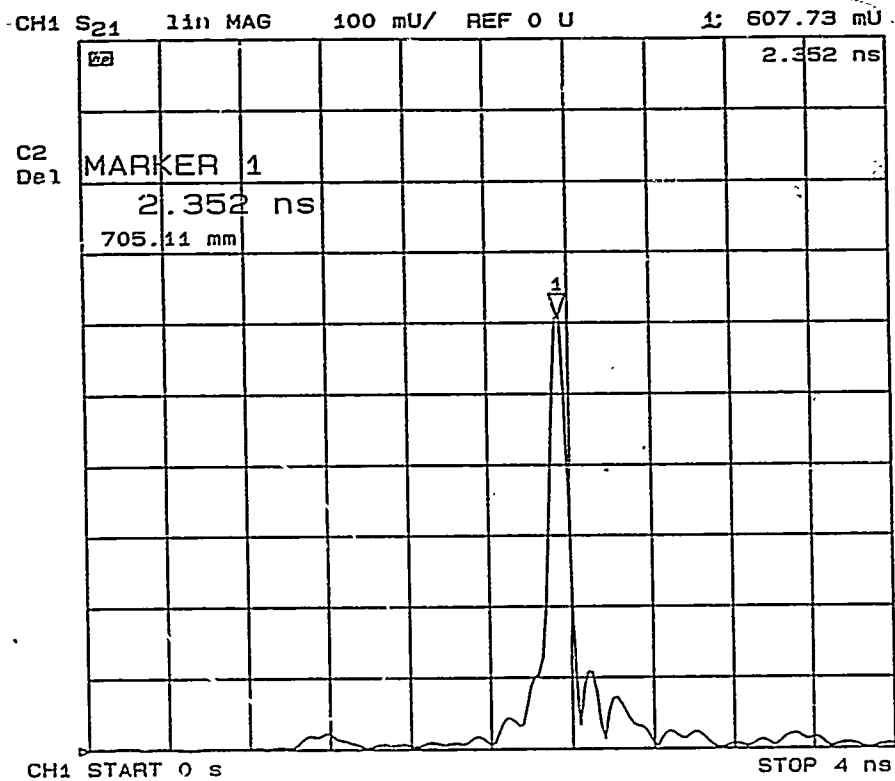
Figure 91. 2 nsec HTS delay line electrical delay.

```
MAG S21 (dB)

 0.0
-2.5
-5.0
-7.5
-10.0
-12.5
-15.0
-17.5
-20.0
     1.0  2.0  3.0  4.0  5.0  6.0  7.0  8.0  9.0  10.0  11.0  12.0
                        Frenquency (GHz)
```
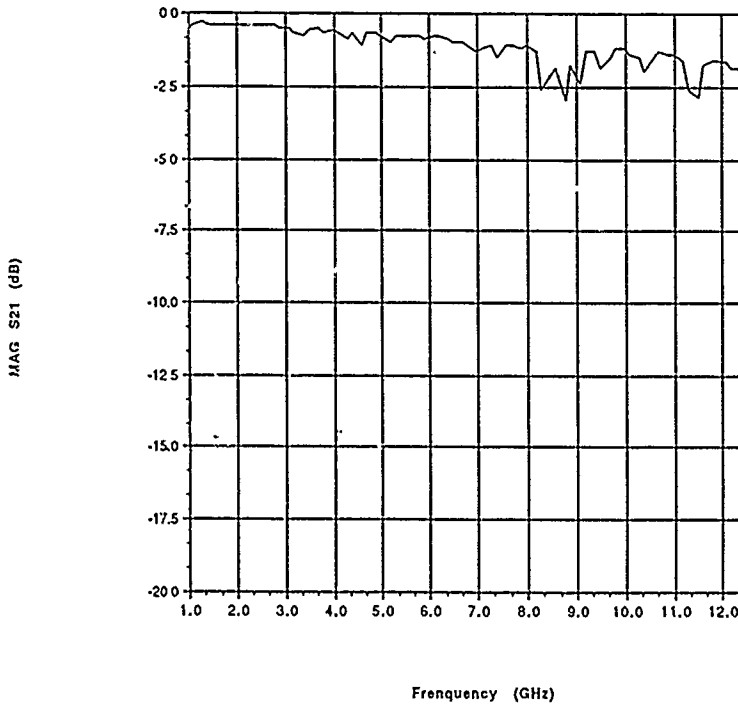
Figure 92. 2 nsec HTS delay line transmission loss.

The design uses a proprietary coplanar wave guide (CPW) structure. The gold crossovers are necessary to preserve the CPW mode of propagation and are implemented as quasi lumped capacitors. High impedance CPW lines between these crossovers are used as quasi-lumped

inductors to realized a low pass filter. This keeps size to a minimum while maximizing delay. Connection to the system was achieved by mounting the circuit into a low thermal mass housing that includes a CPW to Coax transition (see Figure 93).
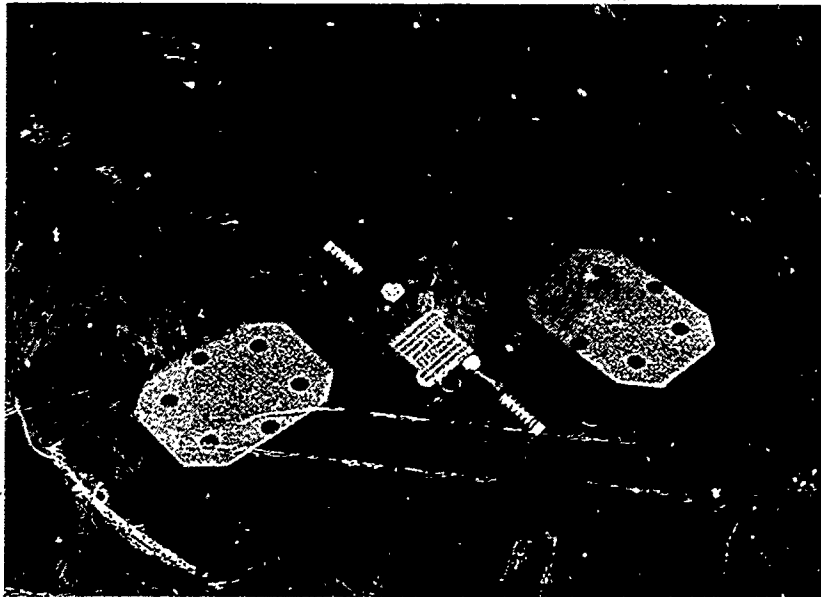
Figure 93. 2 nsec HTS delay line and housing.

The line was fabricated using STI's standard production process. The process deposits TBCCO film onto a single crystal LaAlO$_3$. The standard process also includes an ohmic contact gold layer, a polyimide dielectric layer and a top gold layer.

The same design and fabrication technique has also been used to produce a $1.00 \times 1.00"$ delay line (see Figure 94). The measured delay of this line is shown in Figure 95. This demonstrates that very long delays can be realized using CPW designs on HTS films.
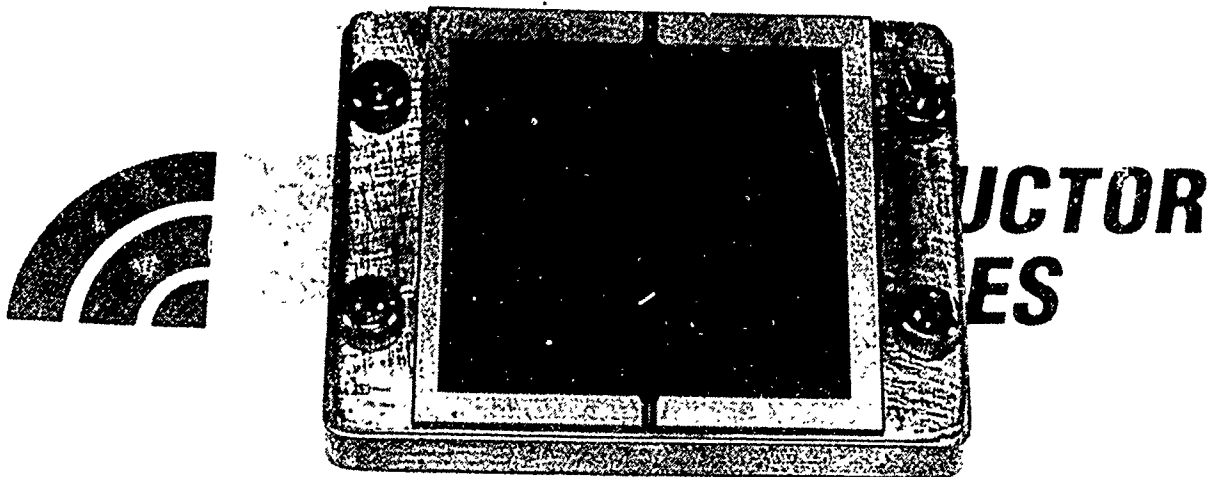
Figure 94. 29 nsec HTS delay line.
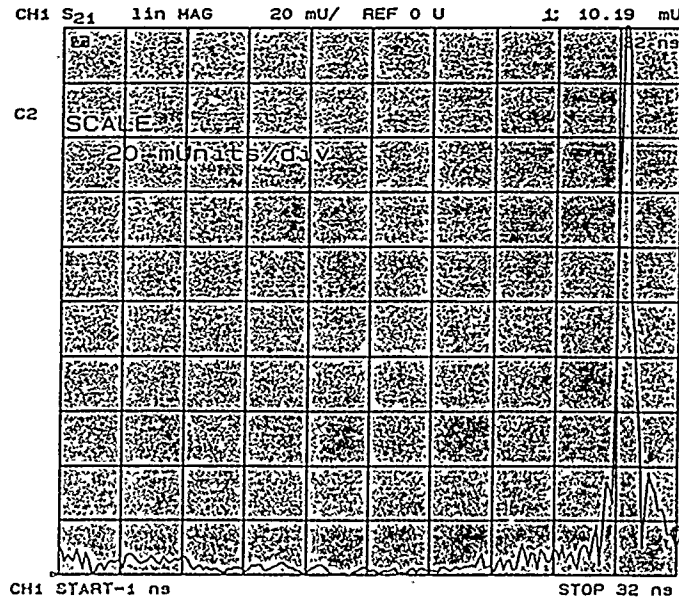
Figure 95. 29 nsec HTS delay line electrical delay.

Dewar Description

• First Demonstration Of Functional HTS Circuit In Permanently Sealed Dewar With Closed Cycle Cooler

• Packaging Is In Early Stages Of Development

• STI Development Efforts Are Focused On:

> Thermal Mass Reduction (Shortens Cooldown Time)
> Vacuum Computability (Improves Dewar Lifetime)
> Microwave Performance (Wider Band Width, Lower Insertion Loss, etc.)

The vacuum dewar is very similar to the common household "Thermos" bottle, except it contains the HTS device and the necessary components to make it reliable and functional for systems applications. A cutaway drawing of the dewar with the final closure cover removed has been shown in Figure 85.

The HTS delay line is mounted inside of the delay line housing which is in thermal contact to the heatsink of the coldfinger. The microwave signals from the delay line are carried by the coaxial cables through the vacuum walls via a feedthru (not shown in Figure 85). To maintain insulating vacuum, two types of getters are utilized within the vacuum. The molecular sieve getters are cooled to about 80K by the cryocooler to remove water molecules and hydrocarbons with a molecule size of less than 5Å. The non-evaporable zirconia alloy getters will remove residual

97

outgassing constituents such as hydrogen, nitrogen, oxygen, carbon dioxide, carbon monoxide, and water.

A temperature sensing diode is used by the demand control electronics to maintain the HTS delay line at about 80K. The temperature sensor diode is used by the LED readout to provide a visual indication of temperature near the HTS delay line. The DC vacuum feedthru carries the required electrical current from the diodes and zirconia alloy getters through the vacuum dewar.

The dewar assembly and coldfinger are slipped onto the cryocooler displacer and secured via mounting screws to the mating flange of the cryocooler displacer. Silver filled silicone thermal grease is added between the coldfinger heatsink and the coldtip of the cryocooler displacer.

Cryocooler Description

- Current Cryocoolers Developed For The IR Industry Are Most Costly, Lower In Capacity, And Less Reliable Than Desired For Cryoelectronics

- STI Efforts Focused On Accelerating Development Of Improved Coolers By The Cooler Industry

The cryocooler design is based on a thermodynamic split Stirling cycle, in which work is done by compressing gas inside a compressor. The heat generated is dissipated at approximately room temperature, and the same gas is allowed to expand inside the cold tip of the displacer, thereby producing a cooling effect. For the current application, it will cool the HTS device to a nominal temperature of 80K.

The major components of the cryocooler are shown in the photo in Figure 96. The hermetically sealed cryocooler is made up of the compressor, displacer, stainless steel transfer line, and the demand control electronics (not shown).
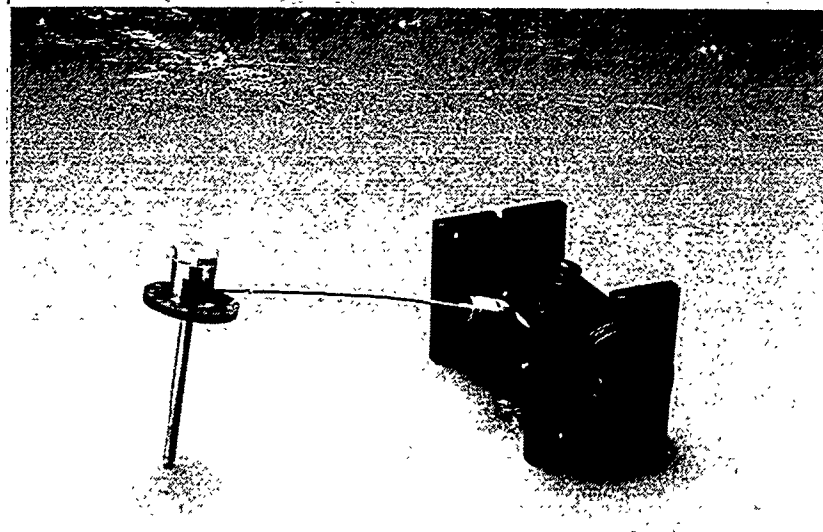
Figure 96. Hughes model 7050H cryocooler.

The compressor consists of a piston mounted on a shaft, which in turn is mounted on diaphragm springs that give axial freedom but are radially rigid. The linear motor causes the shaft, and hence the piston, to oscillate at a frequency of 50 Hz. This superimposes an oscillating pressure cycle of nominally 2:1 on the mean vessel pressure of 325 psi, with helium as the working fluid. This pressure cycle is transmitted to the displacer via a stainless steel transfer tube, which allows flexible independent mounting of these two mechanical units. The free piston displacer contains a reciprocating regenerator stack made of metal mesh with a high specific heat (basically a heat exchanger).

When the motions of these two mechanisms are correctly phased, heat is progressively removed from the cold tip until the operating cryogenic temperature is reached and maintained. The two mechanisms operating at 50 Hz are maintained in a precise phase relationship.

The temperature sensor, mounted in very close proximity to the HTS device, is electrically connected to the demand control electronics. Upon attaining a temperature of 80K, the demand control electronics decreases the power to the compressor, prevents a further decrease in temperature and decreases power consumption. The closed loop feedback control maintains the HTS device at 80K. The cooler can also be tuned to operate at other temperatures, and is therefore not simply a cooler for use at 80K.

Cryocooler Data

When the system is first turned on, the temperature readout will indicate a temperature close to room temperature (~300K). A low pitch sound can be heard from both the compressor and the displacer. The sound can be better heard by placing one's ear closer to the compressor or displacer. A slight vibration can be felt on the compressor due to the oscillation of the pistons within.

The temperature will gradually decrease from ~300K to 80K in about 29 minutes. Figure 97 shows a typical cooldown curve for this unit. The cooldown time can vary a few minutes from the curve shown due to fluctuations of the ambient temperature.

Temperature vs. Cooldown Time
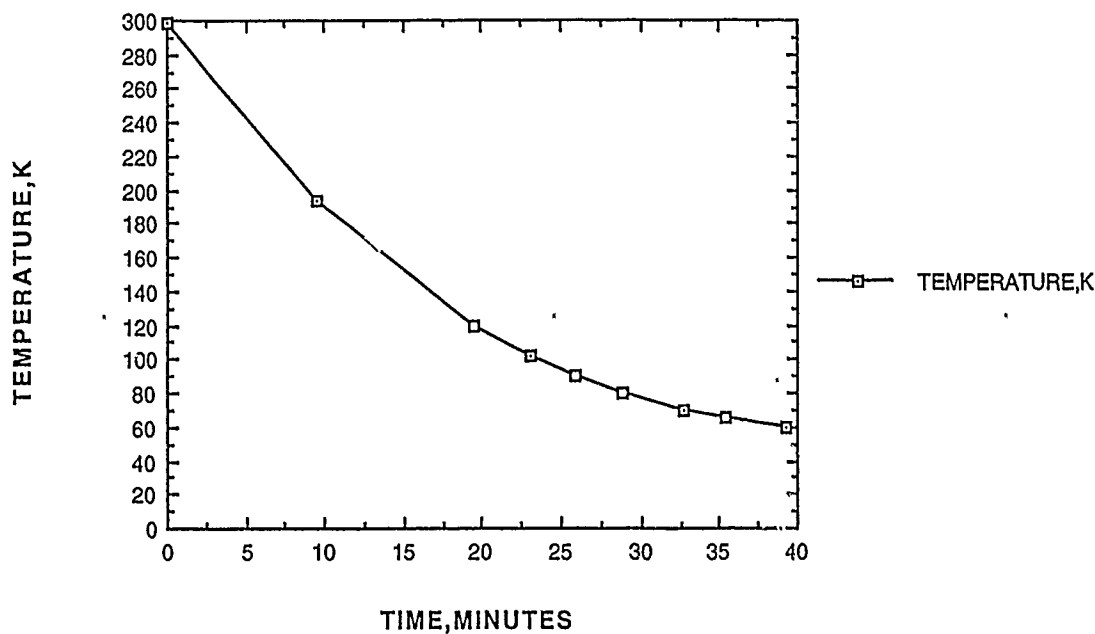
Figure 97. Typical cooldown curve.

When 80K temperature is attained, the cryocooler goes into the demand mode. At this time the compressor and displacer slows down and the oscillation sound will also decrease. The temperature will fluctuate but it will be close to 80K.

During prolonged testing, the displacer and compressor will increase in temperature. The body of the compressor and the warm end of the displacer can reach a steady state temperature of about 70°C.

SUBCONTRACTOR RESEARCH AND RESULTS

BEI Electronics

BEI was included in the original proposal to evaluate thin films for linear actuator coils. Early engineering specifications exceeded the materials properties in a magnetic field and this program was dropped in the first year.

Avantek

Work was subcontracted to Avantek Inc. with an objective of using their expertise in oscillator design, subassembly and device packaging of traditional MIC technology. A copy of the Final Technical Report from Avantek is contained in Volume 2 and expands on the information given below.

Package Development

This portion of the subcontract was intended to perfect the packaging of HTS components at 77K to meet military hermeticity screening requirements. Two housing materials were considered: aluminum and stainless steel. A 50Ω microstrip transmission line was installed in the housings and RF connection was made through 50Ω soldered in glass feedthrus. A total of 75 temperature cycles (300K to 70K) were completed on the two styles of package.

After the 75 cycles were completed, 80% of the stainless steel and 100% of the aluminum housings passed the leak test. The leak failures appeared to be the result of poor soldering of the RF feedthrus into the housings. Also, 100% of the stainless steel and 80% of the aluminum housings passed the electrical tests. The RF failures were due to broken gold ribbons used to connect the RF feedthru pin to the 50Ω circuit trace and appears to be the result of insufficient stress relief.

Oscillator Development

Two approaches to HTS oscillators operating at approximately 10 GHz were studied as outlined below.

Parallel feedback oscillator

An oscillator was built using a bipolar device as the first stage in the amplifier and GaAs FETs in subsequent stages. The phase noise at a center frequency of 10 GHz was measured at

-100 dBc/Hz at 10 kHz from the carrier. It was unclear from these experiments what was limiting phase noise performance.

Series feedback oscillator

Initially the HTS resonator was packaged in a separate housing from the active part of the oscillator circuit. Only the HTS resonator was cooled to 77K. The phase noise performance of this oscillator was measured as -95 dBc/Hz at 10 kHz from the center frequency (approximately 10 GHz). When the HTS resonator was integrated with the active portion of the oscillator in the same housing and the whole assembly cooled to 77K, the phase noise performance degraded by about 30 DB. The causes of this degradation could be due to the reduced quality factor of the resonator in the oscillator package and the uncertainty of correct performance of the active part of the oscillator circuit when operated at 77K. However, the oscillator performed significantly better when compared to one using a gold microstrip resonator as the resonant element in the integrated oscillator. In this case, the phase noise of the HTS resonator stabilized oscillator was about 20 dB better than the gold resonator stabilized oscillator.

Summary

Packaging of HTS assemblies for operation at 77K can be done with high yield when exposed to the leak check of military screening requirements.

HTS stabilized oscillators offer the promise of highly stable oscillators with low phase noise. Parallel feedback oscillators, although not very efficient, achieved good phase noise performance while the series feedback versions operated very efficiently but with relatively poor phase noise performance. It is expected that significant improvements in phase noise can be achieved with better resonators and improvements in packaging design for low phase noise performance and operation at 77K.

LMSC

One possible device application for thin film HTSs is for interconnect wiring to low temperature satellite systems, e.g., IR sensors operating at 10K. Heat leaks caused by conventional metal interconnects causes rapid loss of the coolant and thereby dramatically reduces the orbital lifetime. We investigated the possibility of constructing such an interconnect board with our thallium films in collaboration with Lockheed Research & Development Division. The objective was to build a small demonstration interconnect board. The HTS interconnects needed to have a current carrying capability of a few hundred amps per cm^2 in order to be useful for

applications. The substrate material must also have very low thermal conductivity. We investigated HTS films on three different types of substrates: (i) polycrystalline ZrO_2, (ii) single crystal $LaAlO_3$ and (iii) single crystalline on ZrO_2. We found that the current carrying capability of films on polycrystalline ZrO_2 was unacceptably low. Films on single crystal $LaAlO_3$ had excellent current carrying capabilities; however the thermal conduction of the $LaAlO_3$ substrate was found to be to high. The interconnects fabricated onto single crystalline on ZrO_2 had current carrying capability of more than 5000 amps per cm^2 at 100K which is sufficient to be practical for applications. The one remaining problem was the degradation of the films with time, probably related to the relatively poor nature films on ZrO_2 as compared to films $LaAlO_3$ where no such degradation is observed. Details of this work are in the Appendix (Volume 2) of this report.

We feel that this area still has real potential for HTS thin films, provided a useful substrate, or possible a buffer layer on single crystalline on ZrO_2, can be found. This would assure that the thallium films are epitaxial, which is the case on $LaAlO_3$ where no film degradation is observed.

Hughes

Hughes Aircraft Co. evaluated two applications for HTS materials. The first involved a multibit phase shifter demonstration. Initially Hughes developed test fixturing for HTS circuit evaluations at 77K (or lower). This equipment was used to measure performance of HTS and gold circuits in a standard fixture, so direct comparisons of performance could be made. STI fabricated circuits for evaluation as well as supplying Hughes with unpatterned films for them to pattern and test. The results of these tests are covered in the Hughes final report. A multibit phase shifter design was developed using PIN diodes as switches. Evaluation of the phase shifter design resulted in the conclusion that it does not appear to be manufacturable due to the complicated physical layout with PIN diodes. Also PIN diodes dissipate a significant amount of heat relative to cooling available from current cryocoolers suitable for a radar application. Further development will be required.

The second application involved an IR focal plane interconnect cable to minimize heat loss from the IR detector cold stage (10K) to intermediate processing electronics (30-50K). However, the Hughes design approach required a flexible cable, not a rigid interconnect as was the case for LMSC. The flexibility requirement could not be changed in the system design and further development was dropped.

Sanders

The sub-contract objectives were to design the test circuits for STI to fabricate and test the resulting devices, comparing the results to existing devices. Early in the contract it was apparent that development of the device fabrication technology for etching and bonding to the superconductor was a key technology requirement before devices could be made routinely. Consequently, Sanders provided critical expertise in pioneering some of the device fabrication tools. However, this held up the design and building of the local oscillator, which was the main goal of the sub-contract. The contributions to the program are outlined below.

Ion Milling

Patterning of superconducting films, both YBCO and TBCCO, is routinely achieved using wet chemical etches. However, undercutting of the photoresist and variability in the etch rate not only puts a practical limit on the minimum achievable linewidth, but gives rise to rough edges. An attractive but expensive alternative is to use ion milling. YBCO and TBCCO films grown at STI were ion milled into a standard 2.3 GHz resonator at Sanders to compare the performance and linewidth control of the two techniques.

Figure 98 shows the device performance of the two films. The high unloaded Qs indicate little, if any degradation from the patterning process.
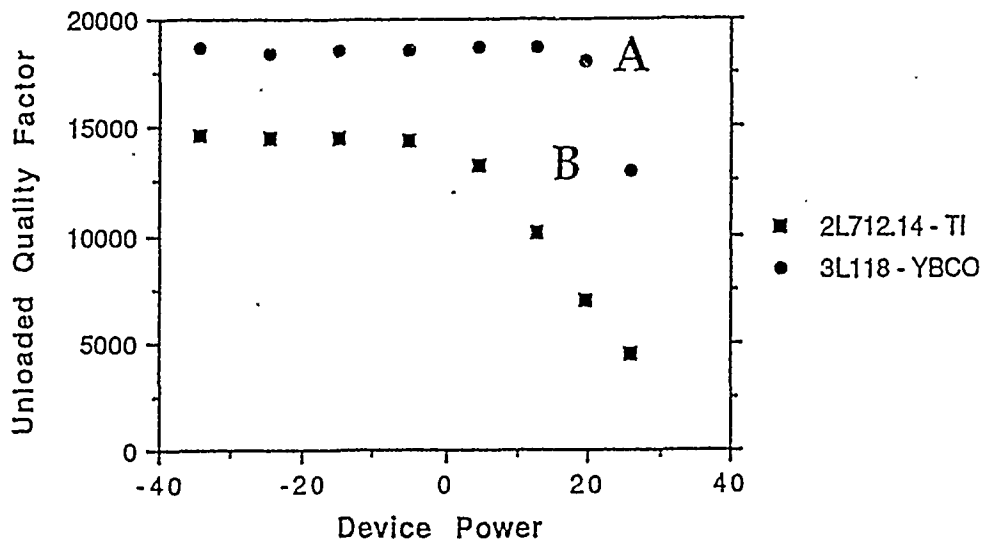
Figure 98. 2.3G Hz device performance for two films, one YBCO and one TBCCO, patterned using ion milling.

In addition Table 5 illustrates the excellent dimensional control achievable using ion milling, when compensation for undercutting is not required.

Table 5. Comparison of dimensional control between ion milling and wet chemical etching.

Film No.	Mask Dimensions μm	Film Dimensions μm	Delta μm	Etch Method
2L712.2	25	24.6	-0.4	Ion
2L712.2	25	25.4	+0.4	Ion
2L683.3	25	12.4	-12.6	Acid
2L683.3	25	14.8	-10.2	Acid

The original mask dimension was 25μm in width. The small variability in the deviations from this value observed for ion milling is within the error of the measurement. However, as can be clearly seen in the case of the acid etched sample, an undercutting of ~5.7μm per edge is evident. This study indicates ion milling is an excellent alternative to wet chemical etches. As smaller features are required the need for ion milling will increase.

Passivation

Exposure of TBCCO superconducting films to thin layers of moisture have been shown to degrade the performance of these films in microwave applications. STI has developed a passivation layer capable of protecting the superconductor against repeated exposure to different environments. The first results are shown in Figure 99.

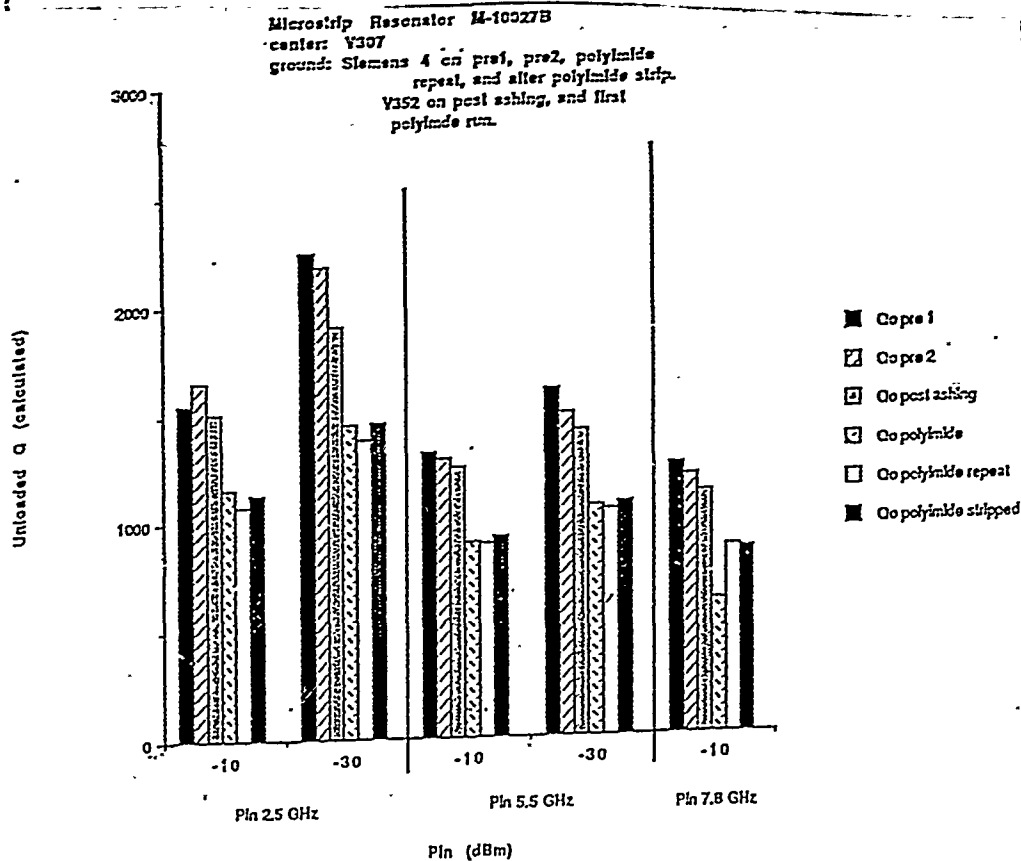Figure 99. Performance data for film V307 at three different frequencies, before and after coating with polyimide passivation layer.

The film used to qualify the process was not of the highest standard; however it did show that coating the resonator with a layer of polyimide did not severely degrade the performance. Figure 91 shows the fundamental frequency (2.5GHz) and the first to harmonics (5.5 and 7.8 GHz) for an S-shaped resonator. Data was collected at two input power levels (-10 and -30dBm) for a sequence of experiments. The baseline performance of the resonator was tested prior to any fabrication steps. This was done twice to assess repeatability. The circuit was then ashed, retested, coated with polyimide, retested and finally stripped of the polyimide layer and retested. The data shows a 30% drop in performance, however, subsequent fine tuning of the polyimide and the use of high quality films has produced a very effective passivation coating which has a minimum effect on device performance.

STI has now developed this passivation coating into an effective barrie.· which maintains the high performance of the device. For example, passivated resonators have been exposed to hydrochloric acid and have shown no significant change in performance.

Bondable Ohmic Contacts

The first ohmic contacts to be used on TBCCO devices which gave the desired low contact resistance were made sputter depositing gold directly onto superconductor. Although low contact resistances were measured, the bond pads often detached from the superconductor and a detailed study of adhesion was an essential step to producing bondable ohmic contacts capable of performing to MILSPEC standards.

Figure 100 shows the improvements in bond pull strength achieved using 0.001" gold wire on bond pads deposited by sputtering or evaporation and surfaces cleaned by bromine etching or ashing. The matrix of experiments was designed to find the optimum combination of superconductor surface preparation and and deposition technique.
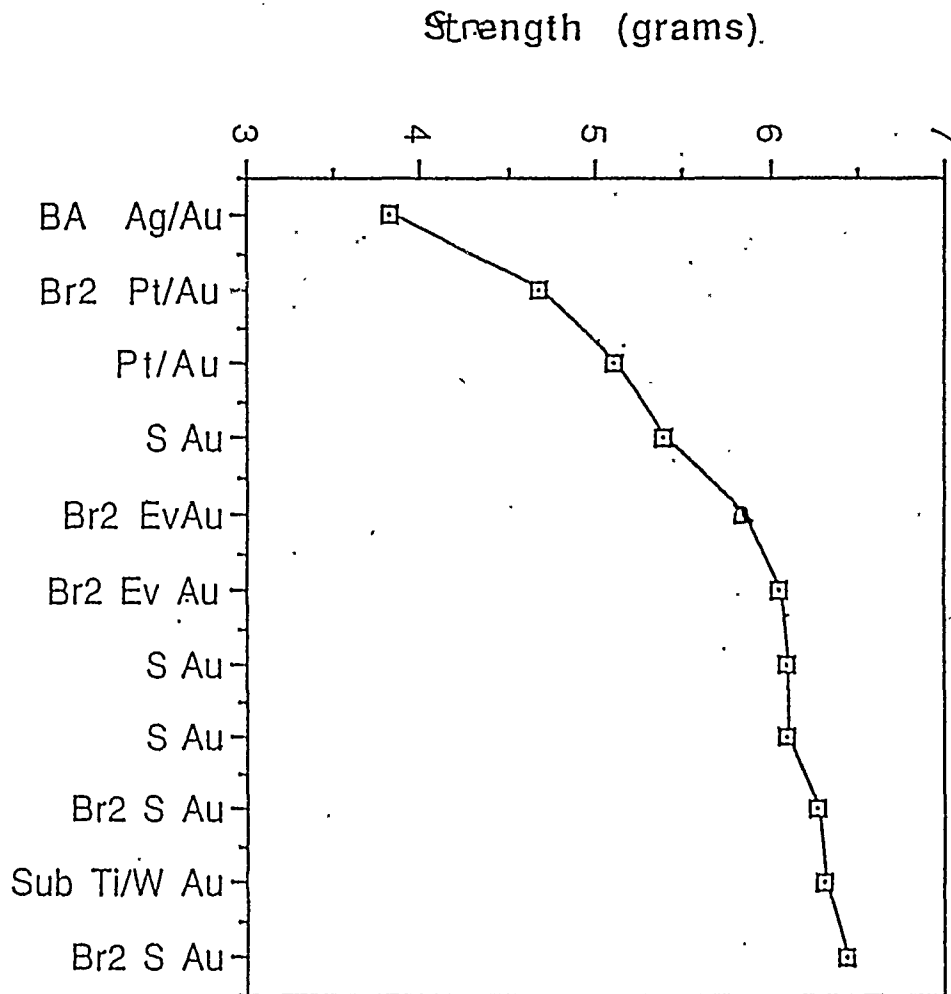

Figure 100. Bond pull strength for different contacts to the superconductor.

The lowest bond pull strength was resulted from barrel ashing (BA) the surface followed by deposition of silver and gold as the contact. As can be seen from Figure 100, deposition of

107

other metals as adhesion or barrier layers such as platinum or silver reduces the strength of the contact. The most robust contacts resulted from sputtered (S) gold on a bromine etched surface. The bromine etch removes a thin layer of material from the superconductor surface. The integrity of the contact is demonstrated by comparing the contact to a gold bond pad on the substrate itself. The best bond to the superconductor is superior in bond pull strength to a bond onto the substrate which has a Ti/W adhesion layer at the interface.

Miscellaneous

Electroplating

For many of the microwave applications envisaged both in this program and in others, a cheap and convenient method for depositing thick gold is required. This is traditionally done by electroplating. This was also seen as a significant advantage for building the gold air bridges required as cross-overs in the proposed circuit layout for this program. It was found that all gold plating solutions severely degraded the superconducting films. A 3μm thick sputtered gold film did not protect the film when immersed in the plating solution. However, the electroplating technique used by Sanders was successfully transferred to STI to allow for further investigation at some future date.

Substrate thinning

The need for high frequency operation of the TBCCO films which are grown on LaAlO$_3$ has led to the drive for thin substrates; LaAlO$_3$ has a dielectric constant close to 24, which for standard substrate thicknesses of 0.020" and 0.010" will result in substantial radiation losses at high frequency. Also, 0.004" thick LaAlO$_3$, prepared at Sanders by backlapping from 0.010", was supplied to STI for evaluation. However, the brittleness of the material and resulting breakage limits the use of the thin substrates.

The contributions made by Sanders in developing the device fabrication technology overcame a critical hurdle to the building of useable microwave hardware.

SUMMARY AND CONCLUSIONS

At the beginning of this three-year program research in the field of high temperature superconductivity was just getting underway. Dramatic advances have been made over the course of the contract. Our work on this program is a good example of the rapid rate of progress. We were successful in:

- developing a synthesis process for producing high quality thin films of TlBaCaCuO, putting that process into routine production, and scaling the wafer size to 2 inches;

- developing microstructural and electrical characterization techniques to allow the rapid measurement of film quality to permit rapid progress in process development;

- developing the needed fabrication processes of patterning, metallization, passivation, and bonding to allow the fabrication of practical HTS microwave and IR focal plane interconnect devices; and

- developing the design tools and the packaging techniques to demonstrate the promise for HTS microwave devices operating at 77K.

The most significant conclusions from this work are that it is possible to bring all the technologies together that are necessary to produce useful HTS passive microwave and IR focal plane interconnect devices that operate at 77K: Thin film manufacturing, device fabrication, device design, and packaging. These devices can offer 100 times the performance possible with the best normal metals (even at 77K).

RECOMMENDATIONS FOR FUTURE WORK

It is most important at this point in time to not lose the momentum we have gained in developing the technologies necessary for passive microwave applications of HTS thin films. It is now critically important to speed the insertion of the technologies into actual systems applications. There are a number of important programs underway that address applications in electronic warfare, radar, and space communications. We must keep pushing these technologies into the high leverage system applications.

In addition, it is of critical importance to keep our eyes on the future of potential applications for HTS thin films. Digital applications offer the highest leverage in terms of potential for both military and commercial systems. HTS multi-chip modules, on-chip interconnects, and fast A/D converters are all applications where HTS can provide solutions to critical needs.

If we look from the technology side rather from the applications side, we can also identify important areas for future work. A critical need for microwave applications of HTS thin films is the development of a more attractive substrate than $LaAlO_3$. It suffers from a twinning induced by a phase transition that occurs below the growth temperature for HTS films. We need a non-twinning substrate with low loss tangent that supports the growth of microwave quality HTS films. Also, a lower dielectric constant than 24 will be important for many applications, particularly at millimeter wave frequencies. Another technology development of far reaching importance will be the development of a process for growing TBCCO films *in-situ*. This will

allow films with lower numbers of defects, higher T_cs, and multilayers. Such films, if produced at low cost, will replace all other HTS films for applications.